Removal of Pharmaceuticals and Personal Care Products from Aqueous Solutions with Metal-Organic Frameworks

Isil Akpinar

This thesis is presented to UCL in partial fulfilment of the requirements for the Degree of Doctor of Philosophy

Supervisors

Dr Ozgur Yazaydin

Professor Asterios Gavrilidis

Department of Chemical Engineering

2017

DECLARATION

I, Isil Akpinar confirm that the work presented in this thesis is my own. Where information has been derived from other sources, I confirm that this has been indicated in the thesis.

Isil Akpinar

ABSTRACT

This thesis focused on synthesising metal-organic frameworks (MOFs) and using them in liquid phase adsorption because of their tunable textural and chemical functional properties. Zirconium based MOFs, Zeolitic Imidazolate Frameworks (ZIFs) and MIL (Matérial Institut Lavoisier) family of MOFs have gained particular attention for many potential applications owing to their exceptionally high chemical, thermal and mechanical stability.

The aim of this research was to determine MOFs`s viability as adsorbents for the remediation of water contaminated with pharmaceuticals, personal care products and also endocrine disrupting compounds, a known emerging class of organic contaminants. Removal of pharmaceutical compounds and endocrine disrupting compounds from water is of utmost importance due to the need for clean water and pollution prevention/mitigation.

The selected MOFs, ZIF-8, UiO-66, UiO-67 and MIL-100(Fe) were synthesised. The materials were characterised using standard characterisation techniques including: Powder X-ray diffraction (PXRD), N_2 sorption isotherm at 77 K and scanning electron microscopy (SEM). The materials were evaluated by batch adsorption experiments for the adsorptive removal of atrazine (pesticide), carbamazepine (antiepileptic), triclosan (antibacterial) and a binary mixture of carbamazepine and atrazine with having different hydrophobicity and hydrophilicity and kinetic diameter. Moreover, the regenerability of MOFs was investigated for the removal of range of organic contaminants of interest in this thesis. The observed results revealed that the MOF materials have potential use as promising adsorbents in treatment of contaminated water.

IMPACT STATEMENT

The pharmaceutical and pesticide removal from water is of paramount importance as they could be toxic and carcinogenic to the aquatic environment and human, respectively. In the water treatment, activated carbons are the widespread adsorbents used to remove organic pollutants. However, activated carbons may suffer from slow kinetic uptake or poor removal of many relatively hydrophilic or charged pollutants. MOFs are a young class of hybrid inorganic/organic porous crystalline materials, particularly zirconium-based MOFs due to their exceptional chemical and thermal stability have received a great deal of attention. In this thesis, to elucidate the adsorption ability of MOFs, the adsorptive removal of representative drug molecules, atrazine, carbamazepine and triclosan, for the first time, with using various water and chemical stable MOFs (UiO-66, UiO-67, ZIF-8, MIL-100(Fe) and HKUST-1) were studied. Due to the strong Zr(IV)−O bonds and high connectivity of the Zr node, Zr_6-based MOFs are intriguingly stable over a wide range of pH. Combined with UiO-67`s great affinity for emerging organic pollutants and an exceptional faster kinetic uptake, UiO-67 `s performance highlights its superiority over commercial activated carbon. Moreover, UiO-67, can be simply regenerated through multiple adsorption-desorption cycles expanding lifetime of the materials and proving its potential in large-scale purification applications. Thus, UiO-67 is a potent candidate and will assuredly extend the use of the MOF for water remediation.

ACKNOWLEDGEMENTS

First of all, I would like to sincerely thank to my supervisor Dr Ozgur Yazaydin for his guidance during my PhD journey at UCL. Thank you for reading and correcting my manuscripts and for all the interesting conversations. I also give my sincere thanks to my secondary supervisor Prof Asterios Gavrilidis.

I am also grateful to Turkish Ministry of Education for financially supporting my PhD studies.

My sincere thanks to Dr Simon Barrass who was easy to turn to when I had trouble using HPLC and thanks to him for his all technical help in the laboratory.

I would like to thank Toby Neville and Dina Ibrahim for their valuable help and time regarding SEM and BET measurements and also thanks to them for being a good friend to me.

My special thanks to my group friends, Benjamin , Aydin Ozcan and Naghmeh Saeidi Bidokthi each one of you has contributed in this thesis with their sincere advice and discussion. I would also like to thank to my 311 friends, Marti, Victor, Evita, Benjamin, Naghmeh, Teng and Din. I will miss you all guys and thank you for everything.

I would like to thanks to my friend Sevgi for being always such a good friend and showing me around in Canterbury.

I would like to thanks to my friend Dr Karl Smith for being a good friend and helping me enjoy my busy PhD life in London.

I am also very thankful to Professor Omar K. Farha to give the opportunity to work as a visiting scholar in Farha group and laboratory at Northwestern University and for the discussion and advice.

I would also like to thank my friend, Dr Timur Islamoglu, thank you for helping me patiently everything about experiments, for all advices and discussion on my PhD and being a good friend and behaving me like his little sister.

Finally, I am very grateful to members of my family, particularly my dear parents Birgul and Mahmut Akpinar for their big support, concern and care. Also, big thanks to my brother, Guven Murat Akpinar, he is always my best friend and listens to me all the time and gives me always advice since our childhood. My family were the source of my inspiration, strength and encouragement. It was impossible to do the PhD without their support and love.

PUBLICATIONS

List of publications associated with this thesis:

1. Akpinar, I.; Yazaydin, A. O., Adsorption of Atrazine from Water in Metal–Organic Framework Materials. Journal of Chemical & Engineering Data 2018, Article ASAP, DOI: 10.1021/acs.jced.7b00930

2. Isil Akpinar and A. Ozgur Yazaydin, Rapid and Efficient Removal of Carbamazepine from Water by UiO-67, Industrial & Engineering Chemistry Research Article, 2017, 56 (51), 15122-15130.

3. Isil Akpinar and A. Ozgur Yazaydin, Effective Uptake of a Personal Care Product, Triclosan by Metal-Organic Frameworks. (Manuscript in preparation)

4. Isil Akpinar and A. Ozgur Yazaydin, Simultaneous Removal of Mixture of Antiepileptic Drug and Endocrine Disrupting Compound by a Zr-based MOF (Manuscript in preparation)

CONTENTS

ABSTRACT **3**

IMPACT STATEMENT **4**

ACKNOWLEDGEMENTS **5**

CONTENTS **8**

Chapter 1: INTRODUCTION **25**

1.1: PHARMACEUTICALS IN WATER SUPPLIES 25

1.2: OVERVIEW of TREATMENT TECHNIQUES OR REMOVAL of PPCPs AND EDCs 28

1.2.1: Adsorption 31

1.2.1.1: Introduction to Adsorption Theory 31

1.2.1.2: Adsorption Isotherm Models in Liquid Phase 32

1.2.2: Adsorbent materials-Porous Materials 36

1.2.2.1: General background on porous materials 36

1.2.2.2: Activated Carbon 39

1.2.2.3: Zeolites 40

1.2.2.4: Graphene and Graphene Oxide 41

1.2.2.5: Carbon nanotubes 42

Chapter 2: LITERATURE REVIEW **43**

2.1: METAL-ORGANIC FRAMEWORKS (MOFs) 43

2.2: SYNTHESIS and ACTIVATION METAL-ORGANIC FRAMEWORKS ..46

2.2.1: General Background of MOF Synthesis 46

2.2.1.1: Hydrothermal Synthesis: 47

2.2.1.2: Solvothermal Synthesis Method: 48

2.2.1.3: Electrochemical Synthesis Method: 49

2.2.1.4: Microwave Assisted Synthesis: 50

2.2.1.5: Sonochemical Synthesis: 51
2.2.1.6: Mechanochemical Synthesis: 52
2.2.2: Activation and Characterisation of MOFs 52
2.3: APPLICATIONS OF METAL ORGANIC FRAMEWORKS 55
2.3.1: Metal-Organic Frameworks for Adsorptive Removal of PPCPs and EDCs from Liquid Phase 57
2.4: THESIS AIM AND OUTLINE 60
Chapter 3: MATERIALS AND METHODS 64
3.1: CHEMICALS 64
3.2: SYNTHESES PROCEDURES of MOFs 64
3.2.1: Synthesis of ZIF-8: 65
3.2.2: Synthesis of UiO-66: 65
3.2.3: Synthesis of UiO-67: 66
3.2.4: Synthesis of MIL-100(Fe): 67
3.3: CHARACTERISATION OF THE ADSORBENTS 68
3.3.1: Powder X-ray Diffraction 68
3.3.2: Nitrogen adsorption and desorption isotherms 68
3.3.3: Scanning Electron Microscopy 69
3.3.4: Zeta Potential 69
3.4: ADSORPTION BATCH EXPERIMENTS 70
3.4.1: Adsorption isotherms 71
3.4.2: Adsorption Kinetics 73
Chapter 4: ADSORPTIVE REMOVAL OF ATRAZINE FROM WATER BY METAL-ORGANIC FRAMEWORKS 75
4.1: INTRODUCTION 75
4.2: MATERIALS AND METHODS 78
4.2.1: Chemicals 78

4.2.2: Syntheses procedures of ZIF-8, UiO-66, UiO-67 78
4.2.3: Characterisation of the adsorbents 78
4.2.4: Adsorption Experiments.....79
4.3: RESULTS AND DISCUSSION 82
4.3.1: Characterisation of the synthesised MOFs.....82
4.3.2: Screening of MOFs and F400 for the removal of atrazine.....87
4.3.3: Effect of Adsorbent Amount on the Removal of Atrazine.....88
4.3.4: Kinetics of Atrazine Adsorption 89
4.3.5: Adsorption Isotherms of Atrazine 92
4.3.6: Effect of pH on Adsorption of Atrazine.....95
4.3.7: Regeneration and Stability of UiO-67.....96
4.4: CONCLUSIONS.....98
Chapter 5: RAPID AND EFFICIENT REMOVAL OF CARBAMAZEPINE FROM WATER BY UIO-67 99
5.1: INTRODUCTION.....99
5.2: EXPERIMENTAL METHODS.....101
5.2.1: Materials.....101
5.2.2: Synthesis and Characterisation of adsorbents 102
5.2.3: Liquid phase adsorption experiments:.....103
5.2.4: Initial comparison of adsorbents for carbamazepine adsorption:.....103
5.2.5: Effect of adsorbent concentration on carbamazepine adsorption.....104
5.2.6: Kinetics of carbamazepine adsorption: 104
5.2.7: Adsorption isotherms of carbamazepine:.....104
5.2.8: Effect of pH on carbamazepine adsorption:.....105
5.2.9: Regeneration of UiO-67.....105
5.3: RESULTS AND DISCUSSION 106
5.3.1: Characterisation of adsorbents: 106

5.3.2: Initial comparison of carbamazepine removal in UiO-67, UiO-66 and F400:.....109

5.3.3: The effect of adsorbent concentration:.....110

5.3.4: Adsorption Kinetics: 115

5.3.5: Effect of pH:.....116

5.3.6: Adsorption Mechanism: 117

5.3.7: Stability and Regeneration of UiO-67:.....118

5.4: CONCLUSIONS.....120

Chapter 6: SIMULTANEOUS REMOVAL OF MIXTURE OF ANTIEPILEPTIC DRUG AND ENDOCRINE DISRUPTING COMPOUND BY A ZIRCONIUM BASED MOF-UIO-67 121

6.1: INTRODUCTION.....121

6.2: EXPERIMENTAL METHODS.....122

6.2.1: Synthesis and characterisation of UiO-67:.....122

6.2.2: Liquid phase adsorption experiments:.....123

6.2.3: Regeneration of UiO-67:.....124

6.3: RESULTS AND DISCUSSION 125

6.3.1: Characterisation of UiO-67: 125

6.3.2: Calibration Curves of atrazine and carbamazepine:.....126

6.3.3: The simultaneous adsorption of carbamazepine and atrazine in UiO-67 127

6.3.4: Kinetic Studies of UiO-67 for carbamazepine and atrazine mixture:128

6.3.5: The effect of salt on the adsorption of carbamazepine and atrazine mixture.....130

6.3.6: Regeneration of UiO-67 for the mixture of carbamazepine and atrazine 131

6.4: CONCLUSION 132

Chapter 7: EFFECTIVE UPTAKE OF A PERSONAL CARE PRODUCT BY METAL-ORGANIC FRAMEWORKS 134

7.1: INTRODUCTION 134

7.1.1: Preparation and characterisation of adsorbents: 137

7.2: MATERIALS AND METHODS 138

7.2.1: Triclosan batch adsorption experiments: 138

7.2.2: Stability of the regenerated MOFs under batch adsorption experiments conditions: 140

7.3: RESULTS AND DISCUSSION 140

7.3.1: Characterisation of adsorbents: 140

7.3.2: Adsorptive removal of hydrophobic triclosan using MOFs and activated carbon (F400): 142

7.3.3: Adsorption Kinetics of UiO-66 and UiO-67: 143

7.3.4: Zeta Potential measurements and pH effect on triclosan adsorption: 146

7.3.5: Adsorption isotherms for triclosan 149

7.3.6: Adsorption mechanism 150

7.3.7: Regeneration and Stability 151

7.4: CONCLUSION 153

Chapter 8: CONCLUDING REMARKS and FUTURE RECOMMENDATIONS 154

8.1: GENERAL CONCLUSION-COST ANALYSIS 156

Chapter 9: APPENDICES 160

9.1: APPENDIX I: Calibration Curves in Chapter 4 160

9.1.1: Atrazine Calibration Curve in Water 160

9.1.2: Atrazine calibration curves in water for pH effect Study 160

9.2: APPENDIX II: Calibration Curves in Chapter 5 162

9.2.1: Carbamazepine calibration curve in water 162

9.2.2: Carbamazepine calibration curves in water for pH effect Study 163
9.3: APPENDIX II: Calibration Curves in Chapter 7 165
9.3.1: Triclosan Calibration Curve in Water 165
9.3.2: Triclosan calibration curves in water for pH effect Study 166
RERERENCES 168

LIST OF FIGURES

Figure 1-1 Schematic flow chart shows the sources and pathways of PPCPs. Reprinted from (Yang et al., 2017) Copyright (2017), with permission from Elsevier. 27

Figure 1-2 Schematic representation of adsorption 32

Figure 1-3 Schematic view of monolayer adsorption 34

Figure 1-4 Schematic representation of multilayer adsorption 35

Figure 1-5 Six types of adsorption isotherms based on IUPAC classification (Sing, 1985) 36

Figure 1-6 Schematic representation of general classification of polymers (organic porous materials) and zeolites (inorganic porous materials) and MOFs (hybrid organic-inorganic porous materials) on the top and the formation procedure of a MOF at the bottom. Reprinted (adapted) with permission from Li et al. (Li et al., 2012) Copyright (2012) American Chemical Society. 39

Figure 1-7. Activated Carbon 40

Figure 1-8 Zeolite rho-solid cages (left) and zeolite ZK5 (right) 40

Figure 1-9 Graphene sheet 41

Figure 1-10 Carbon nanotube 42

Figure 2-1 The structure of MOF-5. a) the MOF-5 structure: ZnO4 tetrahedra (blue) and benzenetricarboxylate linkers (red: oxygen and black: carbon) and pore aperture of 0.8 nm and pore diameter of 1.2 nm (yellow sphere). b) represents the topology of the MOF-5 structure (primitive cubic net) and it is shown as a ball and-stick model. Reprinted from (Omar M. Yaghi, 2003) with permission. 44

Figure 2-2 Illustration of structuring of a MOF. Reproduced from Ref. (Furukawa et al., 2014) with permission from The Royal Society of Chemistry. 44

Figure 2-3 Cambridge Structure Database and MOF structures entries reported in the CSD from 1972 to 2016. The inset display the MOF self-assembly process from

building blocks: metals (red spheres) and organic ligands (blue struts). Reprinted (adapted) with permission from (Moghadam et al., 2017). Copyright (2017) American Chemical Society. 46

Figure 2-4 Schematic diagram of Teflon®-lined stainless steel autoclave Reproduced from (Walton, 2002) with permission from The Royal Society of Chemistry and source: web for the picture on the right. 48

Figure 2-5 Schematic view of solvothermal synthesis approach of MOFs materials Reprinted from (Lee et al., 2013) with permission. 49

Figure 2-6 a) Schematic representation of electro synthesis anodic dissolution cell, b) the formation of HKUST-1 on the anode electrode. c) HKUST-1 structure. Reproduced from Ref. (Rubio-Martinez et al., 2017) with permission from The Royal Society of Chemistry and the structure of HKUST-1.....50

Figure 2-7 Schematic view of traditional ultrasonic rig (Bang and Suslick, 2010) Copyright © 2010 WILEY-VCH Verlag GmbH & Co. KGaA, Weinheim. 51

Figure 2-8 Plausible adsorption mechanisms proposed for the adsorptive removal of organic compounds on MOFs. Adapted with permission from (Hasan and Jhung, 2015), copyright Elsevier, 2015. 60

Figure 3-1 Schematic view of a defect site in single crystal of UiO-66. The missing carboxylates linker is replaced by H_2O to counterbalance the l charge by hydroxide anion. (O: red, C: black, Zr: blue) (Trickett et al., 2015). Copyright © 2015 WILEY-VCH Verlag GmbH & Co. KGaA, Weinheim.....66

Figure 3-2 Schematic representations of defect free UiO-67 and an idealized representation of missing linker defects in UiO-67 leading to terminal Zr–OH groups on select Zr_6 nodes. Zr: light purple; O: red; C: grey. Reproduced from Ref. (Howarth et al., 2015) with permission from The Royal Society of Chemistry. ..67

Figure 3-3 Schematic illustration of the batch adsorption experimental procedure 71

Figure 4-1 Chemical structure of atrazine (top) and the structural models of ZIF-8, UiO-66 and UiO-67 (bottom, from left to right). Colour code: carbon (black), oxygen (red), nitrogen (blue), zinc (orange) and zirconium (cyan). 77

Figure 4-2 PXRD patterns of UiO-67 a), UiO-66 b) and c) ZIF-8 and d) HKUST-1 82

Figure 4-3 N_2 adsorption-desorption isotherm of a) UiO-67, b) UiO-66, c) ZIF-8, d) F400 and e) HKUST-1.....84

Figure 4-4 Pore size distributions of a) ZIF-8, b) F400, c) UiO-67 and d) UiO-66 and e) HKUST-1 85

Figure 4-5 SEM images of (a) ZIF-8, (b) UiO-66, (c) UiO-67 and d) HKUST-1 86

Figure 4-6 Removal efficiency of atrazine with different MOFs and F400 (15 mg each of adsorbents and initial concentration of 25 mg L^{-1} in 25 mL of solution. The experiments were repeated in duplicates and the mean of the values are given here. 88

Figure 4-7 The effect of adsorbent amount on the removal efficiency of atrazine from water. Different adsorbent amount of MOFs and F400 were exposed to 25 mL of 25 mg L^{-1} of atrazine concentration. The experiments were repeated in duplicates and the mean of the values are given here.....89

Figure 4-8 Removal efficiency as a function of time (150 mg of adsorbents was placed in contact with 25 mL solution of an initial atrazine concentration of 25 mg L^{-1}) (Error bars are too small.).....91

Figure 4-9 Pseudo-second order kinetic model fit in a) UiO-67, b) ZIF-8 and pseudo first order kinetic model fit in c) F400 91

Figure 4-10 Adsorption isotherm of atrazine in UiO-67, ZIF-8 and F400 and the Freundlich model, Langmuir-Freundlich and Langmuir adsorption model fit for UiO-67, ZIF-8 and F400, respectively. 93

Figure 4-11 Reusability of UiO-67 for atrazine removal after acetone washing (Ci= 25 mg L^{-1} and 15 mg adsorbent) 97

Figure 4-12 (a) N_2 adsorption-desorption isotherms of prepared UiO-67 and regenerated UiO-67 in acetone followed by thermally activated and (b) PXRD patterns of starting UiO-67 before adsorption of atrazine, regenerated after atrazine adsorption and the simulated PXRD pattern of UiO-67 is also included for comparison. 97

Figure 4-13 SEM images of (a) pristine UiO-67 before atrazine adsorption and (b) regenerated UiO-67 after atrazine adsorption 98

Figure 5-1 PXRD patterns of UiO-67 (a) and UiO-66 (b) 107

Figure 5-2 a) N_2 adsorption-desorption isotherms at 77 K for UiO-67, UiO-66 and F400 (filled and empty symbols are represented for adsorption and desorption, respectively) and pore size distribution and pore volumes of b) UiO-67, c) UiO-66, d) F400 107

Figure 5-3 SEM images and particle size distributions of (a) UiO-66, (b) UiO-67 and (c) F400.....109

Figure 5-4. Removal efficiency of carbamazepine from water at initial carbamazepine concentrations of (a) 10 mg L^{-1} and b) 100 mg L^{-1}. Experiments were performed in triplicate, and the mean values are reported. Error bars correspond to standard deviation. (Adsorbent concentration 1.2 mg mL^{-1}).....110

Figure 5-5. Effect of adsorbent concentration on carbamazepine removal. The initial carbamazepine concentration is 100 mg L^{-1}. Experiments were performed in triplicate and the mean values are reported. Errors are smaller than the symbols. The solid lines are given as guides to the eye. Adsorption isotherms:.....111

Figure 5-6. Adsorption isotherm of carbamazepine in (a) UiO-67 and b) F400. Solid lines show the Langmuir and Freundlich model fits. Experiments were performed in triplicate, and the mean values are reported. Errors are smaller than the symbols. 113

Figure 5-7 Freundlich adsorption isotherm model fittings of carbamazepine in (a) UiO-67 and (b) F400, and Langmuir adsorption isotherm model fittings of carbamazepine in (c) UiO-67 and (d) F400.....114

Figure 5-8. (a) Adsorption of carbamazepine in UiO-67 and F400 as a function of time and (b) The corresponding pseudo second order kinetic plots. Adsorbent concentration is 1.2 mg mL^{-1}. Experiments were performed in triplicate, and the mean values are reported. Errors are smaller than the symbols. Solid lines are given as guides to the eye. 116

Figure 5-9. Effect of pH on adsorptive removal of carbamazepine. Experiments were performed in triplicate, and the mean values are reported. Errors are smaller than the symbols. The solid lines are guides to the eye. 117

Figure 5-10. The adsorbed amount of carbamazepine by UiO-67 after consecutive regeneration cycles. (12 mg UiO-67 was in contact with 5 mL solution of 100 mg L^{-1} initial concentration) 119

Figure 5-11 N_2 adsorption-desorption isotherms and pore size distributions of pristine UiO-67 and regenerated UiO-67 after carbamazepine adsorption (from left to right) 119

Figure 6-1 a) N_2 adsorption-desorption isotherms of UiO-67 (filled and empty symbols represent adsorption and desorption, respectively) and b) the pore volume and pore size distribution of UiO-67 and c) PXRD patterns of synthesized and simulated UiO-67 125

Figure 6-2 Calibration Curves of carbamazepine (a) and atrazine (b) in water .. 126

Figure 6-3 A representative chromatogram of binary mixture of carbamazepine and atrazine with initial concentrations of 20 mg L^{-1} and 5 mg L^{-1}, respectively..... 126

Figure 6-4 Removal Efficiency of carbamazepine and atrazine as pure components and as binary mixtures by UiO-67 (20 ppm carbamazepine and 5 ppm atrazine in binary mixture was contacted with 15 mg UiO-67 at 25 ˚C for 24 h.) 127

Figure 6-5 Removal Efficiency of UiO-67 for mixture of carbamazepine and atrazine with initial concentrations of 20 mg L^{-1} and 5 mg L^{-1} in a mixture, respectively and individually 20 mg L^{-1} of carbamazepine and 5 mg L^{-1} atrazine. Error bars represent standard deviation. 129

Figure 6-6 Adsorption capacity of UiO-67 for carbamazepine and atrazine mixture as a function of time (a) and pseudo second order fit for triclosan in UiO-67 (15 mg UiO-67 added into in 25 mL of solution with an initial concentration of 20 mg L^{-1} of carbamazepine and 5 mg L^{-1} of atrazine as binary mixture).....129

Figure 6-7 Pseudo Second Order Kinetic Fitting of mixture of carbamazepine (20 mg L^{-1}) and atrazine (5 mg L^{-1}). 130

Figure 6-8 The effect of salt on the adsorption of carbamazepine and atrazine as pure components and mixture. 131

Figure 6-9 Regeneration of UiO-67 for adsorption of carbamazepine atrazine in binary mixture (30 mg of UiO-67 with an initial concentration of 20 mg L^{-1} of carbamazepine and 5 mg L^{-1} atrazine as a binary mixture).....132

Figure 7-1 Chemical structure of triclosan and shows the kinetic diameters of triclosan in width, length and depth. 136

Figure 7-2 Structural analysis for the synthesized MOFs. 141

Figure 7-3 Zeta Potential of a) UiO-67and b) UiO-66.....142

Figure 7-4 Removal Efficiency of triclosan on different adsorbents by adding various amounts of adsorbents. (Column bar represent for 5 mg and green line represents 1 mg of each of adsorbents). 143

Figure 7-5 The adsorbed amount of mg of triclosan per g of UiO-66 and UiO-67 (a), pseudo second order plot for triclosan on UiO-66 and UiO-67 and removal efficiency (in %) of triclosan by UiO-66 and UiO-67 at two different concentrations as a function of time. (The data are reported as the mean of duplicate experiments). 145

Figure 7-6 Effect of solution pH on triclosan adsorption on UiO-67 (a) and UiO-66(b) (initial concentration of triclosan was 9 mg L^{-1} contacting with 5 mg of each adsorbents for 24 h at 25 ˚C) and the zeta potential of UiO-67 (navy line, a) and UiO-66 (green line, b). 148

Figure 7-7 Langmuir-Freundlich fitting of triclosan on UiO-67 (a) and UiO-66 (b) 150

Figure 7-8 a) Adsorption Cycles of UiO-67 in the adsorption and b)XRD patterns of pristine UiO-67 and regenerated UiO-67. 152

Figure 7-9 a) N_2 adsorption-desorption isotherms and b) pore size distributions of pristine UiO-67 and regenerated UiO-67 after triclosan adsorption (filled circle and empty circle represent adsorption and desorption, respectively). 152

Figure 8-1 Flow chart of the total process cost 158

Figure 9-1 Atrazine Calibration Curve obtained by HPLC at pH 6.9 160

Figure 9-2 Atrazine Calibration Curve obtained by HPLC at pH 2.8 160

Figure 9-3 Atrazine Calibration Curve obtained by HPLC at pH 4.5 161

Figure 9-4 Atrazine Calibration Curve obtained by HPLC at pH 8.9 161

Figure 9-5 Atrazine Calibration Curve obtained by HPLC at pH 9.8 162

Figure 9-6 Carbamazepine Calibration Curve obtained by UV-vis at pH 5 162

Figure 9-7 Carbamazepine Calibration Curve obtained by UV-vis at pH 3 163

Figure 9-8 Carbamazepine Calibration Curve obtained by UV-vis at pH 5 163

Figure 9-9 Carbamazepine Calibration Curve obtained by UV-vis at pH 6 164

Figure 9-10 Carbamazepine Calibration Curve obtained by UV-vis at pH 7 164

Figure 9-11 Carbamazepine Calibration Curve obtained by UV-vis at pH 9 165

Figure 9-12 Triclosan Calibration Curve at pH 7 165

Figure 9-13 Triclosan Calibration Curve obtained by HPLC-UV at pH 3 166

Figure 9-14 Triclosan Calibration Curve obtained by HPLC-UV at pH 5 166

Figure 9-15 Triclosan Calibration Curve obtained by HPLC-UV at pH 7 167

Figure 9-16 Triclosan Calibration Curve obtained by HPLC-UV at pH 9 167

LIST OF TABLES

Table 1-1 Conventional and advanced chemical, physical and biological treatment methods for the removal of PPCPs and EDCs 29

Table 2-1 MOF materials, their surface areas and maximum adsorption capacity for pharmaceuticals adsorption in MOFs in the literature 57

Table 4-1 Physicochemical properties and molecular dimensions of atrazine 78

Table 4-2 Surface and pore size characteristics of ZIF-8, UiO-66 and activated carbon (F400). 85

Table 4-3 Kinetic parameters for pseudo-first and pseudo-second order model. .92

Table 4-4 Langmuir-Freundlich, Langmuir and Freundlich adsorption isotherms fitting parameters of atrazine on UiO-67, ZIF-8 and F400. 94

Table 4-5 The effect of pH on atrazine adsorption by the studied MOFs and F400. 95

Table 5-1 Chemical structure and physicochemical properties of carbamazepine 101

Table 5-2 Surface area and pore volume properties of UiO-66, UiO-67 and F400. 108

Table 5-3. Comparison of Freundlich rate constant values (K_F) for adsorption of carbamazepine by various adsorbents reported in the literature. 112

Table 5-4 Langmuir and Freundlich Adsorption Models Fitting Parameters. 114

Table 5-5. Pseudo first order and pseudo second order kinetic models fitting parameters. 116

Table 6-1 Pseudo Second Order Kinetic Model Parameter Fittings of UiO-67 towards mixture of carbamazepine and atrazine. 130

Table 7-1 Physicochemical properties of triclosan. 137

Table 7-2 Textural Properties of the studied MOFs in this study 141

Table 7-3 Pseudo Second Order Fitting for triclosan on UiO-67 and UiO-66....145

Table 7-4 Langmuir-Freundlich isotherm model fitting parameters.....150

LIST OF ABBREVIATIONS

AC	Activated Carbon
ATZ	Atrazine
BET	Brunauer, Emmett and Teller
BTC	Benzene tricarboxylic acid
BDC	Benzene dicarboxylate
BPDC	4,4 Biphenyl carboxylic acid
CBZ	Carbamazepine
Cu	Copper
DMF	N, N-dimethylformamide
DEF	N, N-diethyl formamide
EDCs	Endocrine Disrupting Compounds
F400	Filtrasorb® 400
GAC	Granular Activated Carbon
GC	Gas Chromatography
HPLC	High Performance Liquid Chromatography
HKUST	Hong Kong University of Science and Technology
IPA	Isopropanol/isopropyl alcohol
MIL	Matérial Institut Lavoisier

MOFs	Metal-Organic Frameworks
PAC	Powdered Activated Carbon
PPCPs	Pharmaceuticals and Personal Care Products
PCP	Porous Coordination Polymers
pK_a	Acid dissociation constant
K_{ow}	Octanol-water partition coefficient
SEM	Scanning Electronic Microscopy
TRC	Triclosan
UiO	University of Oslo
USEPA	United States Environmental Protection Agency
UV-Vis	Ultraviolet-Visible
WHO	World Health Organization
XRD	X-ray Diffraction
ZIF	Zeolitic Imidazole Framework
Zr	Zirconium

Chapter 1: INTRODUCTION

1.1: PHARMACEUTICALS IN WATER SUPPLIES

The amount of environmental water pollution is increasing globally and has become one of the most widespread problems due to the rapid industrialization, urbanization and the growth in population throughout the world (Shannon et al., 2008, Han et al., 2015). The severity of this issue is magnified by the growing demand for clean water supplies. Access to safe and clean water has always been a challenge, but its accomplishment is becoming even more difficult.

At least 2 billion people used contaminated water , in other words used without a safely managed drinking-water service estimated by World Health Organization (Organization-WHO, 2017). The total concentration for all pesticides has been limited to 0.50 µg/L in water for human use by the EU Directive 98/83/EC (Lima et al., 2009). EU law does not have a particular regulatory limit on levels of pharmaceuticals water (Union, 1998). EU Directive 2008/105/EC has been amended by Directive 2013/39/EU enforce the European Commission to establish a strategic approach to contaminated water with pharmaceuticals (European Parliament, 2013).

Contamination of surface and ground waters by the increasing occurrence of organic pollutants such as pharmaceuticals (Daughton and Ternes, 1999), polyaromatic hydrocarbons (Tobiszewski and Namiesnik, 2012), dyes (Tichonovas et al., 2013), pesticides (Carvalho, 2017) and toxic residuals arises from the release of effluents from industrial, agricultural and domestic activities into water sources.

This has become a major concern since these chemicals pose potential hazards both to the aquatic environment and to human health (Schwarzenbach et al., 2006, Richardson and Ternes, 2014, Grundgeiger et al., 2015, Petrie et al., 2015, Alsbaiee et al., 2016). Among these organic micropollutants, pharmaceuticals, personal care products and endocrine disrupting compounds have great potential to elicit adverse effects because of their persistence in aquatic environments (Mompelat et al., 2009, Calisto et al., 2015). Furthermore, it is reported that more than 20 million tons of Pharmaceuticals and Personal Care Products (PPCPs) are annually produced (Wang and Wang, 2016, Xu et al., 2017). The production of PPCPs shows a continuous gradual increase because of their use for treating and preventing diseases in humans or animals is still in great demand (Wang and Wang, 2016, Xu et al., 2017).

PPCPs and Endocrine Disrupting Compounds (EDCs) (an emerging class of environmental contaminants) continuously enter our water supply by means of various direct or indirect routes; including human and animal excretion, hospital waste, therapeutic drugs, discharge of wastewater effluents from pharmaceuticals plants and veterinary drugs disposal (Rivera-Utrilla et al., 2013, Petrie et al., 2015). **Figure 1-1** depicts the sources and transport pathways of pharmaceuticals entering drinking water. The occurrence of these emerging micropollutants leads to environmental water pollution, which represents a threat to living organisms and human beings, even though their concentrations in the aquatic environment are within a very low concentration range (ppm or even ppb level) (Petrovic´ et al., 2003, Joss et al., 2006, Wang and Wang, 2016). The low concentrations at which these emerging micropollutants exist makes their detection in environmental

samples a further challenge. With advances, however, in analytical technology, scientists are now able to detect these PPCPs at trace level (Wang and Wang, 2016). Their qualitative and quantitative analyses have been successfully achieved by advanced analytical techniques such as Gas Chromatography (GC) and Liquid Chromatography (LC). These analytical techniques are the most commonly used for the determinations of these trace levels of pharmaceuticals in the environment.

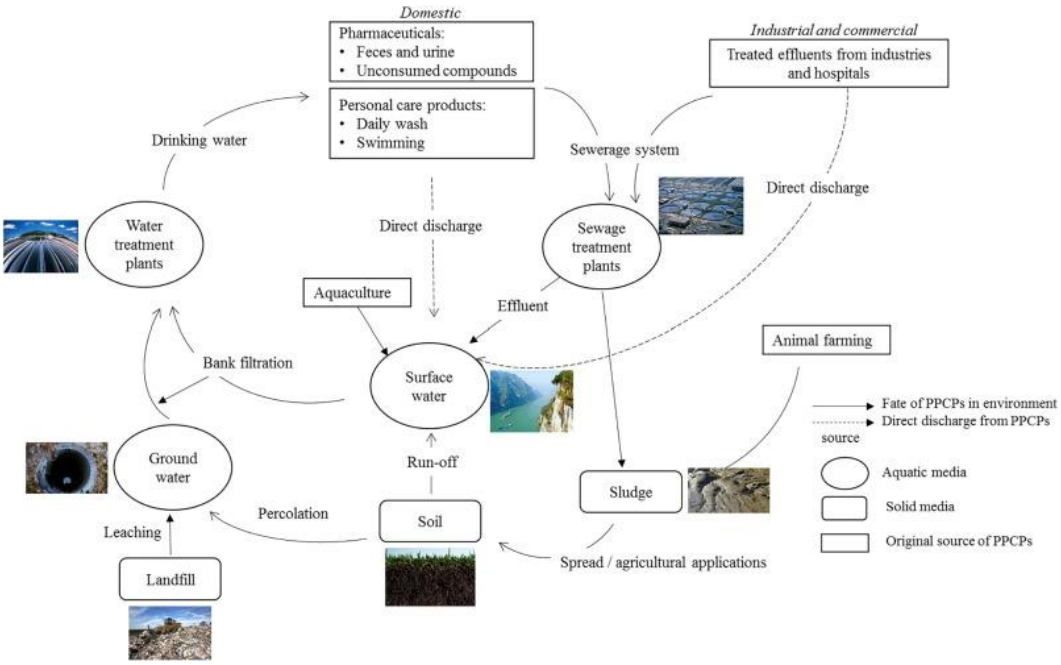

Figure 1-1 Schematic flow chart shows the sources and pathways of PPCPs. Reprinted from (Yang et al., 2017) Copyright (2017), with permission from Elsevier.

Anti-inflammatories and analgesics (acetaminophen, ibuprofen, aspirin and diclofenac), anti-depressants, anti-epileptics (carbamazepine), lipid lowering drugs, β-blockers, antihistamines and antibiotics are ubiquitous in surface, ground and drinking waters (Corcoran et al., 2010, Rivera-Utrilla et al., 2013). These pharmaceuticals are infused continually in the form of unmetabolized or active

metabolites through human/animal excretion or urination. They are also persistent in the aquatic environment and not readily biodegradable (Jones et al., 2001, Khetan and Collins, 2007, Mompelat et al., 2009, Calisto et al., 2015).

The Organization of Economic and Cooperative Development (OECD) describes an EDC as an exogenous substance/agent that disrupts the function of endocrine systems and afflicting humans and wildlife (Esplugas et al., 2007). Pesticides (e.g. DDT, vinclozolin, TBT, atrazine), persistent organochlorines and organ halogens (e.g. dioxin, furans, brominated fire retardants, alkyl phenols, phytoestrogens, and synthetic and natural hormones) are chemical compounds that have a potentially adverse impact on the endocrine systems of wildlife and humans and these various chemical compounds interact with the endocrine system, which give rise to the generation or interruption of hormones (Campbell et al., 2006, Esplugas et al., 2007). Prompted by this, the removal of PPCPs and EDCs from water has therefore become a necessity and is crucial before discharging/releasing wastewater into the environment.

1.2: OVERVIEW of TREATMENT TECHNIQUES OR REMOVAL of PPCPs AND EDCs

During the last decade, several conventional chemical, physical and biological treatment methods (Adams et al., 2002), including coagulation-flocculation (Westerhoff et al., 2005), chlorination (Adams et al., 2002, Joss et al., 2006, Simazaki et al., 2008), biodegradation, activated sludge (Joss et al., 2006) and filtration (Clara et al., 2005) have been explored and used for the removal of PPCPs and EDCs from drinking water or wastewater **(Table 1-1)**. Most of the

pharmaceuticals have not been eliminated effectively or only a low removal level was achieved for these conventional treatment methods (Stackelberg et al., 2007, Vieno et al., 2007, Rahman et al., 2009, Rossner et al., 2009, Calisto et al., 2015). Although advanced chemical and physicochemical treatment methods, such as ozonation and Advanced Oxidation Processes (AOPs) have been found to be effective methods in the removal of pharmaceuticals (Esplugas et al., 2007, Klavarioti et al., 2009), there are some detrimental effects associated with these techniques . For example, the formation of by-products from ozonation which could be of toxicological concern and vulnerable to biodegradation (Hoigné, 1998). Likewise, AOPs will generate some more toxic by-products and require relatively high energy to operate, so incurring an increase in the costs. Alternatively, an inexpensive treatment option to remove and degrade can be activated sludge biological treatment; however, activated sludge does not remove the micropollutants and some of these pharmaceuticals may be adsorbed in the sludge.

Table 1-1 Conventional and advanced chemical, physical and biological treatment methods for the removal of PPCPs and EDCs

Methods	References
Coagulation-flocculation	Westerhoff et al., 2005
Chlorination	(Adams et al., 2002, Joss et al., 2006, Simazaki et al., 2008)
Biodegradation, activated sludge	Joss et al., 2006
Filtration	Clara et al., 2005
Ozonation and advanced oxidation	Esplugas et al., 2007

Highlighting the disadvantages of these advanced treatment methods makes it clear that simple, efficient, inexpensive method for purifying water is needed.

Adsorption-based methods are considered to be one of the most promising, alternative methods for the removal of pharmaceuticals from aqueous solutions (Yu et al., 2008, Bui and Choi, 2009, Yu et al., 2009, Nam et al., 2014, Calisto et al., 2015). These techniques involve the use of a porous adsorbent material. Common adsorbents that have been used, include but are not limited to activated carbons, polymers, silica and zeolites (Streat and Horner, 2000, Moreno-Castilla, 2004, Deng, 2006, Snyder et al., 2007, Bui and Choi, 2009, Cabrera-Lafaurie et al., 2014). Activated carbon is the most commonly studied adsorbent for the adsorption of a variety of pharmaceutical compounds because it is inexpensive (Mestre et al., 2012, Mestre et al., 2014, Galhetas et al., 2015, Mestre et al., 2016), particularly for hydrophobic pharmaceuticals. However, it is found to be ineffective in removing either electrically charged (e.g., ibuprofen, gemfibrozil) (Westerhoff et al., 2005) or hydrophilic pharmaceuticals (e.g., clofibric acid, atenolol, sotalol, and ciprofloxacin) (Vieno et al., 2007, Bui and Choi, 2009, Domínguez et al., 2011). Besides, their moderate surface areas limit the number of available adsorption active sites and their relative lack of tunability impedes their use for contaminant-specific applications.

Recent extensive research into the design and synthesis of metal-organic frameworks (MOFs) has resulted in their development for use in various practical applications. MOFs have held great promise over conventional activated carbons and zeolites as adsorbents in water purification applications. MOFs are structurally porous materials that consist of metal nodes bridged by multidentate organic ligands (such as carboxylates, tetrazolates, sulfonates). Their chemical and physical properties are tunable by rational design and they provide a class of crystalline

materials with high surface areas, porosity and stability. One of the greatest advantages of MOFs over other well-understood nanoporous materials (e.g., activated carbon, zeolites and molecular sieves) is that MOFs possess relatively larger specific surface areas (e.g., MOF-5 has a surface area of 3631 m^2 g^{-1}). The larger surface area is one of the commonly measured features in the evaluation of sorption performance of adsorbents. Therefore, adsorbents with higher surface areas have an enhanced availability of vacant active sites for the adsorbates, yielding a higher adsorption capacity (Jiang and Ashekuzzaman, 2012).

1.2.1: Adsorption

1.2.1.1: Introduction to Adsorption Theory

Adsorption occurs whenever a solid surface is exposed to a gas or liquid, resulting in the accumulation of a substance at an interface between two phases, such as a liquid and a solid or a gas and a solid. The adsorption of organic compounds from aqueous solutions could occur in different ways, including physisorption in which van der Waals forces (nonspecific) are involved or chemisorption in which stronger specific forces are involved and the molecules are held to the solid surface by chemical bonding (Rouquerol et al., 2013). Physisorption does not induce a strong change in the properties of the adsorbed molecules. The energies of adsorption for physisorption and chemisorption are lower than 50 kJ mol^{-1} and higher than 50 kJ mol^{-1}, respectively.

Figure-1-2 depicts the principal terms relating to the adsorption process. The species to be adsorbed or adsorbable, prior to its adsorption on the solid surface, is named the adsorptive. Once the adsorptive has been adsorbed onto the solid surface,

it is then termed the adsorbate. The adsorbent is the solid substance in which adsorption takes place on its surface.

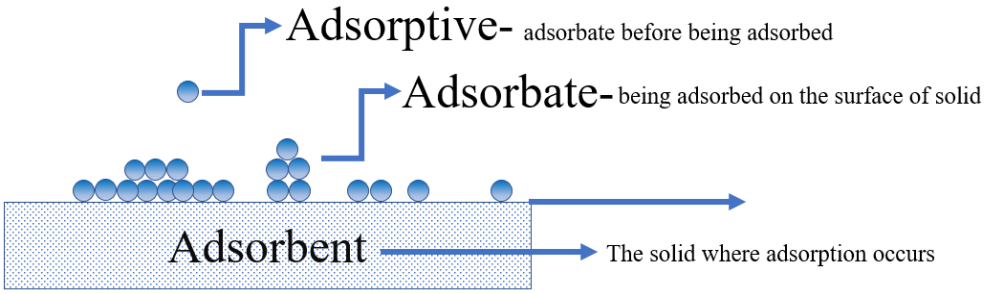

Figure 1-2 Schematic representation of adsorption

The surface area of the adsorbents is a key parameter in the adsorption process because adsorption is considered a surface phenomenon. Thus, a promising adsorbent should have a large surface area on a per unit mass or volume basis (m^2 g^{-1} or cm^3 g^{-1}), which makes pores accessible to adsorbates. The adsorbent capacity is generally proportional to the surface area since adsorption occurs on surfaces, Therefore, microporous materials with a large internal surface area are regarded as promising adsorbents (Brenner, 2013). The pore network of the solid materials as well as high surface area or micropore volume play a significant role in the transport of the adsorbate to the interior. Thus, a combination of these main properties should be provided by the solid materials in order to offer a high adsorptive capacity (Do, 1998). The surface functional groups are also other important properties that can trigger an increase or a decrease in the adsorption capacity of the adsorbents.

1.2.1.2: Adsorption Isotherm Models in Liquid Phase

Adsorption isotherms are visual representations of the amount of adsorbate adsorbed at the equilibrium concentrations, constant temperature and a range of

partial pressures. In order to assess the adsorption capacity of the adsorbent materials for the compounds of interest, adsorption isotherm models and equations are developed. These adsorption isotherm equations are dependent of the specific theoretical model exploited. There are a variety of adsorption isotherm models such as Freundlich (Freundlich, 1906), Langmuir (Langmuir, 1916), Brunauer–Emmett–Teller (Brunauer et al., 1938), Redlich–Peterson (Redlich and Peterson, 1959), Dubinin–Radushkevich (Dubinin, 1975), Temkin, Toth, Koble–Corrigan, Sips (Langmuir-Freundlich), Khan, Hill, Flory–Huggins and Radke–Prausnitz (Foo and Hameed, 2010). Freundlich (1906) and Langmuir (1918) are typical representatives of the group of two-parameter isotherms, which are the most commonly used to describe the adsorption process (Worch, 2012). In this thesis, Langmuir, Freundlich and Langmuir-Freundlich isotherm models were used because these models have been the most applied for modelling/calculating the adsorptive removal of organic pollutants from water by MOFs in the literature: they are explained in detail in section **1.2.2.2.1** and **1.2.2.2.2.**

1.2.1.2.1: Langmuir Isotherm Model

The Langmuir model is the simplest and the most widely used model, which can be applied to both physisorption and chemisorption in the liquid phase. The adsorbed amount of adsorbate on an adsorbent as a function of concentration at a given temperature is quantified by the Langmuir adsorption model. The Langmuir theory relies on four assumptions:

- The adsorbent surface is homogenous in which all adsorption sites are energetically constant.

- Each adsorbate is adsorbed on only one active site of adsorbent.
- No interaction occurs between the adsorbed molecules
- There are a certain number of active sites on the adsorbent surface which are proportional to the surface area of an adsorbent.

Based on the assumptions, in the Langmuir model, the only interaction is taken place between the adsorbed molecule and the adsorbent material. This results in single molecular layer (monolayer) adsorption **(Figure 1-3)** on the adsorbent surface and the formation of a plateau or a constant adsorbent capacity. In monolayer adsorption, all the adsorbed molecules are assumed to be in contact with the adsorbent surface.

Figure 1-3 Schematic view of monolayer adsorption

1.2.1.2.2: Freundlich Isotherm Model

The Freundlich isotherm is an empirical model which is used to represent the adsorption process that corresponds to a heterogeneous surface, multi-layer manner of adsorption **(Figure 1-4)** with non-uniform energy distribution of adsorption heat and affinities. In multilayer adsorption the adsorption surface possesses more than one layer, thus, not all the adsorbed molecules are in contact with the adsorbent surface layer. The adsorption heat and affinities are assumed to derive from the various functional groups of the surface and several adsorbate and adsorbent interactions. For adsorption in the liquid phase, the Freundlich equation takes the

form of an exponential equation, which assumes that the amount of adsorbate on the adsorbent surface continuously increases when the concentration of the solution increases. Hence, an infinite amount of adsorption can take place (Freundlich, 1906).

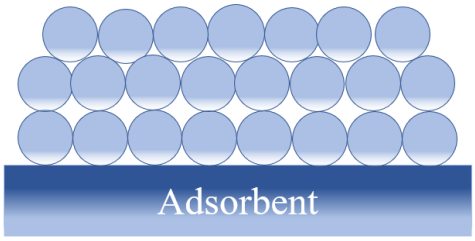

Figure 1-4 Schematic representation of multilayer adsorption

The shape of the isotherms provides the information on the nature of the specific adsorption phenomenon. There are six sorption isotherm types classified by International Union of Pure and Applied Chemistry (IUPAC) in 1985(Sing, 1985). The isotherm types (Type I, II, III, IV, V, VI) are depicted in **Figure 1.5**. Type I isotherms are obtained with microporous and the accessible micropore volume governs the limiting uptake rather than by internal surface area. Types II are given by nonporous or macroporous in which shows the unrestricted monolayer-multilayer adsorption at high relative pressure. Type III are also obtained with nonporous and in this type the interactions between adsorbate-adsorbate are stronger than the interactions between adsorbent surface and adsorbate. In the Types IV and V, adsorption on mesoporous adsorbents proceeds by multilayer adsorption followed by capillary condensation. The characteristic features of the Type IV isotherm are its hysteresis loop. The hysteresis loop is related to the filling and emptying by capillary condensation occurs in mesopores. The initial part of the Type IV isotherm follows the same pattern as the corresponding part of the Type

II. The Type V also shows the hysteresis loop that is related to the mechanism of the pore filling and emptying. The Type VI isotherm is called stepped isotherm which is related to the layer by layer adsorption on a highly uniform surface.

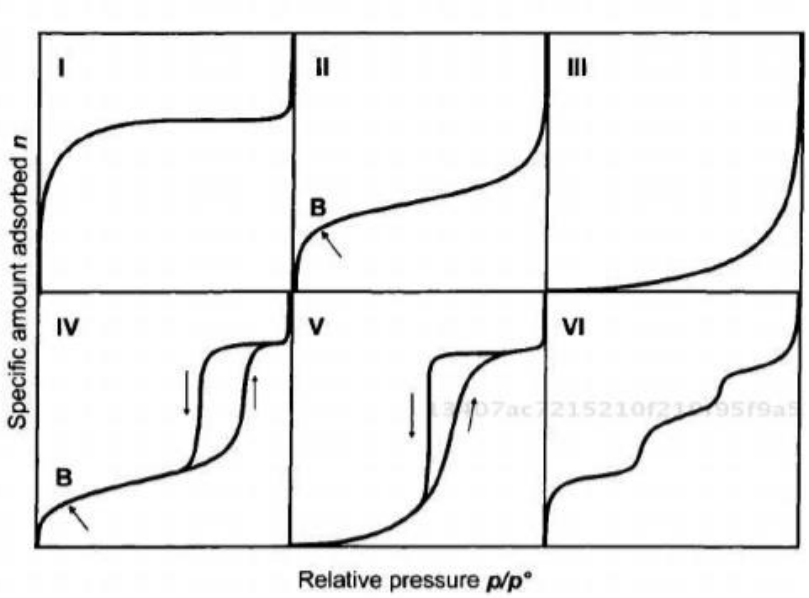

Figure 1-5 Six types of adsorption isotherms based on IUPAC classification (Sing, 1985)

1.2.2: Adsorbent materials-Porous Materials

In this section, the importance of the adsorbent materials and the general definitions are covered since the adsorption process obtained on the surface of the adsorbent surface.

1.2.2.1: General background on porous materials

Due to their ability to interact with atoms, ions and molecules at their surfaces and throughout the bulk material, porous materials have received interest (Davis, 2002). Porous materials are used in a wide variety of applications, such as

adsorption, separation, ion exchange, drug storage and delivery and catalysis (Kuppler et al., 2009). The pore width of porous materials can be categorized based on size by the International Union of Pure and Applied Chemistry (IUPAC). Pores of internal width in the range of equal and less than 2 nm in diameter are named micropores, those in the range of between 2 nm and 50 nm are called mesopores and those in the range of greater than 50 nm are denoted macropores (McCusker et al., 2001). Besides, it is worth noting that nanoporous materials are subgroup of porous materials having pores between 1 and 100 nm in diameter (Lu and Zhao, 2004). Pores are in the nanometre size are generally as a nanopores. Porous materials can be either organic or inorganic materials based on their material composition/constituents. Activated carbons (Sontheimer et al., 1988) are the most common known organic porous materials and they are prepared by elevated temperature pyrolysis of carbon-rich materials (i.e. coal, carbon black and wood char). They possess high surface areas and porosities and offer high adsorption capacities; however, they lack in ordered structures. Despite not having ordered structures, activated carbons are used in a range of applications, such as water remediation, gas storage and separation (Kuppler et al., 2009). The performance of activated carbons however is found to be dependent on the type of carbon and their selectivity has been demonstrated insufficient (Mohan and Pittman, 2006).

Inorganic porous materials, such as zeolites are well-known a class of crystalline aluminosilicates with interconnected pores of 4- 13 nm (Li et al., 2012). Although their structures are highly ordered, these porous inorganic solids suffer from a lack of tunability in pore sizes. While zeolites selectively separate small molecules from mixtures containing small and large molecules, the larger

molecules may not enter in their pores (Davis, 2002). It is very certain that their ability to separate mixture molecules with variable size can be limited by the pore size distributions. Their performances for the separation of molecules therefore rely on the sizes of the molecules. Moreover, the interior of the pores of inorganic porous materials is constructed from walls resulting in relatively lower specific sorption capacity (Omar M. Yaghi, 2003). Inorganic porous materials, however, have found a range of applications in many fields such as separation (Krystl et al., 2001, Jensen et al., 2012, Matito-Martos et al., 2014) and catalysis (Heinemann, 1981, Weitkamp, 2000).

MOFs, as a relatively new class of hybrid porous crystalline materials, have the properties of both organic and inorganic porous materials and well-defined structure and large surface areas (Kuppler et al., 2009). One of their important advantages over organic carbons and inorganic zeolites is the tunability of their composition by changing the metal ions and/or the organic linker. Moreover, MOF structures offer various pore sizes and shapes (i.e. tunnels and cages) and they may have flexibility that provides MOFs adaptation to the pore size to the adsorbate (Horcajada et al., 2012). **Figure 1-6** represents the examples of some typical organic (polymers), inorganic porous materials (zeolites), the combination of organic-inorganic hybrid porous materials (MOFs), as well as, showing the schematic representation of the formation procedure of a MOF (Li et al., 2012). The synthesis procedure of a MOF will be explained more in Chapter 2.

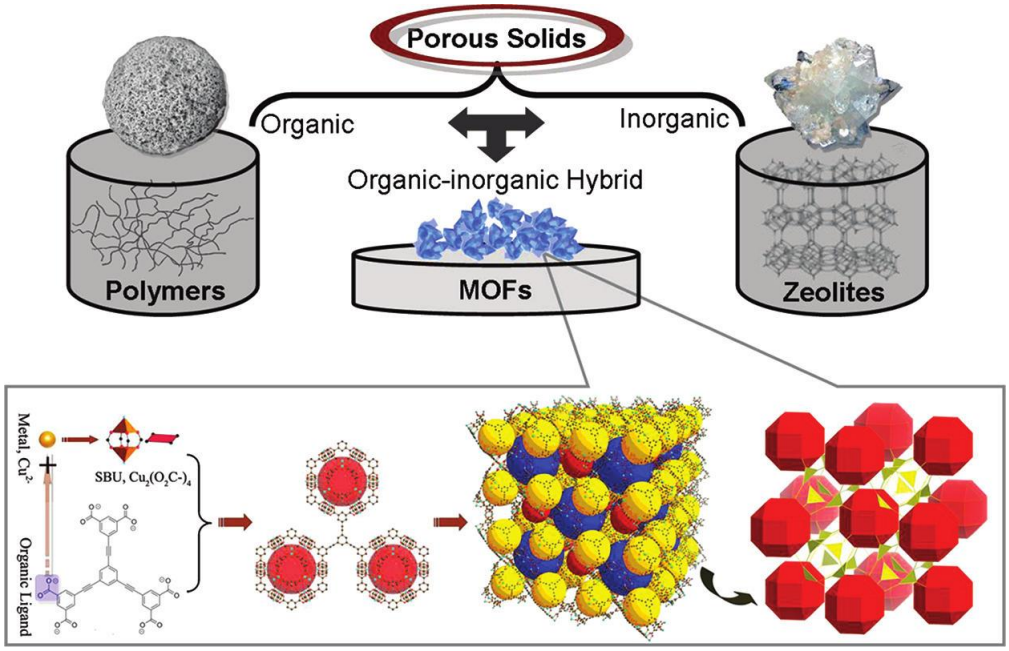

Figure 1-6 Schematic representation of general classification of polymers (organic porous materials) and zeolites (inorganic porous materials) and MOFs (hybrid organic-inorganic porous materials) on the top and the formation procedure of a MOF at the bottom. Reprinted (adapted) with permission from Li et al. (Li et al., 2012) Copyright (2012) American Chemical Society.

1.2.2.2: Activated Carbon

Activated carbons **(Figure 1-7)** are crystalline porous materials are considered the most excessively used traditional adsorbent in the treatment of organic pollutants from water. Activated carbons are amorphous and not providing uniform structures; as mentioned above, they possess however relatively large surface areas and higher surface areas compared to zeolites (Li et al., 2012). Activated carbons are found in two forms as powdered activated carbon (PAC) and granular activated carbon (GAC) (Kyriakopoulos and Doulia, 2006, Calisto et al., 2015). PAC offers kinetically faster adsorption owing to its smaller particle size compared to GAC,

however, PAC cannot be regenerated. On the other hand, GAC can be regenerated (Altmann et al., 2014, Calisto et al., 2015). Many studies were conducted on using activated carbons as an adsorbent for the pharmaceuticals removal from water (Nowotny et al., 2007, Snyder et al., 2007, Yu et al., 2008, Yu et al., 2009, Mestre et al., 2012)

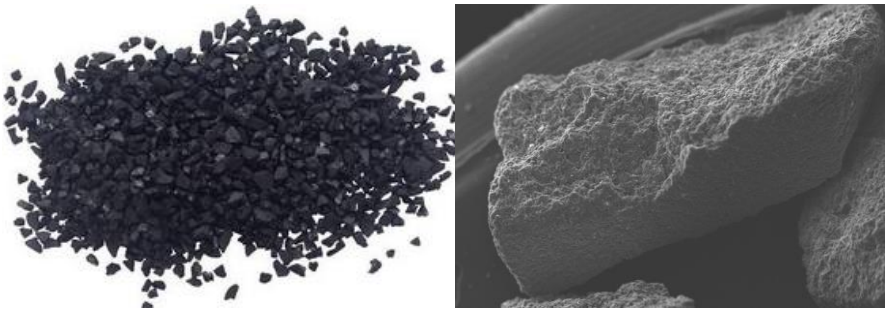

Figure 1-7. Activated Carbon

1.2.2.3: Zeolites

Zeolites **(Figure 1-8)** are inorganic microporous crystalline and natural aluminasilicate minerals which consist tetrahedral units of SiO_4 and AlO_4 and these units covalently linked by sharing oxygen atoms to form $Si(Al)O_4$ (Park et al., 2006, Baerlocher et al., 2007, Martucci et al., 2012). Zeolite polarity was defined by the Si/Al ratio (Martucci et al., 2012). The three-dimensional frameworks composed of

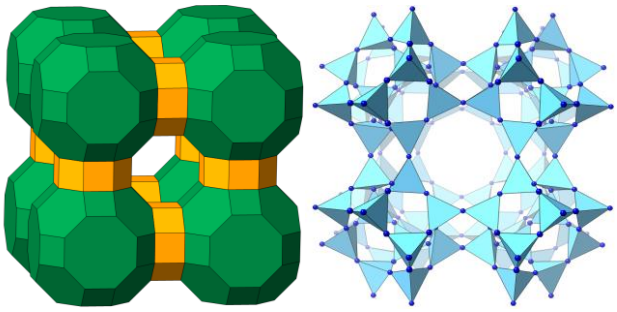

Figure 1-8 Zeolite rho-solid cages (left) and zeolite ZK5 (right)

channels and cages which can allow small guest molecules to diffuse into pores. Their channels can be found in different shape such as elliptical or circular, straight or zigzag (Martens and Jacobs, 1987), which can significantly impact their adsorptive properties towards guest molecules.

1.2.2.4: Graphene and Graphene Oxide

Graphene **(Figure 1-9)** is a single chip structure that composed of carbon atoms. The graphene structure basically is a two-dimensional carbon atom covalently connected to form a honeycomb sheet. Graphene oxide is prepared by the oxidation of graphite. Due to their high specific surface area, they are considered as promising adsorbents for removing the PPCPs compared to activated carbon. The studies showed that the physiochemical properties of PPCPs, pH of the solution and contact time affect strongly the performance of graphene and its oxide towards the removal of PPCPs (Kyzas et al., 2015, Wang and Wang, 2016).

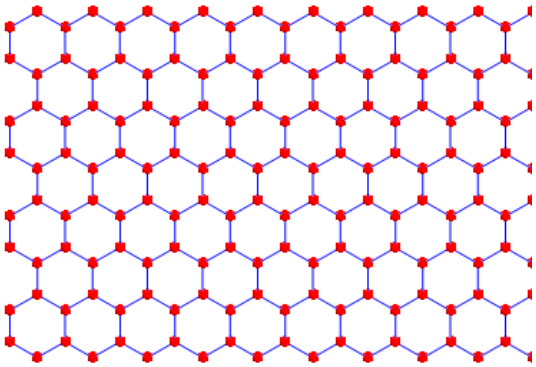

Figure 1-9 Graphene sheet

1.2.2.5: Carbon nanotubes

Carbon nanotubes (CNTs) **(Figure 1-10)** are built up by rolling up graphene sheets (hexagonal structures) into cylindrical form. CNTs have classified as single walled nanotubes (SWNTs) and multiwalled nanotubes (MWNTs). They are also categorised as three types of structures such as zigzag, armchair and chiral structures based on atomic arrangement. Their features are strongly dependent of their morphology and size. Their atomic arrangement makes CNTs metallic or semiconducting (Mittal et al., 2015).

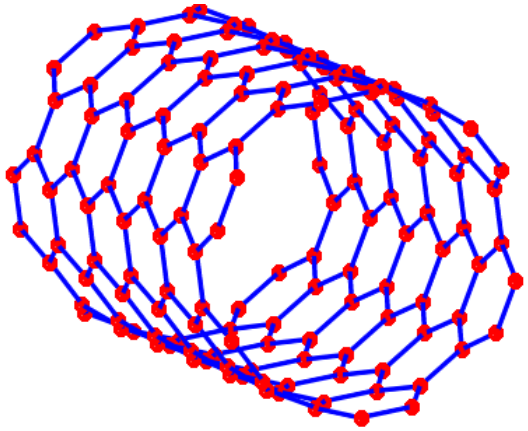

Figure 1-10 Carbon nanotube

Chapter 2: LITERATURE REVIEW

In this chapter, general background on metal-organic frameworks, their synthesis and characterisation methods, as well as, their potentials as adsorbents in environmental remediation applications are explained.

2.1: METAL-ORGANIC FRAMEWORKS (MOFs)

In the late 1980s, Hoskins and Robson discovered porous structures with 3D infinite framework structures by the assembly of organic and inorganic linkers, which was expected to have large empty cavities and low densities (Hoskins and Robson, 1989, Hoskins and Robson, 1990). In 1995, Yaghi et al. defined MOFs with a 3D crystalline structure by inspiring the study of Hoskins and Robson (Yaghi et al., 1995). Afterwards, Yaghi et al. (1999) synthesised the first known robust and highly porous crystalline three-dimensional framework called MOF-5 (IRMOF-1). MOF-5 was built up by connecting $Zn_4O(CO_2)_6$ octahedral secondary building units (SBUs) each with six chelating 1,4-benzenedicarboxylate (BDC) units to form a cubic framework with formula of $Zn_4O(BDC)_3.(DMF)_8(C_6H_5Cl)$ **(Figure 2-1)** (Hailian Li, 1999). The surface area values of MOFs reached at least 3000 $m^2 g^{-1}$ and above. For example, MOF-5 provided much greater surface area of 3631 $m^2 g^{-1}$ than the reported zeolite Y with the highest surface area of 904 $m^2 g^{-1}$ (Frost et al., 2006) and activated carbons having surface area of 2030 $m^2 g^{-1}$ (Chae et al., 2004). Up to date, the apparent surface areas of MOFs can exceed almost 10,000 $m^2 g^{-1}$ while zeolites and activated carbons reach 1000 $m^2 g^{-1}$ and up to 3500 $m^2 g^{-1}$, respectively (Farha et al., 2012, Gomez-Gualdron et al., 2016, Moghadam et al., 2017).

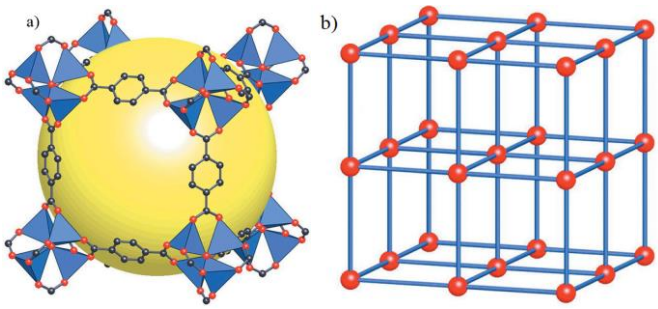

Figure 2-1 The structure of MOF-5. a) the MOF-5 structure: ZnO4 tetrahedra (blue) and benzenetricarboxylate linkers (red: oxygen and black: carbon) and pore aperture of 0.8 nm and pore diameter of 1.2 nm (yellow sphere). b) represents the topology of the MOF-5 structure (primitive cubic net) and it is shown as a ball and-stick model. Reprinted from (Omar M. Yaghi, 2003) with permission.

MOFs, also known as porous coordination polymers (PCPs), are crystalline hybrid materials with permanent porosity. MOF structures consist of inorganic nodes (metal ions or metal-containing clusters) and organic bridging ligands. They are therefore constructed from inorganic nodes bridged by multitopic organic ligands through coordination bonds resulting in three-dimensional (3D) structures with one-dimensional (1D), two-dimensional (2D) or three-dimensional (3D) channel systems (Eddaoudi et al., 2002, Omar M. Yaghi, 2003, V. Krungleviciute et al., 2007, Patil et al., 2011, Furukawa et al., 2013a). The schematic illustration of a MOF is briefly depicted in **Figure 2-2.**

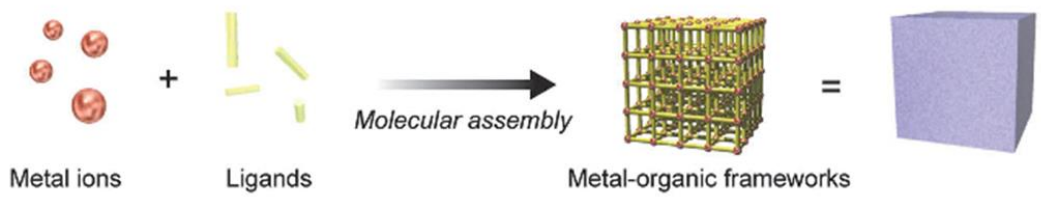

Figure 2-2 Illustration of structuring of a MOF. Reproduced from Ref. (Furukawa et al., 2014) with permission from The Royal Society of Chemistry.

MOFs have gained substantial attention in recent years owing to a wide number of intriguing properties, including their structural periodicity, accessible cages and tunnels (Yang and Yan, 2011), high surface areas, high pore volume and low densities (from 0.21 to 1 g cm^{-3}). Furthermore, their tunable shapes and pore sizes from microporous to mesoporous scale by simply changing the connectivity of the inorganic moiety and organic ligands (Khan et al., 2013b) and adjustable chemical functionalities allow MOFs to be used for various targeted applications.

Synthesising isoreticular MOFs (IRMOFs) having the same topology but a wide range of pore sizes and surface areas by choosing an appropriate combination of inorganic and organic "building blocks" resulted in a huge number of MOF materials with various chemical functionalities (Eddaoudi et al., 2002). Theoretically, numerous MOF materials can be synthesised by simply changing the organic linkers and metal ions. There are a wide range of the choices of multidentate linkers including polycarboxylates, phosphonates, sulfonates, amines, imidazolates, pyridyl and phenolates (Horcajada et al., 2012). In 2016, the Cambridge Structure Database (CSD) documents more than 850,000 entries of small molecule crystal structures consisting of MOFs and other porous materials over the last 44 years. In the last two decades, the number of MOFs has also substantially exceeded to around 70,000 materials among these porous materials **(Figure 2-3)** (Moghadam et al., 2017).

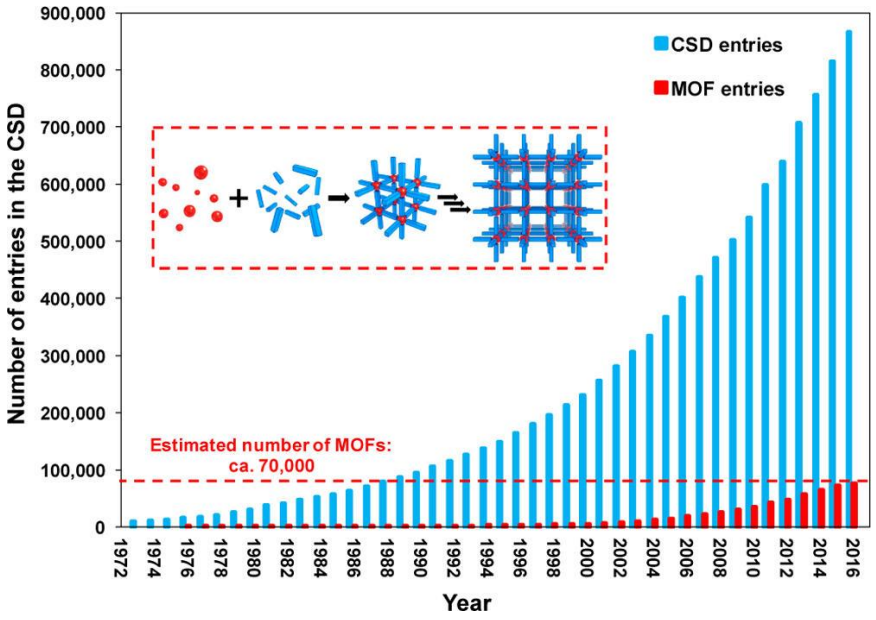

Figure 2-3 Cambridge Structure Database and MOF structures entries reported in the CSD from 1972 to 2016. The inset display the MOF self-assembly process from building blocks: metals (red spheres) and organic ligands (blue struts). Reprinted (adapted) with permission from (Moghadam et al., 2017). Copyright (2017) American Chemical Society.

2.2: SYNTHESIS and ACTIVATION METAL-ORGANIC FRAMEWORKS

2.2.1: General Background of MOF Synthesis

In the literature, a variety of synthesis methods were reported to synthesise MOFs (Meek et al., 2011, Stock and Biswas, 2012, Sun and Zhou, 2015). The synthesis of MOFs is generally carried out by modular synthesis or self-assembly reactions in which organic linkers and metal ions in organic solvents mixture are heated from room temperature to elevated temperature. In the literature, various syntheses strategies have been employed to obtain a MOF crystalline material including hydrothermal synthesis (Yaghi and Li, 1995), solvothermal synthesis (Al-Kutubi et

al., 2015), electrochemical synthesis (Al-Kutubi et al., 2015), microwave assisted synthesis (Klinowski et al., Ni and Masel, 2006), ultrasonication synthesis (Khan and Jhung, 2015) and mechanochemical synthesis (Do and Friscic, 2017). Solvothermal synthesis method is the most widely used method because it is the most straightforward, practical method (Howarth et al., 2017) and also industrially feasible for the kt/year scale production (Yilmaz et al., 2012). Moreover, the system does not require for specialist equipment to be operated and the fast crystals growth with prominent level of crystallinity and phase purity were afforded.

The aforementioned synthesis of crystalline MOFs methods, hydrothermal, solvothermal, electrochemical, sonochemical and microwave assisted, are explained briefly in the following sections.

2.2.1.1: Hydrothermal Synthesis:

In hydrothermal synthesis, the reactions occur in closed vessel under autogenous pressure (Qiu and Zhu, 2009). Typically, organic ligand and inorganic metal salts are mixed in the solvents and placed in a sealed Teflon-lined autoclave. The generation of an autogenous pressure is obtained through heating the solvents at their boiling points or greater than that of their boiling points. Finally, the chemical reactions between organic solids and solvents take place under these conditions (Al-Kutubi et al., 2015). The decrease in solvent viscosity and dielectric constant of the solvent enhance the diffusion process and crystal growth, accordingly. **Figure 2-4** displays a schematic of a typical Teflon-lined stainless-steel autoclave, which is used for hydrothermal synthesis.

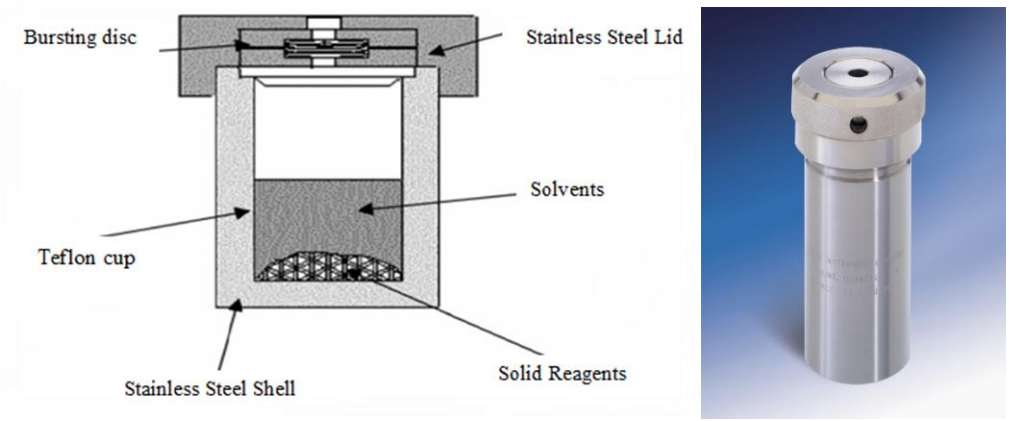

Figure 2-4 Schematic diagram of Teflon®-lined stainless steel autoclave Reproduced from (Walton, 2002) with permission from The Royal Society of Chemistry and source: web for the picture on the right.

2.2.1.2: Solvothermal Synthesis Method:

The conditions of solvothermal synthesis method are in common with hydrothermal method approach/route, however the use of polar organic solvents (i.e. dimethylformamide, diethylformamide) was employed in solvothermal synthesis method. The synthesis carries out at lower temperatures (80 - 250 ^{o}C) and atmospheric pressures (Al-Kutubi et al., 2015). Typically, in solvothermal synthesis method, a metal salt and a multidentate organic linker are mixed in a solvent with a high boiling point such as dimethylformamide (DMF) or diethylformamide (DEF) in a screw-top vial **(Figure 2-5).** The mixture is then placed in a conventional oven or a hot plate equipped with a non-flammable silicone-based oil bath to be heated for typically 12 to 48 h. The topology, crystal size, shape, and phase purity/crystallinity of the material can be affected by varying parameters including reaction temperature, time, solvent, reagent concentration and pH. The solvothermal method represents a versatile strategy for the preparation of

hybrid MOF materials that facilitate control over the crystal size and purity of the materials (Zhao et al., 2016).

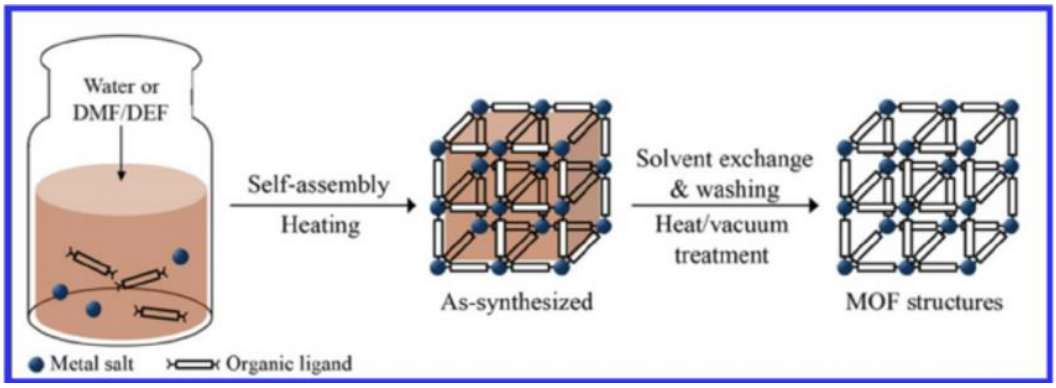

Figure 2-5 Schematic view of solvothermal synthesis approach of MOFs materials Reprinted from (Lee et al., 2013) with permission.

2.2.1.3: Electrochemical Synthesis Method:

Electrochemical synthesis was developed by researchers at BASF in 2005 (Biswas et al.2005). In the electrochemical synthesis of MOFs, the main aim was to exclude anions such as nitrate, perchlorate and chloride during the synthesis. Therefore, metal ions are continuously provided via anodic dissolution that consists of dissolved linker molecules and a conducting salt. The metal ions are continuously being introduced to a synthesis mixture of organic linker and electrolyte (Stock and Biswas, 2012). It is expected to have highly crystalline and pure materials during this synthetic procedure. Moderate synthesis conditions, shorter synthesis time and the ability to control the synthesis rate/yield can be determined as advantages of using the electrochemical synthesis (Al-Kutubi et al., 2015). This method can also allow the large-scale synthesis of MOFs to be obtained (Al-Kutubi et al., 2015). To give an example, Muller et al. synthesised copper based HKUST-1 (HKUST stands for Hong Kong University of Science and Technology)

using this method, which is built from 1,3,5 benzenetricarboxylate (BTC) ligands and copper (Cu) ions. The schematic representation of electrosynthesis and structure of HKUST-1 are given in **Figure 2-6** (Mueller et al., 2006).

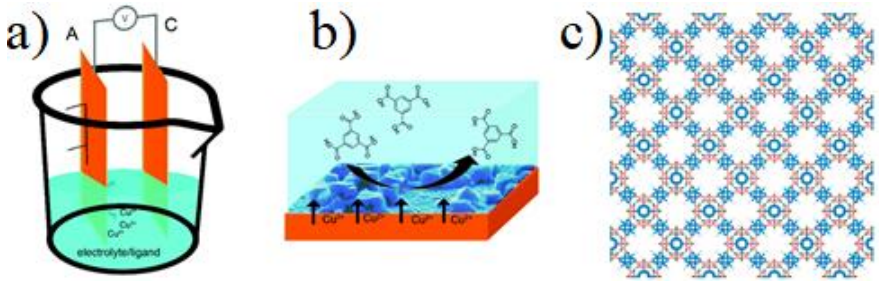

Figure 2-6 a) Schematic representation of electro synthesis anodic dissolution cell, b) the formation of HKUST-1 on the anode electrode. c) HKUST-1 structure. Reproduced from Ref. (Rubio-Martinez et al., 2017) with permission from The Royal Society of Chemistry and the structure of HKUST-1.

2.2.1.4: Microwave Assisted Synthesis:

Microwave assisted synthesis method depends upon the interaction of electromagnetic waves with mobile electric charges (Stock and Biswas, 2012), may these be polar solvent molecules in a solution or electron in a solid. The operational temperatures of above 100 °C and very short reaction times (i.e., a few seconds or minutes) have been identified for microwave-assisted synthesis of MOFs. Generally, microwave irradiation decreases the synthesis time for the materials with having smaller crystal size compared to conventional heating (Stock and Biswas, 2012). Microwave heating occurs almost instantaneous and enables the use of the temperatures above the boiling point of a solvent in pressurised vessels (Klinowski et al., 2011). The main focuses of microwave assisted MOF synthesis are the acceleration of crystallization, the formation of nanoscale products,

improvement the purity of production and selective synthesis of polymorphs. Direct heating of the solvents is related to higher nucleation rate (Stock and Biswas, 2012).

2.2.1.5: Sonochemical Synthesis:

This method relies generally on the chemical reactions by employing high-energy/intensity ultrasound. Ultrasonic **(Figure 2-7)** irradiation offers unusual reaction conditions such extremely high local temperatures and high pressures in liquids for a very short duration of time. These conditions are created because acoustic wavelengths are much greater than molecular dimensions. Molecular level interaction between ultrasound and the chemical species do not directly occur. Acoustic cavitation, the process of generation, growth and collapse of bubbles in liquids are obtained by high energy ultrasound in the sonochemical process (Bang and Suslick, 2010, Khan and Jhung, 2015). These transient and local hot spots provided by cavitation lead to the rapid release of energy with heating and cooling rates of 1010 K s^{-1} and have around 5000 K of temperatures and 1000 atmospheres of pressures (Stock and Biswas, 2012).

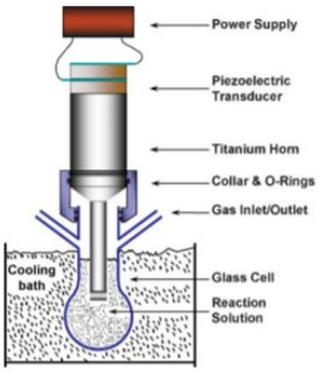

Figure 2-7 Schematic view of traditional ultrasonic rig (Bang and Suslick, 2010) Copyright © 2010 WILEY-VCH Verlag GmbH & Co. KGaA, Weinheim.

2.2.1.6: Mechanochemical Synthesis:

By applying mechanical force, many physical phenomena and chemical reactions in the presence of solvents can emerge. In mechanochemical synthesis, the intramolecular bonds are mechanically broken in such a way that chemical transformations may take place (Stock and Biswas, 2012). The starting materials are placed in a steel reactor containing a steel ball for a period of time (2-10 min) and then a highly crystalline and single-phase product of MOFs with guest molecules inside the pores are formed. These guest molecules inside the pores can be thermally removed in order to afford a guest-free porous material.

2.2.2: Activation and Characterisation of MOFs

The MOF material initially composes solvent or unreacted/residual linkers inside the pores. In order to discard unreacted linkers trapped inside the pores, the as-synthesized MOF product is firstly washed with the solvents (e.g., DMF) by centrifugation. The non-volatile solvent used during the synthesis is exchanged with an organic volatile solvent (e.g., methanol, acetone or ethanol) which can be easily removed from the pores by simply applying heating. Exchange process is carried out by soaking the material in a volatile solvent for an extended period of time (e.g., overnight). The solvent is then evacuated by heating under vacuum thus leading to an activated material with having large pore volume and large surface area (Howarth et al., 2017).

The crystallinity and phase purity of a MOF is basically determined by means of powder X-ray diffraction in addition to N_2 adsorption-desorption isotherm. Furthermore, N_2 sorption isotherm is also used for the confirmation of the porosity

and calculating a surface area. Specific apparent surface area, pore volume and pore size distribution of a MOF are measured through adsorption isotherms for nonreactive gases at cryogenic temperatures. The adsorption-desorption isotherms shape can provide also information about the material characteristic (e.g., micropores, mesopores, macropores) (Thommes, 2010, Thommes et al., 2015). For obtaining the adsorption-desorption isotherms, N_2 gas adsorption at -196 ˚C is most widely used.

Powder X-ray diffraction is used to establish the crystal structure of a MOF. Other information (e.g., unit cell size) can be derived from powder pattern once a sample is confirmed to be a crystalline. The new material`s crystallinity is obtained from single crystal X-ray data as to confirm the phase purity of a MOF (Howarth et al., 2017). Thus, the experimental powder X-ray pattern is compared to simulated powder pattern derived from the single crystal.

Prior to an adsorption-desorption isotherm measurement, the MOF should be properly activated in order to be able to attain reliable information. The amount of sample plays an important role in the analysis, thus, the multiplication of the amount of sample in grams by the apparent surface area of the sample in $m^2 g^{-1}$ should be equal or above 100 m^2 for reliable data. If the amount of sample in the analysis is measured incorrectly, it is more likely to either underestimate or overestimate specific surface areas. For specific apparent area measurements of MOFs, Brunauer Emmet Teller (BET) theory (Brunauer et al., 1938) is the most appropriate one because the pore sizes of most of the MOFs support multilayer gas adsorption. On the other hand, the Langmuir theory is used only for monolayer adsorption (Langmuir, 1918). Therefore, the apparent Langmuir surface areas are

likely to be overestimated around by 50% or more (Howarth et al., 2017). The apparent surface area of a MOF can be calculated with the BET equation (Equation 2-1) through plotting $(P/P_0)/n(1-P/P_0)$ vs relative pressure (P/P_0).

$$\frac{P/P_0}{n(1-P/P_0)} = \frac{1}{n_m C} + \frac{C-1}{n_m C}(P/P_0) \qquad (2-1)$$

where n is the amount of gas molecules adsorbed, C is the BET constant, P is the equilibrium pressure and P_0 is the saturation pressure of adsorbate and n_m is the monolayer capacity (Rouquerol et al., 2013).

The other essential information provided by adsorption-desorption isotherm is the pore volume and pore size distribution of a MOF. Several methods such as density functional theory (DFT) method (Tarazona et al., 1987) and Barrett Joyner Halenda method (Barrett et al., 1951) among the most used have been proposed to utilize for analysing pore volume and pore size distribution of a MOF. The DFT model is commonly used for the analysis of MOF pores, particularly when mesopores is close to 2 nm or micropores is less than 2 nm. In 1989, Seaton et al. (Seaton et al., 1989) first proposed a DFT model to calculate the pore structure characterisation (i.e. pore size distribution) from nitrogen adsorption isotherms. On the other hand, Barrett, Joyner and Halenda was published BJH method in 1951. (Barrett et al., 1951). BJH is used for the mesopores range materials (2 nm <pores<50 nm), thus, this method describes the adsorption occurs in mesopores.

Lippens and de Boers was published t-plot method in 1965 (Lippens et al., 1964, Lippens and De Boer, 1965). The t-plot method is a technique used to establish the micropores and/or mesopores volumes and the surface area of a

sample. The film thickness of an adsorbate on non-porous surface are established and the relation between the volume adsorbed and the film thickness is expressed in Equation 2-2.

$$\frac{V}{V_m} = \frac{t}{\sigma} \qquad (2-2)$$

where t is an average film thickness of an adsorbate on surface (Å), σ is thickness of single molecular layer of nitrogen molecule (3.54 Å), V is the adsorbed volume of gas at the relative pressure P/P_0 ($cm^3\ g^{-1}$), V_m is the adsorbed volume of gas at monolayer ($cm^3\ g^{-1}$).

To calculate the film thickness, Harkins-Jura equation is used (de Boer et al., 1966). Therefore, in this research, the Harkins-Jura equation was used for calculating the thickness. Harkins-Jura thickness equation is given in Equation 2-3 for nitrogen at 77 K. By plotting the graph, the adsorbed volume of gas (V) against average film thickness of an adsorbate (t) which allows micropore volume to be calculated.

$$t = \left(\frac{13.99}{0.034 + \log(P/P_0)}\right)^{1/2} \qquad (2-3)$$

2.3: APPLICATIONS OF METAL ORGANIC FRAMEWORKS

In the last few years, due to the aforementioned functional properties, MOFs are investigated for a numerous potential applications, including gas storage/separation (Li et al., 2009), carbon dioxide adsorption and separation (Britt et al., 2008, Britt et al., 2009, D'Alessandro et al., 2010, McDonald et al., 2015), methane and hydrogen storage (Rosi et al., 2003, Wei Zhou et al., 2007, Peng et al., 2013, Mason

et al., 2014), heterogeneous catalysis (Lee et al., 2009), drug delivery and release (Horcajada et al., 2006, Teplensky et al., 2017, Huxford et al., 2010), heavy metals removal (Feng et al., 2013, Yee et al., 2013, Abney et al., 2014, Li et al., 2015, Vu et al., 2015, Wang et al., 2015), removal of hazardous chemicals materials from air (Barea et al., 2014, DeCoste and Peterson, 2014) and degradation of chemical warfare agents (Moon et al., 2015, Islamoglu et al., 2017, Bobbitt et al., 2017).

In addition to these applications, there are many current studies revealed that MOFs have also proven to be used as efficient adsorbents for separation and purification of organic pollutants (e.g., dyes and pharmaceuticals) in the liquid phase (Khan et al., 2013a, Van de Voorde et al., 2014, Ahmed and Jhung, 2016, Wang et al., 2016a). The adjustability/tunability pore size, shape and the functionalization of MOFs enable them to be used in the selective adsorption of various guest molecules with specific chemical functional groups (Khan et al., 2013a). In addition, the pore structures and size and shape of the adsorbents are one of the most important parameters to understand the separation mechanism toward adsorbates. The design of MOFs with permanent porosity can be achieved and the pore size, shape and chemical composition of the pores can also be adjusted for water remediation and adsorption applications in order to favour the uptake of specific compounds with great affinity and high selectivity. Moreover, some MOFs possess quite low density (i.e., NU-1301`s density is 0.125 g cm^{-3}) (Li et al., 2017) leading to have exceptional pore volumes and BET specific areas, which is of interest in the adsorption-based applications.

2.3.1: Metal-Organic Frameworks for Adsorptive Removal of PPCPs and EDCs from Liquid Phase

Intensive research into MOFs for diverse organic pollutants adsorption and separation in the liquid phase have recently attracted great research interest as an alternative to traditional adsorbent materials in the last past decades. It is worth noting that the efficiency of adsorption is strongly defined by the characteristics of the adsorbents (Van de Voorde et al., 2014). Hence, their abundant active vacancy sites and versatile chemical functional groups, revealed that MOFs are exploited as promising adsorbents for wastewater treatment remediation applications (Jiang et al., 2013, Hasan and Jhung, 2015, Seo et al., 2015b, Wang et al., 2016a, Wei et al., 2016, Bhadra and Jhung, 2017, Sarker et al., 2017, Seo et al., 2017, Song and Jhung, 2017). The reported MOFs, their corresponding surface areas, maximum adsorption capacity to date, for the studied analytes in the literature are represented in **Table 2-1**. As explicitly seen in **Table 2-1**, the studied MOFs offered greater maximum adsorption capacity/affinity for the studied PPCPs or EDCs than activated carbons or zeolites. These findings suggested that MOFs could be potentially leveraged as adsorbents due to their huge surface areas and chemical functional tailorability for removing contaminants from water.

Table 2-1 MOF materials, their surface areas and maximum adsorption capacity for pharmaceuticals adsorption in MOFs in the literature

MOF-material	Surface Area (m^2 g^{-1})	Analytes	Uptake capacity (mg g^{-1})	Reference
MIL-100-Fe	1492	Naproxen	115	(Hasan et al., 2012a)

MIl-101	3014	Naproxen	132	(Hasan et al., 2012a)
Activated carbon	871	Naproxen	81	(Hasan et al., 2012a)
MIL-101	3014	Clofibric acid	312	(Hasan et al., 2012a)
Activated carbon	871	Clofibric acid	244	(Hasan et al., 2012a)
MIL-53(Cr)	1438	2,4-dichlorophenoxy-acetic acid	556	(Jung et al., 2013)
Activated carbon	1068	2,4-dichlorophenoxy-acetic acid	286	(Jung et al., 2013)
Zeolite	720	2,4-dichlorophenoxy-acetic acid	256	(Jung et al., 2013)
ZIF-8	1106	*p*-arsanilic acid	730	(Jung et al., 2015)
Mesoporous ZIF-8	1134	*p*-arsanilic acid	791	(Jung et al., 2015)
Activated carbon	1068	*p*-arsanilic acid	293	(Jung et al., 2015)
UiO-66	710	phthalic acid	187	(Khan et al., 2015)
UiO-66-NH_2	651	phthalic acid	224	(Khan et al., 2015)
ZIF-8	1501	phthalic acid	654	(Khan et al., 2015)
Activated carbon	1016	phthalic acid	249	(Khan et al., 2015)
UiO-66	982	Methylchloro-phenoxypropionic acid	370	(Seo et al., 2015b)
Activated carbon	871	Methylchloro-phenoxypropionic acid	303	(Seo et al., 2015b)
UiO-66	1082	Diclofenac sodium	189	(Hasan et al., 2016a)
UiO-66-SO_3H	910	Diclofenac sodium	263	(Hasan et al., 2016a)
UiO-66-NH_2	902	Diclofenac sodium	106	(Hasan et al., 2016a)
Activated carbon	870	Diclofenac sodium	76	(Hasan et al., 2016a)
MIL-101	3030	Saccharin	53.4	(Seo et al., 2016c)

MIL-101-urea	1970	Saccharin	86.4	(Seo et al., 2016c)
MIL-101-melamine	1350	Saccharin	70.1	(Seo et al., 2016c)
MIL-101-NO_2	1620	Saccharin	18.7	(Seo et al., 2016c)
MIL-101	3030	Naproxen	114	(Seo et al., 2016a)
MIL-101-OH	2170	Naproxen	185	(Seo et al., 2016b)
MIL-101-$(OH)_2$	990	Naproxen	136	(Seo et al., 2016a)
MIL-101-NO_2	1620	Naproxen	66.1	(Seo et al., 2016a)
MIL-101-NH_2	1892	Naproxen	147	(Seo et al., 2016b)
MIL-101	3030	Dimetridazole	141	(Seo et al., 2017)
MIL-101-urea	1970	Dimetridazole	185	(Seo et al., 2017)
UiO-66	1155	Sulfachloropyra-dazine	417	(Azhar et al., 2017)
MIL-53(Al)	1401	Dimetridazole	467.3	(Peng et al., 2018)

Stability of MOFs in water and chemical is of the crucial points in the liquid phase adsorption. Considering the huge number of MOFs in the literature, it is anticipated that some of them are not stable in the presence of water or moisture leading to the decomposition of frameworks (Burtch et al., 2014, Wang et al., 2016b). The decomposition of frameworks give rise to lower surface area and eventually poor adsorption capacities. Therefore, water and chemical stable MOFs should be considered for the liquid phase adsorption (Hu et al., 2013) as it is not practical to examine organic pollutants adsorption capacities of each MOF reported in the literature using experimental methods.

Both the physical and chemical interaction can be involved in the adsorption of organic pollutants in the liquid phase. Several types of possible adsorption

mechanisms can be proposed to determine the mechanism, which include electrostatic interaction, hydrogen bonding, acid-base interaction, influence of metal ions, hydrophobic interaction and π-π stacking **(Figure 2-8)** (Hasan and Jhung, 2015). In many cases, there might be more than one type of adsorption forces that determines the dominant forces involved in the liquid phase adsorption.

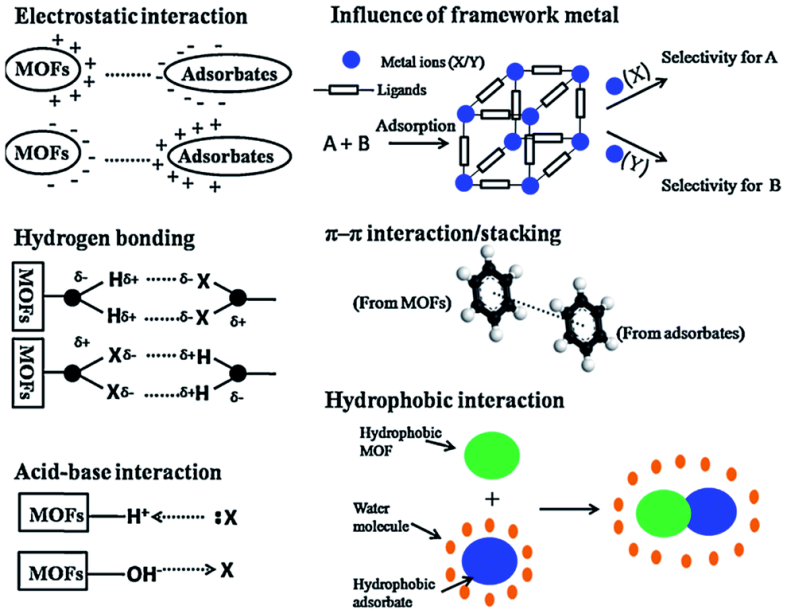

Figure 2-8 Plausible adsorption mechanisms proposed for the adsorptive removal of organic compounds on MOFs. Adapted with permission from (Hasan and Jhung, 2015), copyright Elsevier, 2015.

2.4: THESIS AIM AND OUTLINE

The aim of this research is to evaluate the adsorption ability of metal-organic frameworks for the adsorptive removal of emerging contaminants, particularly, pharmaceuticals and personal care products and endocrine disrupting compounds in water. However, the intended contribution to the area of the research is not only to prepare MOFs that could be used in PPCPs and EDCs removal, but the

enhancement of the removal of emerging contaminants from water. In this thesis, atrazine, carbamazepine and triclosan were chosen as probe molecules because their prolonged exposure to the aquatic environment and human has raised concern on the ecological system and human health. Hence, their removal from water has become of ultimately importance.

The specific objectives of this project are given in the following:

- To synthesise and characterise the selected MOFs.
- To compare the adsorption capacity of the synthesised MOFs towards the target PPCPS and EDCs with commercially available activated carbon of Filtrasorb-400 for water treatment.
- To elucidate the adsorption capacity of the MOFs for the binary mixture of pharmaceuticals since pharmaceuticals are found as a mixture in natural waters.
- To verify the adsorption forces that drive the uptake of organic pollutants of interest.
- To demonstrate the MOF stability after the uptake of organic pollutants from water.
- To demonstrate the maximum adsorption capacity towards the selected organic pollutants by fitting to adsorption isotherm models.

An introduction on the occurrence of PPCPs and EDCs in water and treatment technologies proposed to remove them from water is given in Chapter 1. Adsorption based treatment method is particularly explained and some previous porous adsorbents and MOFs which have been used for the organic pollutants removal are described.

A literature review on metal-organic frameworks, various synthesis methods that have been used for the synthesis of MOFs and variety applications of MOFs are thoroughly described in Chapter 2. In addition to these, MOFs for environmental water remediation applications are presented.

Chapter 3 demonstrates the experimental method for the synthesis of the selected MOFs, the characterisation techniques that were used for the prepared MOFs and the adsorption batch experiments.

Chapter 4 demonstrates the uptake of atrazine, is the common used pesticide and priority pollutants listed by the European Union. The adsorptive removal was examined by using the selected MOFs and compared with commercially available granular activated carbon (Filtrasorb F400). The adsorption uptake of atrazine is enhanced as well as adsorption removal rate was found to be very fast by UiO-67.

Chapter 5 provides another example of removal of carbamazepine adsorption by MOFs. Carbamazepine is one of the persistent organic compounds and resistant to biodegradation. The results show that UiO-67 demonstrates carbamazepine uptake enhancement with very fast uptake.

Chapter 6 examines UiO-67 for the competitive removal towards mixture of carbamazepine and atrazine and demonstrates the effect of salt ions on the carbamazepine and atrazine removal.

Chapter 7 exhibits another example of adsorption of hydrophobic antibacterial triclosan from water by using MOFs. The observations reveal that both UiO-66 and UiO-67 for the triclosan uptake are found to outperform granular activated carbon.

Chapter 8 concludes the main observations covered in this thesis, as well as demonstrates recommendations for the future.

Chapter 3: MATERIALS AND METHODS

In this chapter, chemicals and the details of all experimental procedures of synthesis, characterisation techniques used during the research are described in this chapter.

3.1: CHEMICALS

Zinc nitrate hexahydrate ($Zn(NO_3)_2.6H_2O$, 98%, Sigma Aldrich), 2-methylimidazole ($C_4H_6N_2$, Sigma Aldrich), zirconium chloride ($ZrCl_4$, Merck), 1,4 benzene-dicarboxylic acid (BDC, Sigma Aldrich for synthesis), C_6H_4-1,4-$(CO_2H)_2$, (VWR International), 4,4' biphenyl dicarboxylic acid (BPDC, Sigma Aldrich), iron(III) nitrate nonahydrate ($Fe(NO_3)_3.9H_2O$, Sigma Aldrich), benzene-1,3,5-tricarboxylic acid (H_3BTC), Sigma Aldrich), HKUST-1 (Cu-BTC) (Sigma Aldrich), sodium hydroxide solution (NaOH, Sigma Aldrich), atrazine (Cambridge), N,N dimethylformamide (DMF, Sigma Aldrich, SIAL, ≥99.8), methanol (HPLC Grade, Fisher Scientific), absolute ethanol (Merck), hydrochloric acid (HCl, 36.5-38 wt%, Sigma Aldrich), sulphuric acid (H_2SO_4, Sigma Aldrich, 95-98 %) were purchased and used as received. Filtrasorb-400 (F400) was supplied by Chemviron Calgon, Belgium. All chemicals were used as received without further activation.

3.2: SYNTHESES PROCEDURES of MOFs

This section consists of the syntheses procedures of the selected MOFs (ZIF-8, UiO-66, UiO-67, MIL-100(Fe) according to the synthesis methods reported previously. The detail of the syntheses procedures is described in this section.

3.2.1: Synthesis of ZIF-8:

ZIF-8 was prepared based on the procedure reported by Fu et al. (Fu et al., 2013) 3.0 g of zinc nitrate hexahydrate was dissolved in 60 mL of methanol and 8.3 g of 2-methylimidazole was dissolved in 60 mL of methanol separately. The two solutions were then mixed together in a 250-mL glass jar. The mixture was then sonicated for 15 min at 70°C and a milky white solution was obtained. The ZIF-8 powder was collected by washing with methanol by centrifugation (Thermo Scientific, Sorvall-Legend X1R) at 10000 rpm for 10 min several times and dried at 100°C overnight under vacuum (Heraeus Instruments Vacutherm, VT6025 Vacuum Oven and Pump-PC3001 VarioPro, Vario).

3.2.2: Synthesis of UiO-66:

UiO-66 was prepared with three missing linkers per node **(Figure 3-1)** according to previously procedures reported by Katz et al (Katz et al., 2013, Audu et al., 2016). For UiO-66, 1.25 g of zirconium chloride (5.4mmol), 50 mL of DMF and 10 mL of concentrated HCl were placed in a 250-mL glass bottle and ultrasonicated for 20 minutes until completely dissolved. 1.23 g of 1,4 benzene-dicarboxylic acid (7.5 mmol) and 100 mL of DMF were then added to the mixture and sonicated for further 20 minutes. The consequent mixture was then placed in an oven at 80 °C overnight. After cooling down to the room temperature, the resulting white precipitates were separated from the mother liquor and washed with DMF 2 times (2 x 30 mL) followed by washing with ethanol 3 (3 x 30 mL) times by centrifugation to remove unreacted linkers and DMF trapped from the pores,

respectively. Finally, the sample was collected and dried in a vacuum oven at 90 °C overnight to afford UiO-66 crystals.

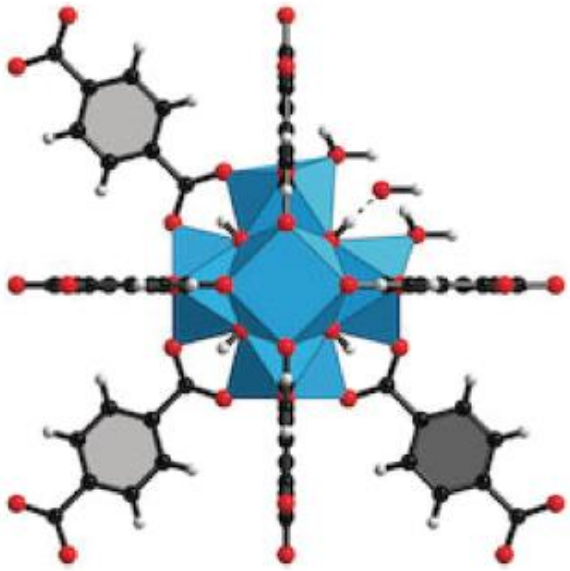

Figure 3-1 Schematic view of a defect site in single crystal of UiO-66. The missing carboxylates linker is replaced by H_2O to counterbalance the l charge by hydroxide anion. (O: red, C: black, Zr: blue) (Trickett et al., 2015). Copyright © 2015 WILEY-VCH Verlag GmbH & Co. KGaA, Weinheim

3.2.3: Synthesis of UiO-67:

UiO-67 were also synthesised with 3 missing linkers per node **(Figure 3-2)** following the procedures reported by Katz et al (Katz et al., 2013, Audu et al., 2016). Briefly, in a 250-mL glass bottle, 0.67 g of zirconium chloride (2.7 mmol), 50 mL of DMF and 5 mL of HCl were added and ultrasonicated for 20 min followed by adding 0.90 g of 4,4' biphenyl dicarboxylic acid (3.8 mmol) and 100 mL of DMF mixed ultrasonically for further 20 minutes. The resulting mixture was incubated at 80 °C overnight. After cooling to the room temperature, the white solid was washed 3 times with DMF and 4 times with acetone by centrifugation (5000

rpm, 5 min). The solid was finally dried in a vacuum oven at 90 °C overnight to obtain UiO-67 as a white powder.

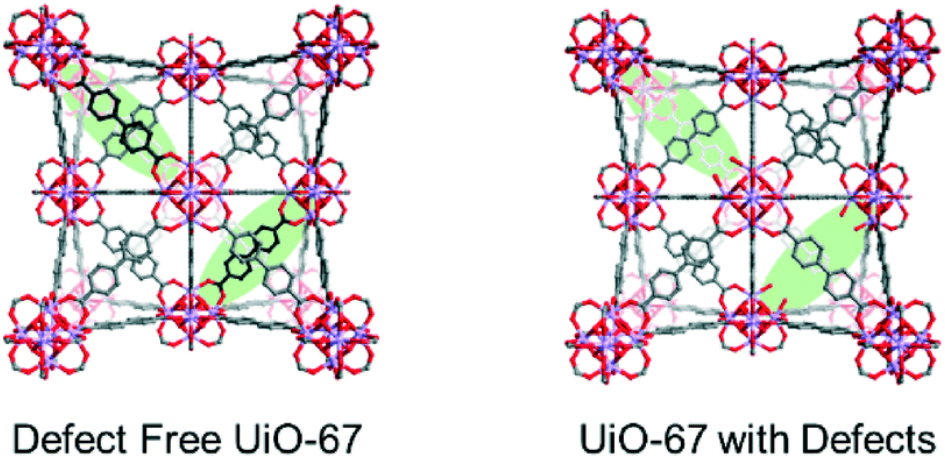

Figure 3-2 Schematic representations of defect free UiO-67 and an idealized representation of missing linker defects in UiO-67 leading to terminal Zr–OH groups on select Zr_6 nodes. Zr: light purple; O: red; C: grey. Reproduced from Ref. (Howarth et al., 2015) with permission from The Royal Society of Chemistry.

3.2.4: Synthesis of MIL-100(Fe):

MIL-100(Fe) was synthesized at low temperature and atmospheric pressure by following the reported procedure with minor modification (Shi et al., 2013). 4 g of iron(III) nitrate nonahydrate, 1.89 g of benzene-1,3,5-tricarboxylic acid and 6 mL of ultrapure water were placed in a flask and stirred at 95 °C for 12 h under reflux. The mother liquor was discarded by centrifugation (4000 rpm, 15 min) followed by 3 times washing with deionized water and 3 times with ethanol by centrifugation. The solid was then collected and left it to be dried in air at room temperature.

3.3: CHARACTERISATION OF THE ADSORBENTS

3.3.1: Powder X-ray Diffraction

Powder X-ray diffraction (PXRD) is an analytical characterisation technique that is used for phase identification of a crystalline material. PXRD patterns were conducted to establish phase purity and bulk crystallinity of the material. The phase purity of a MOF can be determined by comparing the experimental powder X-ray patterns to the simulated patterns. The simulated patterns were accomplished using computational modelling for comparison (Howarth et al., 2017). PXRD patterns of the materials were obtained at ambient temperature using a Bruker-AXS D4 machine with Cu Kα radiation (λ = 1.5418 Å) in transmission mode and in the range of 5˚≤2θ≤50˚ with a step size/width of 0.05˚ and a scan rate of 2 s/step. The PXRD patterns in the last chapters was acquired at room temperature on a Stoe Seifert diffractometer with Mo radiation source (λ = 0.71 Å) in transmission mode and in the range of 2˚≤2θ≤50˚ with a step size of 0.015˚ and a scan rate of 2s/step. Simulated PXRD patterns of the synthesised MOFs were obtained using powder pattern calculation in Mercury software.

3.3.2: Nitrogen adsorption and desorption isotherms

The adsorption isotherms provide significant information with regards to the adsorbate and adsorbent interactions and the adsorption process. It is used to determine the surface area, pore volume and pore size distribution of the adsorbents. N_2 adsorption measurements of the materials were conducted on a Micromeritics Tristar porosity analyser and on a Quantachrome Autosorb IQ MP Physisorption Analyser at 77 K to assess an apparent surface area, total pore volume

and the pore size distribution. The apparent surface areas of the materials were calculated by BET method because the pore sizes of most of the MOFs provide multilayer gas adsorption (Brunauer et al., 1938), micropore volume of the materials were obtained by t-plot method and finally the pore size distributions of the materials were derived by using density functional theory. For the reliable BET data, the amount of material used for the analysis is important because the amount of sample can affect the textural properties of the materials. As a rule of thumb the multiplication of the amount of material in grams by the apparent surface area of the materials of $m^2 g^{-1}$ should be 100 m^2 or above 100 m^2 (Howarth et al., 2017).

3.3.3: Scanning Electron Microscopy

Scanning electron microscopy (SEM) is a characterisation technique for producing images of a sample by scanning the surface with a beam of electrons. SEM is used to identify various features of a material, including morphology, crystal size and elemental composition. In this research, SEM was performed to determine MOF materials and activated carbon properties including crystal size and morphology. The samples were coated with a conducting material (e.g. gold) to avoid charging effects. SEM images of the materials were recorded on a Zeiss evolution MA10 SEM to assess the morphology and particle size of adsorbents. Samples were firstly coated with a thin layer of gold for conductivity and then operated in beam mode at a 15kV of acceleration voltage.

3.3.4: Zeta Potential

Zeta potential is a physical property and associated with the surface charge when a solid dispersed in a liquid. Zeta potential analysis is used to measure the magnitude

of the degree of electrostatic charge or determine attraction/repulsion between particles. Besides, the measurements of zeta potential are used to evaluate the stability of particle and colloidal dispersions in liquid. In this thesis, zeta potential was used to demonstrate the surface of the MOFs in order to assess whether or not electrostatic attraction or repulsion is involved in adsorption mechanism. Zeta potentials of the MOFs at different range of pH. were recorded by Beckman Coulter DelsaMax Pro light scattering analyser and its software.

3.4: ADSORPTION BATCH EXPERIMENTS

The procedure for the batch adsorption experiments and the analysis methods are explained in the following section. **Figure 3-3** illustrated the batch adsorption experiments from preparing the sample to taking the sample for measurements. Stock solutions of the pharmaceuticals are individually prepared on a weight basis at desired concentrations by dissolving the powder pharmaceuticals in ultrapure water. The stock solutions were covered with aluminium foil to eliminate the light effect on the sample and then kept at 4˚C until further use. Aqueous solutions of the target pharmaceuticals were prepared by further diluting stock solutions in deionized water at a various range of concentrations. Prior to adsorption, the adsorbents (MOFs) and granular activated carbon Filtrasorb-400 (F400) were dried overnight under vacuum at 100°C. For each adsorption experiment, an exact amount was added into aqueous pharmaceutical solutions with the fixed concentrations in a set of vials. Vials were sealed and placed in an incubator shaker. The solutions and the adsorbents will then be shaken and maintained for a fixed time (24h) until equilibrium was deemed to be reached at a constant temperature (25°C). Control experiments without adding adsorbents were also conducted to

monitor the change the concentrations. After adsorption for a pre-determined time, the samples were separated from the adsorbents using a syringe filter (0.2 µm cellulose acetate) and the concentrations were determined by means of UV-vis spectrophotometer or high-performance liquid chromatography (HPLC) equipped with UV-vis detector.

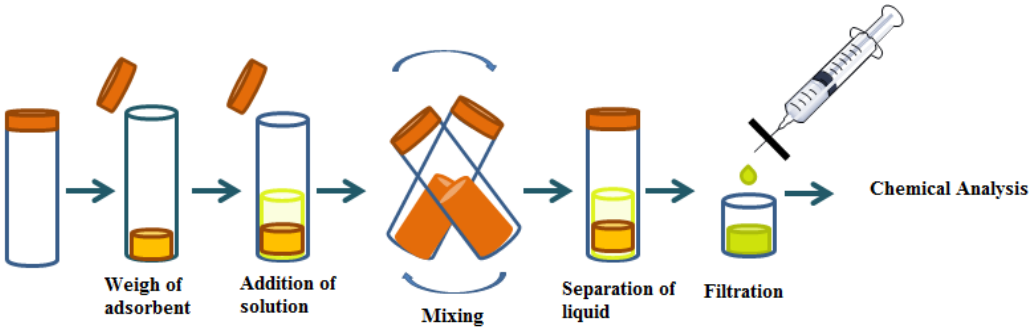

Figure 3-3 Schematic illustration of the batch adsorption experimental procedure

3.4.1: Adsorption isotherms

Adsorption isotherms of each pharmaceutical over the adsorbents was obtained by keeping contact the adsorbate with adsorbent for 24 h at constant temperature to ensure the saturation was reached. The adsorption isotherms are represented as the adsorbed amount of an adsorbate onto an adsorbent when the equilibrium is attained (Q_e, mg g^{-1}) versus the amount of adsorbate remaining in solution at equilibrium (C_e, mg L^{-1}). The amount of adsorbed adsorbate onto adsorbents were calculated by using the mass-balance relationship which is given in **Equation 3-1**:

$$Q_e = \frac{(C_o - C_e).V}{m} \qquad (3-1)$$

where, Q_e (mg/g) is the amount adsorbed per unit mass of adsorbent at equilibrium, C_o and C_e (mg/L) are the initial and the equilibrium concentrations of

the adsorbate, respectively, V (L) is the volume of the pharmaceutical solution and m (g) is the weight of the adsorbent used.

There are a variety of adsorption isotherm models as mentioned in Chapter 2. In this thesis, Freundlich (**Equation 3-2**) (Freundlich, 1906), Langmuir (**Equation 3-3**) (Langmuir, 1916) and Langmuir-Freundlich (**Equation 3-4**) (Koble and Corrigan, 1952, Gao and Deshusses, 2011) are the isotherm models used to describe the adsorption process. Hence, the experimental data can be analysed by using either these non-linear isothermal models or linearized forms of Freundlich (**Equation 3-5**) and Langmuir (**Equation 3-6**) isotherm models. Langmuir adsorption isotherm model was also derived in other linearized form (**Equation 3-7**). Finally, the adsorption isotherms for different adsorbents are plotted according to the linear form of isotherm mode equations as follows:

$$Q_e = K_f {C_e}^{1/N} \qquad (3-2)$$

$$Q_e = \frac{Q_o \, K_L \, C_e}{1 + K_L C_e} \qquad (3-3)$$

$$\mathrm{Q_e} = \frac{\mathrm{Q_m} * {\mathrm{C_e}}^{\mathrm{N}}}{1 + \mathrm{K_L} * {\mathrm{C_e}}^{\mathrm{N}}} \qquad (3-4)$$

$$\ln \mathrm{Q_e} = \ln \mathrm{K_f} + \left(\frac{1}{\mathrm{N}}\right) \ln \mathrm{C_e} \qquad (3-5)$$

$$\frac{1}{\mathrm{Qe}} = \left(\frac{1}{\mathrm{Q_m} * \mathrm{K_L}}\right)\frac{1}{\mathrm{C_e}} + \frac{1}{\mathrm{Q_m}} \qquad (3-6)$$

$$\frac{C_e}{Q_e} = \frac{C_e}{Q_m} + \frac{1}{Q_m K_L} \qquad (3-7)$$

where, Q_e (mg/g) is the amount of adsorbed at equilibrium, C_e (mg/L) is the equilibrium concentration of the adsorbate in the aqueous phase at equilibrium, K_f

((mg g^{-1}) (mL mg^{-1})$^{1/N}$) is the Freundlich adsorption constant, N is the degree of non-linearity and adsorption intensity of the adsorbents, Q_m (mg g^{-1}) is the Langmuir maximum adsorption capacity and K_L (L mg^{-1}) is the Langmuir adsorption constant.

3.4.2: Adsorption Kinetics

To study the adsorption kinetics for the adsorption of each pharmaceutical on the best MOFs and activated carbon, an exact amount (in mg) of each MOF were mixed with corresponding volume of solution of a fixed initial concentration of pharmaceutical. A series of samples were taken at pre-determined time intervals starting from 1 min to 2 h, the concentrations of the solutions were calculated by using UV-vis spectrometry or high-performance liquid chromatography. Finally, the amount of adsorbed adsorbate onto the different adsorbents were calculated by using the mass-balance relationship which is given in **Equation 3-8**:

$$Q_t = (C_o - C_t)\frac{V}{m} \qquad (3-8)$$

where, Q_t (mg/g) is the amount adsorbed per unit mass of adsorbent in time t, C_o (mg/L) is initial liquid-phase concentration of adsorbates at time=0, C_t (mg/L) is liquid phase concentration of adsorbates at time=t, V (L) is the volume of the solution and m (g) is the weight of the adsorbent.

To analyse the experimental kinetic data and calculate the kinetics rate constants, the non-linear pseudo-first order kinetic model and the pseudo second order kinetic model are proposed. These models are utilised for the interpretation of the kinetics of the pharmaceuticals. These models can be converted to their linearized forms

and be used to calculate the kinetic constants because we can simply plot ln (Q_e - Q_t) versus time for the pseudo-first order or plot t/Q_t versus time for the pseudo-second order.

The non-linear pseudo-first order (**Equation 3-9**) and pseudo-second order (**Equation 3-10**) kinetic models and their linearized forms of the pseudo-first order (**Equation 3-11**) and the pseudo-second order (**Equation 3-12**) are expressed as follows:

$$Q_t = Q_e(1 - e^{-k_1 t}) \qquad (3-9)$$

$$\mathrm{Q}_t = \frac{Q_{e^2} k_2 \mathrm{t}}{1 + Q_e k_2 t} \qquad (3-10)$$

$$\ln(\mathrm{Q_e} - \mathrm{Q_t}) = \ln(\mathrm{Q_e}) - \mathrm{k_1} * \mathrm{t} \qquad (3-11)$$

$$\frac{\mathrm{t}}{\mathrm{Q_t}} = \frac{1}{\mathrm{k_2} * \mathrm{Q_e}^2} + \frac{\mathrm{t}}{\mathrm{Q_e}} \qquad (3-12)$$

where Q_t (mg g^{-1}) and Q_e (mg g^{-1}) are the amounts of atrazine adsorbed at time t (min) and at equilibrium, respectively; k_1 (min^{-1}) is the pseud- first order rate constant and k_2 (g mg^{-1} min^{-1}) is the pseudo second order rate constant and t (min) is the adsorption time.

Chapter 4: ADSORPTIVE REMOVAL OF ATRAZINE FROM WATER BY METAL-ORGANIC FRAMEWORKS

4.1: INTRODUCTION

Contamination of surface and ground water with herbicides is a major concern due to the hazards these chemicals pose to the environment and humans (Castro et al., 2009, Zhou et al., 2017, Sanderson et al., 2000). Atrazine, 6-chloro-N-ethyl-N'-(1-methylethyl)-1,3,5-triazine-2,4-diamine, is one of the most commonly used herbicides in agriculture and it is listed as an endocrine disrupting compound by the US Environmental Protection Agency (USEPA) (Environmental Protection Agency, 2015). As a result of extensive use, atrazine has been found in drinking water supplies and groundwater (Lemic et al., 2006, Chen et al., 2009). Moreover, some studies reported that atrazine was determined potentially carcinogenic because atrazine disrupt the endocrine hormone metabolism (Zhou et al., 2017) and has relatively long half-life (250 days) under light (Komtchou et al., 2016). The maximum atrazine concentration has regulated to 0.1 μg L^{-1} by the Directive 98/83 (Lima et al., 2009). Therefore, the removal of atrazine from environmental water has become of utmost importance.

The removal of atrazine from drinking water is known to be challenging and problematic.(Streat and Horner, 2000) Several conventional treatment techniques include coagulation/flocculation, filtration and chlorination have been employed for the removal of atrazine from water. While these conventional techniques do not effectively remove atrazine,(Brown et al., 2004, Broseus et al., 2009) advanced removal technologies; such as ozone-based oxidation (Broseus et al., 2009, Hua et

al., 2006) reverse osmosis, nanofiltration and adsorption (Snyder et al., 2007) have demonstrated to be promising. In particular, adsorption based removal of atrazine from water is attractive due to the ease of operation, low initial cost and the by-product-free removal process (Sotelo et al., 2014). Activated carbon (Paul Westerhoff, 2005), surface modified activated carbon (Chingombe et al., 2006), organo-zeolites (Lemic et al., 2006), clay minerals modified with a cationic surfactant (Sanchez-Martin et al., 2006), carbon nanotubes (Yan et al., 2008), surface oxidized multiwalled carbon nanotubes (Chen et al., 2008, Tang et al., 2012), activated carbon/iron oxide composites (Castro et al., 2009), zeolite-rich tuffs (Salvestrini et al., 2010) and a banana peel based sorbent (Chaparadza and Hossenlopp, 2012) have studied for the adsorptive removal of atrazine so far.

Metal organic frameworks (MOFs) are explained in detail in section 2.1. Exploring novel adsorbents for efficient removal of atrazine is still of great significance. In this study, three MOFs were considered for the removal of atrazine; ZIF-8 (Park et al., 2006), UiO-66 and UiO-67 (Cavka, 2008) due to their excellent water, chemical and thermal stabilities and also the most common used HKUST-1 (Chui et al., 1999) for comparison. Zeolitic imidazolate framework-8 (ZIF-8) is formed by zinc metal ions linked by 2-methylimidazole ligands and has 11.6 Å pores accessible through 3.4 Å apertures. UiO-66 and UiO-67 are isostructural Zr-based MOFs. UiO-66 is formed by hexanuclear zirconium ($Zr_6O_4(OH)_4$) clusters and 1,4 benzene-dicarboxylate (BDC) linker (Moreira et al., 2012, Cavka, 2008) which possess 11 Å octahedral pores and 8 Å tetrahedral pores which are accessed by apertures of 5 and 7 Å, respectively (Bárcia et al., 2011, Moreira et al., 2012). UiO-67 consists of a 4,4’ biphenyl-dicarboxylate (BPDC) linker instead of BDC,

and therefore presents larger pores compared to UiO-66 (i.e. 12 Å tetrahedral and 16 Å octahedral pores) (Chavan et al., 2012). HKUST-1 is formed by 1,3,5 benzenetricarboxylate (BTC) ligands coordinating copper ions in a cubic lattice which has large square-shaped pores of 9 Å by 9 Å. The chemical structure and physicochemical properties of atrazine as well as structural models of ZIF-8, UiO-66 and UiO-67 are given in **Figure 4-1 a**nd **Table 4-1,** respectively. As seen in **Table 4-1**, atrazine is a weak-base herbicide with having a pKa of 1.85. Its octanol-water partitioning coefficient is 2.67 which is attributed to the degree hydrophobicity of the compound. Given its higher $LogK_{ow}$ of 2.67, atrazine is considered as hydrophobic and is high likely to be adsorbed on the surface of adsorbent. MOFs are selected based on their chemical. thermal and stability, and pore size. For comparison purposes, a commercially available granular activated carbon, Filtrasorb-400 (F400) is also included.

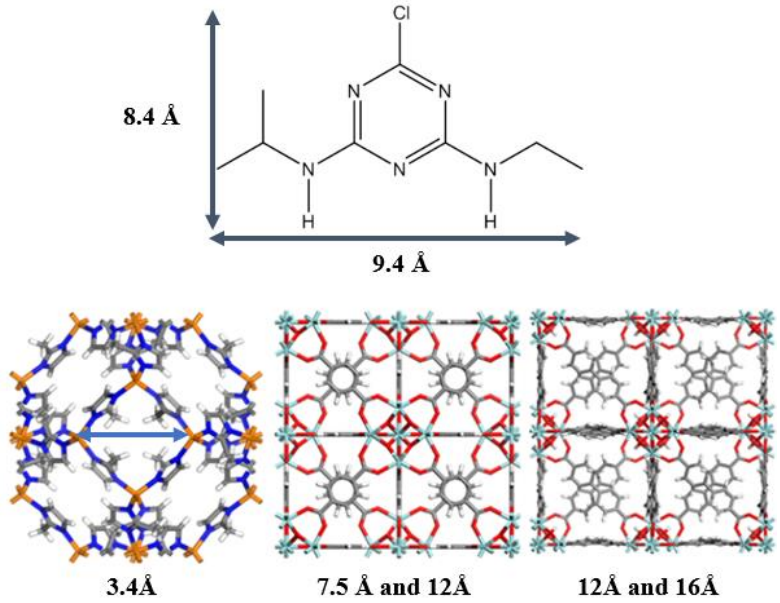

Figure 4-1 Chemical structure of atrazine (top) and the structural models of ZIF-8, UiO-66 and UiO-67 (bottom, from left to right). Colour code: carbon (black), oxygen (red), nitrogen (blue), zinc (orange) and zirconium (cyan).

Table 4-1 Physicochemical properties and molecular dimensions of atrazine

Chemical Formula	Solubility in water (mg L^{-1}) [a] at 25 °C	$LogK_{ow}$ [b]	pK_a [b]	Molecular Dimensions*
$C_8H_{14}ClN_5$	33	2.67	1.85	9.4x 8.4 x 3.2 Å

[a.](Streat and Sweetland, 1998, Streat and Horner, 2000), [b.](Nam et al., 2014) and **as measured with ChemBioOffice 2014-Chembiodraw3D (Cambridge Soft Corporation)*

4.2: MATERIALS AND METHODS

4.2.1: Chemicals

The chemicals in this chapter are given in Chapter 3 (see section 3.1). Atrazine is purchased from Cambridge scientific, UK and used without further activation.

4.2.2: Syntheses procedures of ZIF-8, UiO-66, UiO-67

The procedures of synthesis of MOFs, ZIF-8, UiO-66 and UiO-67 are the same as described in detail in Chapter 3 material and method (see section 3.2.1, 3.2.2 and 3.2.3, respectively).

4.2.3: Characterisation of the adsorbents

The crystallinity of ZIF-8, UiO-66 and UiO-67, was confirmed by powder X-ray diffraction (PXRD). The detail of PXRD measurements of the materials is given in section 3.3.1. N_2 adsorption measurements of ZIF-8, UiO-67, HKUST-1 and F400 were conducted on a Micromeritics Tristar porosity analyser and that of UiO-66 was performed on a Quantachrome Autosorb IQ MP physisorption analyser at 77 K to assess the Brunauer-Emmett-Teller (BET) surface area, total pore volume and

the pore size distribution. 100 mg of each sample were weighed and then degassed at 150°C for ZIF-8, UiO-67, HKUST-1 and F400 overnight and at 120°C for UiO-66 for 16 hours under high vacuum prior to analysis. In order to have enough sample 100 mg UiO-67 was used in the adsorption batch experiments for the confirmation of the stability in terms of the surface area and pore volume measurements and crystallinity after regeneration of UiO-67. The specific apparent surface areas were determined using the BET model in the range of $0.005<P/P_0<0.1$ and the pore size distribution of the studied MOFs and F400 were derived from the adsorption isotherms by density functional theory (DFT).

4.2.4: Adsorption Experiments

A stock solution of atrazine was prepared by dissolving 25 mg of atrazine in 1 L ultrapure water (18 M.Ω.cm) using ultrasonication followed by magnetic stirring until completely dissolved. The solutions of desired concentrations for calibration standards and batch adsorption experiments were obtained by diluting the atrazine stock solution with ultrapure water.

To first test the adsorption efficiency of the selected MOFs towards atrazine, 15 mg of 4 different MOFs (ZIF-8, UiO-66, UiO-67 and HKUST-1) and commercial granular activated carbon F400 were added to 25 mL of atrazine solution at an initial concentration of 25 mg L^{-1}. Based on the removal efficiency achieved by MOFs, the effect of adsorbents concentrations (UiO-66, UiO-67, ZIF-8 and F400) on the removal of atrazine was studied by adding 5 to 150 mg of each adsorbent to 25 mL of atrazine solution with an initial concentration of 25 mg L^{-1}. The glass vials with these solutions and adsorbents were placed in an incubator shaker

(SCQuip) and the solutions were shaken at 250 rpm for 24 hours at 25°C. Control experiments were also carried out without adding adsorbents to check the concentrations. The experiments were conducted in duplicates. After 24 hours, the control solution and samples were filtered through a syringe filter (cellulose membrane, 0.2 μm, Sartorius Minisart Syringe Filter). The atrazine initial and equilibrium concentrations were measured using an HPLC Shimadzu LC2010HT system which consists of a binary pump, a column thermostat, an auto sampler and a UV-Vis detector. The reverse phase HPLC column, C18 (Hichrom, ACE 5 C18, 150 mm x 4.6 mm, 5 μm particle) was used with a water/methanol mobile phase (45:55% v/v) at a flow rate of 1mL min^{-1}. The detector was set at 223 nm wavelength and the column temperature was set to 25°C.

Atrazine concentrations in the control solution and in the filtrate, were calculated by comparing the obtained peak area corresponding to atrazine with respect to the calibration standard. The efficiency of atrazine removal (in %) by the adsorbent was determined by the following equation:

$$\text{Removal } (\%) = \frac{C_0 - C_e}{C_e} * 100 \qquad (4-1)$$

where C_0 (mg L^{-1}) is the initial concentration and C_e (mg L^{-1}) is the residual concentration of atrazine in the stock solution and filtrate, respectively.

Adsorption isotherms of atrazine in ZIF-8, UiO-67 and F400 were measured. For this purpose, 15 mg of ZIF-8, F400 and UiO-67 were weighed into 25 mL of atrazine solution with initial concentrations between 2 and 25 mg L^{-1} in a glass vials. Samples containing adsorbent and the control sample (25 mL of atrazine solution without adsorbent) were then shaken at 250 rpm and 25°C for 24h in the

incubator shaker. Then the samples were filtered off with a syringe filter. HPLC was used to measure the initial and residual atrazine concentrations in water. Finally, the amount of adsorbed atrazine was calculated by using the mass-balance equation (**Equation 3-1**) is given in section 3.4.1 (Hasan et al., 2012b).

Freundlich, Langmuir and Langmuir-Freundlich adsorption models were considered to describe the isotherms. Langmuir-Freundlich (**Equation 3-4**) and their linearized forms of Freundlich (**Equation 3-5**) and Langmuir (**Equation 3-6**) and isotherm models are used, which are given in section 3.4.1

To study the adsorption kinetics of atrazine, an exact amount of ZIF-8, UiO-67 and F400 were separately weighed into glass vials which contained 25 ml atrazine solutions at an initial concentration of 25 mg L^{-1}. Afterwards, the glass vials were placed in the incubator shaker and were shaken at 250 rpm at 25°C. Samples were collected at frequent time intervals (2 min, 5 min, 10 min, 15 min, 30 min, 45 min, 60 min, 90 min and 120 min), filtered through a syringe filter and placed in vials to be analysed by HPLC to determine the concentration of the atrazine at any time in the solution. The amount of adsorbed atrazine on the adsorbents was calculated by using the following mass-balance relationship (**Equation 3-8**) is given in section 3.4.2.

To explore the adsorption kinetics in UiO-67 and ZIF-8 (kinetics of UiO-66 are omitted owing to its poor removal efficiency) the pseudo first order (Ho and McKay, 1998) and pseudo-second order kinetic models (Y.S. Ho, 1999) are calculated by **Equation 3-11** and **Equation 3-12**, respectively, and are represented in linearized form in section 3.4.2.

4.3: RESULTS AND DISCUSSION

4.3.1: Characterisation of the synthesised MOFs

The phase purity of the synthesised materials and the crystalline stability of UiO-67 after atrazine adsorption uptake were characterised by PXRD. **Figure 4- 2** shows the simulated and experimental PXRD patterns of UiO-67, UiO-66, ZIF-8 and HKUST-1 are in good agreement, which confirms their successful preparation. The crystal planes where the crystal grown were also obtained in Figure 4-2 with using planes calculation in Mercury software. The XRD patterns are the characteristic of the solid samples and used to identify the crystalline sample. Thus, **Figure 4-2** showed that the crystal planes of the synthesised samples matched well with the simulated patterns.

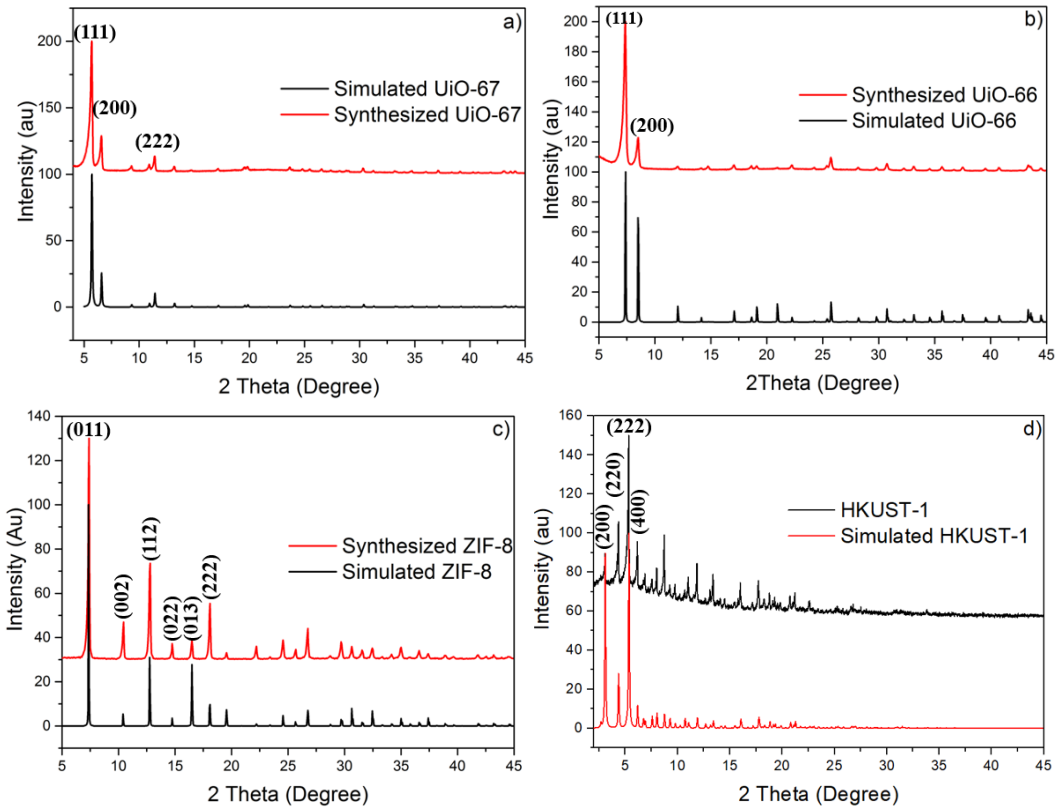

Figure 4-2 XRD patterns of UiO-67 a), UiO-66 b) and c) ZIF-8 and d) HKUST-1

N_2 adsorption isotherms at 77 K for UiO-67, UiO-66, ZIF-8, HKUST-1 and F400 are shown in **Figure 4-3.** From **Figure 4-3**, UiO-67, UiO-66 and ZIF-8 exhibited Type I isotherms with IUPAC characteristic, which is indicative of microporous materials. Also, in UiO-67 showed a small step at 0.1-0.2 relative pressure that is attributed to mesopores step. HKUST-1 showed Type IV isotherm with IUPAC characteristic hysteresis loop. BET surface areas and pore volumes are given in **Table 4-2**, and pore size distributions are presented in **Figure 4-4**. UiO-67 has the highest surface area and the pore volume among the four adsorbents, followed by ZIF-8, UiO-66, F400 and HKUST-1. Pore size distributions, which were determined by density functional theory (DFT) analysis, reveal that UiO-67 possess both micropores and mesopores (i.e. > 20 Å), whereas ZIF-8, UiO-66 and HKUST-1 possess only micropores **(Figure 4-4).**

Conventional t-plot methods from N_2 adsorption data were used to calculate the micropore pore volumes and micropore surface areas for the MOFs and F400. The t range was chosen over the range of 3- 5 Å for ZIF-8, UiO-66, 4-5 Å for HKUST-1 and 5.3-6.5 Å for UiO-67 by fitting the data to Harkins-Jura thickness equation (**Equation 2-3**). These range values of 5.3-6.5 Å for UiO-67 were chosen because UiO-67 exhibits mesoporous step at 0.1-0.2 P/P_0 in adsorption isotherm (Figure 4-3 (a)), the t range selected offers physically logical positive values for micropore volume whilst sustaining a correlation coefficient which is closest to 1 (Audu et al., 2016).

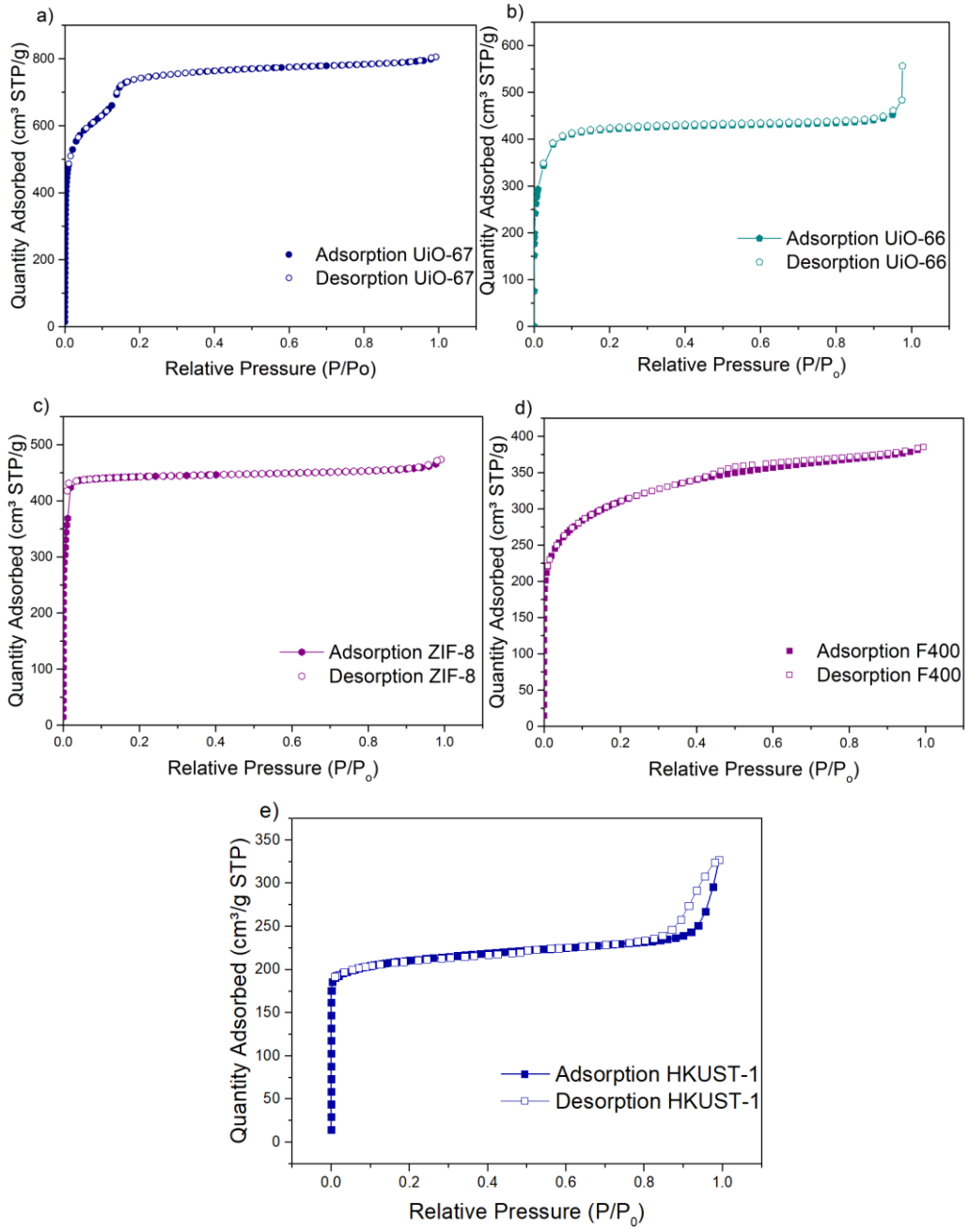

Figure 4-3 N_2 adsorption-desorption isotherm of a) UiO-67, b) UiO-66, c) ZIF-8, d) F400 and e) HKUST-1

Table 4-2 Surface and pore size characteristics of ZIF-8, UiO-66 and activated carbon (F400).

Materials	Surface Area, m^2/g^a	Total Pore Volume, cm^3/g^b	Micropore Volume, cm^3/g
ZIF-8	1875 ±8	0.714±0.006	0.660±0.014
UiO-66	1640 ± 5	0.656± 0.030	0.621± 0.025
UiO-67	2344 ± 7	1.249 ± 0.040	0.930 ± 0.016
HKUST (commercial)	825 ± 30.87	0.506± 0.035	0.281± 0.038
F400	1135± 20	0.584 ± 0.0.33	0.241± 0.030

[a] Calculated within 0.005-0.20 relative pressure (P/P_o) range, [b] Estimated at a relative pressure of 0.95

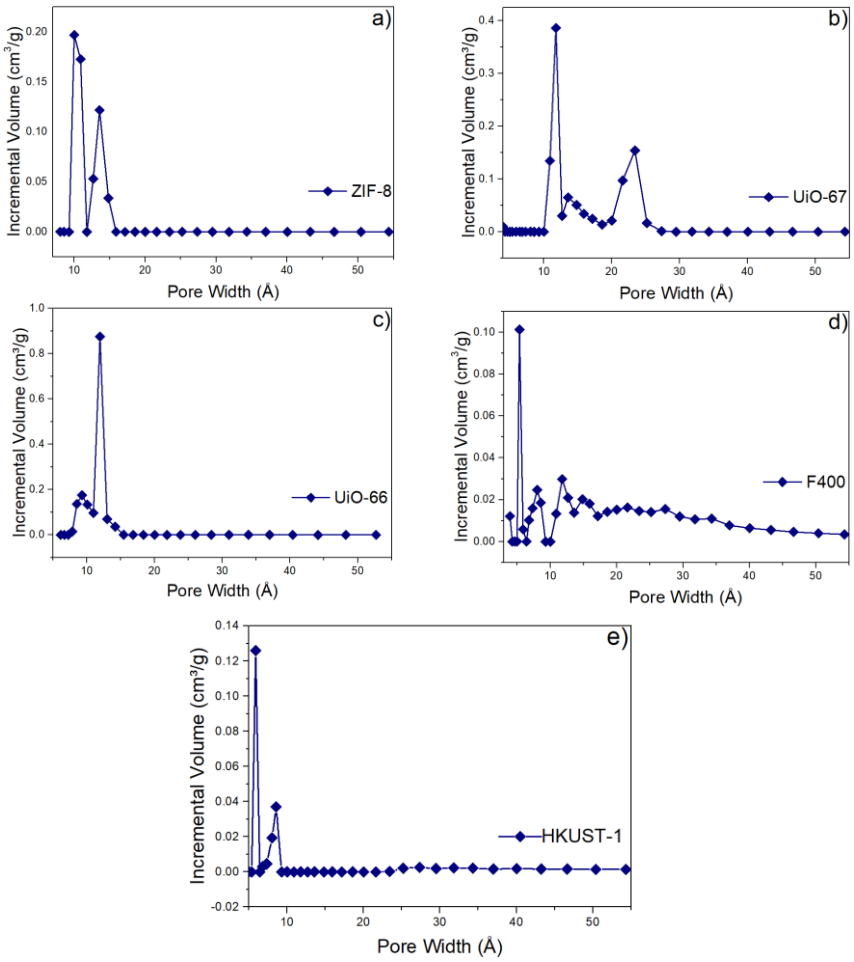

Figure 4-4 Pore size distributions of a) ZIF-8, b) F400, c) UiO-67 and d) UiO-66 and e) HKUST-1

Furthermore, the crystal shape of ZIF-8 **(Figure 4-5 a)** was observed as octahedral with sharp edges and both UiO-66 and UiO-67 were observed in spherical crystals which were the consistent with the literature (. **(Figure 4- 5 b and c)**. As also seen in SEM images in **Figure 4-5**, ZIF-8, UiO-66 and UiO-67 have close average particle sizes of 290 nm, 233 nm and 278 nm, respectively. As also seen in Figure 4-5 d, HKUST-1 has octahedral shape with average diameters of roughly 7 µm. The particle sizes of the MOFs were measured approximately by using Image-J software.

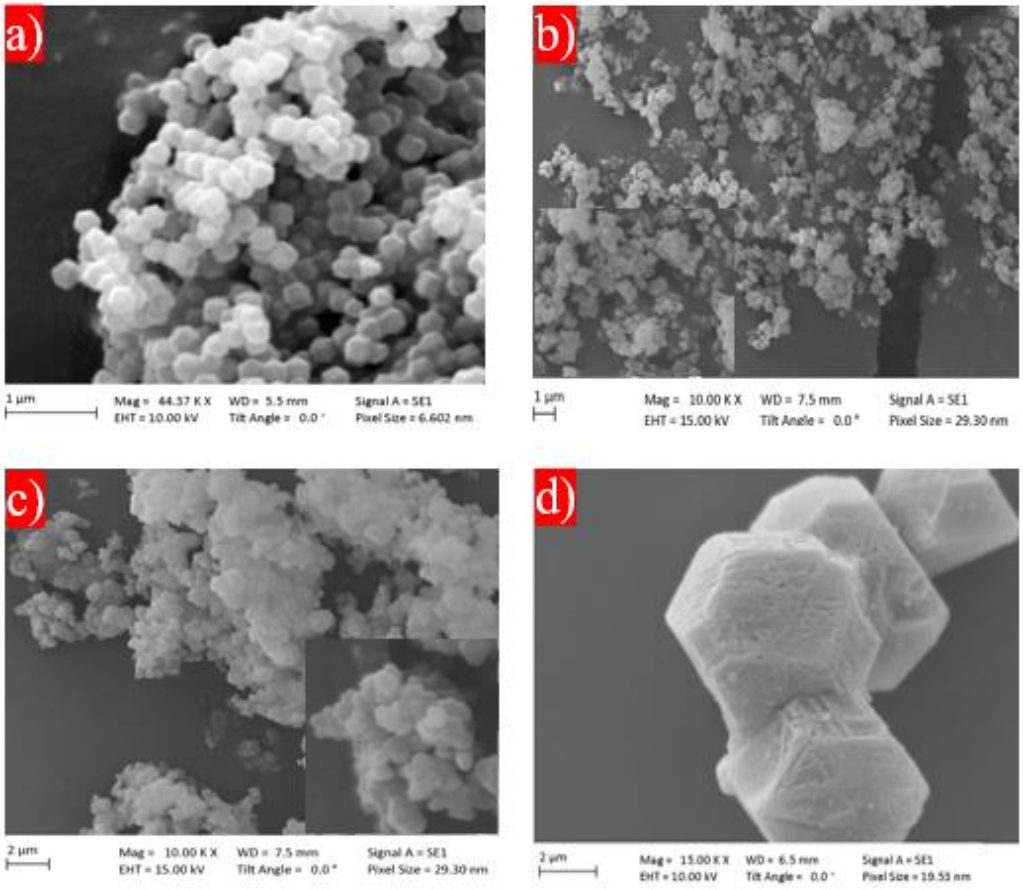

Figure 4-5 SEM images of (a) ZIF-8, (b) UiO-66, (c) UiO-67 and d) HKUST-1

4.3.2: Screening of MOFs and F400 for the removal of atrazine

Figure 4-6 shows the removal efficiency (Equation 4-1) of atrazine by using four various MOFs, UiO-66 and UiO-67, ZIF-8, and HKUST-1. The MOFs have different surface area and pore volume and commercial granular activated carbon F400 is also included for comparison. As seen in Figure 5, the highest removal efficiency was achieved by UiO-67 followed by activated carbon, ZIF-8, UiO-66 and HKUST-1. The removal of atrazine in MOFs might be attributed to not only the surface area and pore volume, but also the pore sizes and apertures of adsorbents. As expected, UiO-67 has the highest surface area and pore size and aperture compared to other adsorbents studied here, thus UiO-67 showed greater adsorption rate of atrazine than the other adsorbents. On the other hand, even though UiO-66 and ZIF-8 have higher surface area than that of F400, the removal efficiency is calculated to be less than that of F400 which may be ascribed to the small pore size and pore apertures of ZIF-8 and UiO-66. It is concluded that, the surface area, pore size and apertures play an important role in the adsorption of atrazine from water.

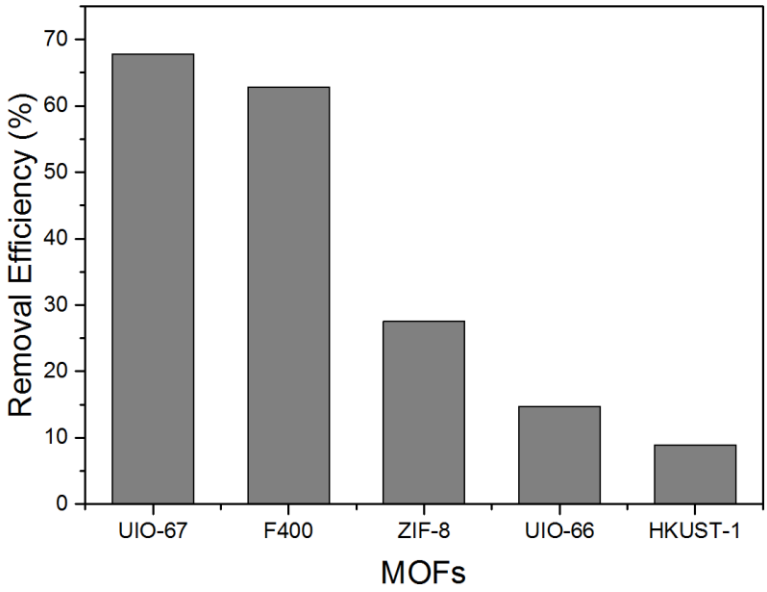

Figure 4-6 Removal efficiency of atrazine with different MOFs and F400 (15 mg each of adsorbents and initial concentration of 25 mg L^{-1} in 25 mL of solution. The experiments were repeated in duplicates and the mean of the values are given here.

4.3.3: Effect of Adsorbent Amount on the Removal of Atrazine

Figure 4-7 shows the removal efficiency of atrazine with increasing amounts of adsorbent in a 25 mg L^{-1} atrazine solution. At 2.4 mg mL^{-1} adsorbent concentration, both UiO-67 and F400 remove more than 90 % of atrazine; whereas, ZIF-8 removes 60% of the atrazine and UiO-66 removes 20% of the atrazine present in the solution. At 6 mg mL^{-1} adsorbent concentration, all adsorbents except UiO-66 remove 98% of the atrazine.

The effectiveness of UiO-67 compared to UiO-66 in removing atrazine may be attributed to the presence of pores in UiO-67 which are large enough to accommodate atrazine (Figure 2c and Table 2). On the other hand, although atrazine is not expected to enter the pores of ZIF-8 due to its narrow pore aperture, ZIF-8 effectively removes almost all atrazine from water. This may be due to the

hydrophobicity of ZIF-8 (Ghosh et al., 2014) which blocks water being adsorbed in significant amounts promoting atrazine adsorption possibly on the external surface. In contrast despite having a pore aperture comparable to the molecular dimensions of atrazine, UiO-66 is ineffective in the removal of atrazine from water. This may be attributed to the hydrophilic character of UiO-66 which leads to the filling of UiO-66's micropores with water and is no effective at removing atrazine from water even by surface interaction (Ebrahim et al., 2013, Ghosh et al., 2014).

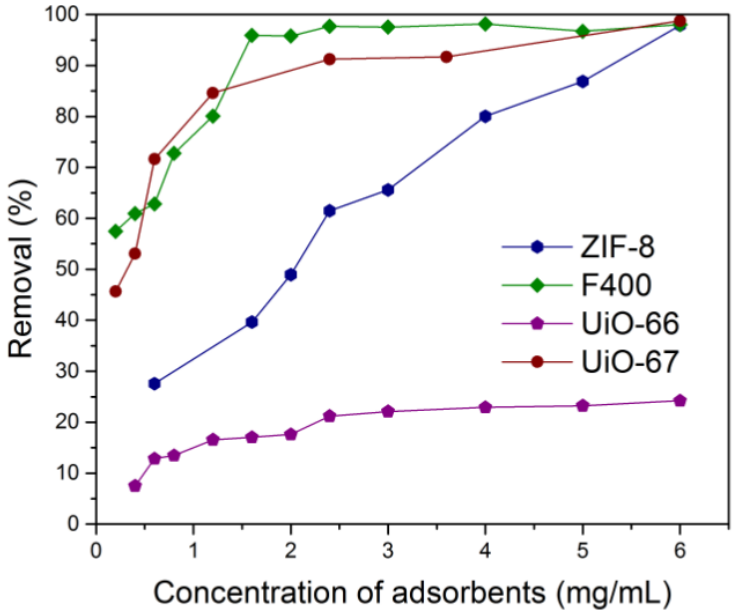

Figure 4-7 The effect of adsorbent amount on the removal efficiency of atrazine from water. Different adsorbent amount of MOFs and F400 were exposed to 25 mL of 25 mg L^{-1} of atrazine concentration. The experiments were repeated in duplicates and the mean of the values are given here.

4.3.4: Kinetics of Atrazine Adsorption

Adsorption of atrazine as a function of time was measured in ZIF-8, UiO-67 and F400 at an adsorbent concentration of 6 mg mL^{-1} (UiO-66 was not considered due to its poor removal efficiency). At this concentration, these three adsorbents

removed 98% of atrazine from the solution (**Figure 4-7**). **Figure 4-8** shows the percentage removal efficiency of atrazine as a function of time. UiO-67 removes atrazine much faster than the other two adsorbents, reaching 98% removal in just 2 minutes. In contrast, ZIF-8 removes only 46% of the atrazine in 2 minutes and requires 40 minutes to reach 98% atrazine removal. The removal kinetics of F400 was even worse with less than 20% atrazine removal in 2 minutes and requiring 50 minutes to reach 98% removal rate.

The kinetics of atrazine adsorption was analyzed by pseudo first order and pseudo second order models **(Figure 4-9).** The calculated kinetic parameters and correlation coefficients are given in **Table 4-3.** Kinetics of atrazine adsorption in UiO-67 and ZIF-8 are well represented by the pseudo second order model with high correlation coefficients (R^2) of 0.9999 and 0.987, correspondingly. Moreover, as seen in Table 2, the calculated Q_e values (adsorbed amount in mg of atrazine per g of both UiO-67 and ZIF-8) by the pseudo second order model are almost same with the experimental Q_e adsorbed amount with high correlation coefficient (R^2) of 0.999. On the other hand, the calculated Q_e values by the pseudo first order model are significantly less than the experimental Q_e as well as having low correlation coefficients **(Table 4-3)**. Therefore, the pseudo second order kinetic model suggests that possible chemisorption of atrazine in UiO-67 and ZIF-8 may be involved. (Zhu et al., 2015, Han et al., 2017). On the other hand, kinetic data of atrazine adsorption in F400 was better represented by the pseudo first order model **(Figure 4-9c).**

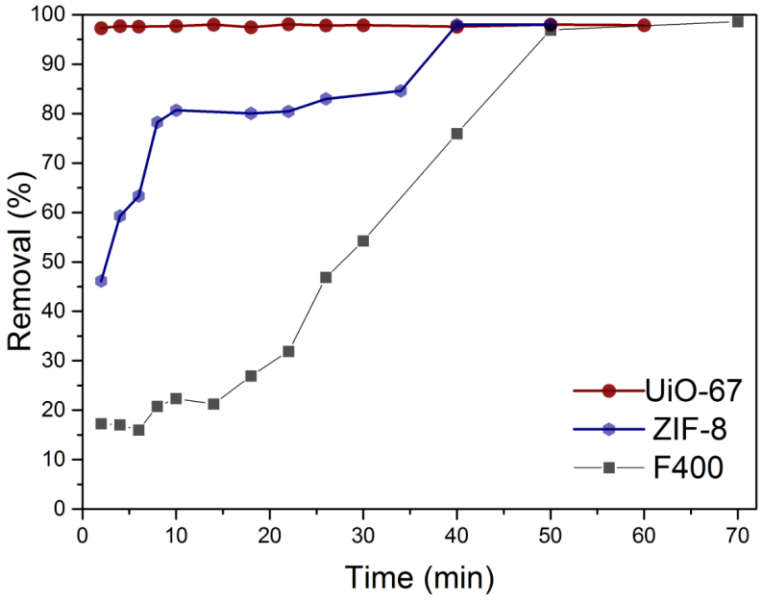

Figure 4-8 Removal efficiency as a function of time (150 mg of adsorbents was placed in contact with 25 mL solution of an initial atrazine concentration of 25 mg L^{-1}) (Error bars are too small.)

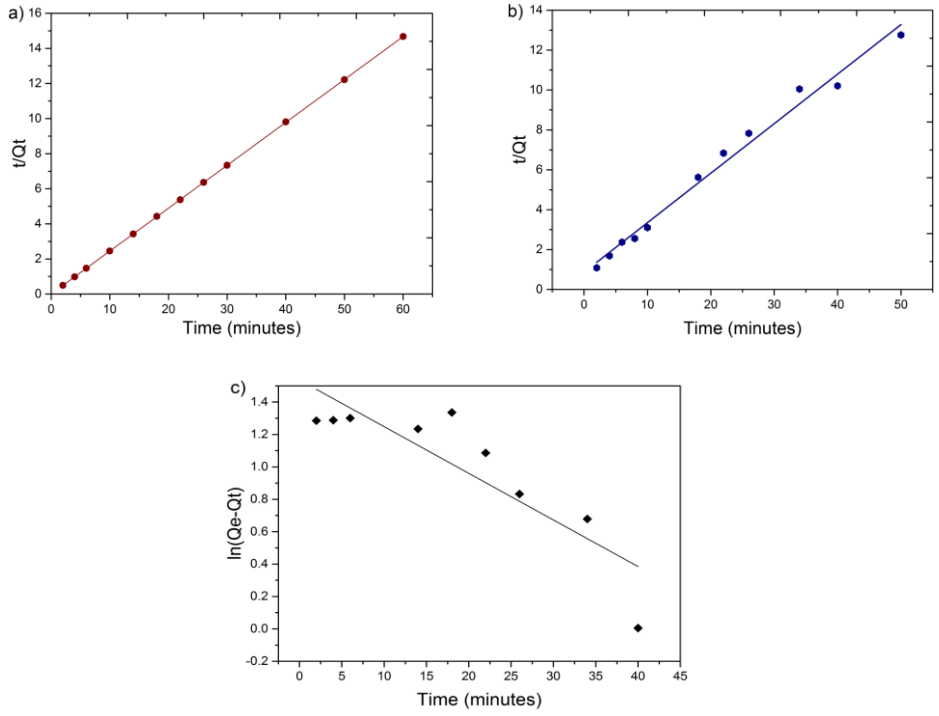

Figure 4-9 Pseudo-second order kinetic model fit in a) UiO-67, b) ZIF-8 and pseudo first order kinetic model fit in c) F400

Table 4-3 Kinetic parameters for pseudo-first and pseudo-second order model.

Adsorbent	Experimental	Pseudo First Order Kinetic Model			Pseudo Second Order Kinetic Model		
	$Q_{e\ (exp.)}$ (mg g^{-1})	k_1 (min^{-1})	$Q_{e\ (calc.)}$ (mg g^{-1})	R^2	k_2 (g mg^{-1} min^{-1})	$Q_{e\ (calc.)}$ (mg g^{-1})	R^2
UiO-67	4.09	0.0068	0.047	0.187	17.58	4.09	1.00
ZIF-8	4.00	0.122	3.64	0.538	0.071	4.02	0.98
F400	4.3	0.028	4.64	0.765	0.105	2.08	0.59

4.3.5: Adsorption Isotherms of Atrazine

Adsorption isotherms of atrazine on UiO-67, ZIF-8 and F400 are given in **Figure 4-10**. Adsorption equilibrium data were fitted to different isotherm models mentioned in the methodology section. As seen in **Table 4-3,** isotherm model parameters, Freundlich model gives the best fit for atrazine adsorption in UiO-67, while Langmuir-Freundlich model and Langmuir model give the best fits for ZIF-8 and F400, respectively. Freundlich adsorption constant of UiO-67 is higher than the other adsorbents studied here, which shows that intensity of the adsorption affinity of the adsorbent towards analyte. Within the atrazine concentration range studied, the gravimetric adsorption capacity of UiO-67 and F400 are about 2.5 times larger than that of ZIF-8 **(Figure 4-10).** ZIF-8 has a larger total pore volume than F400; however, it adsorbs much less atrazine. This is because of the narrow pore aperture of ZIF-8 (3.4 Å) which is small to accommodate atrazine **(Table 4-1)**; therefore, atrazine is expected to only be being adsorbed on the surface. While F400 and ZIF-8 isotherms reach saturation, it is clear that the UiO-67 isotherm is far from saturation and can adsorb more atrazine thanks to its larger pore volume compared to F400 and ZIF-8. Due to the low solubility of atrazine in water it is not

possible to prepare solutions with higher equilibrium concentrations to probe the maximum atrazine adsorption capacity of UiO-67.

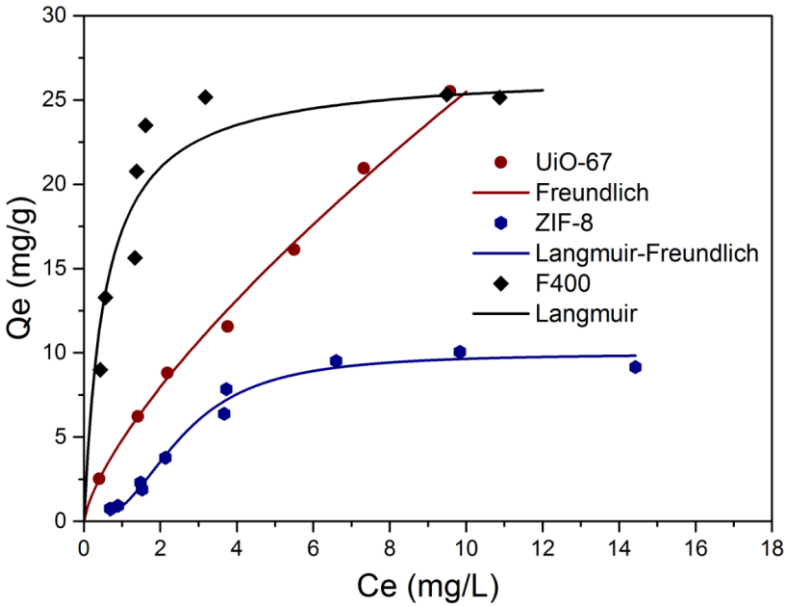

Figure 4-10 Adsorption isotherm of atrazine in UiO-67, ZIF-8 and F400 and the Freundlich model, Langmuir-Freundlich and Langmuir adsorption model fit for UiO-67, ZIF-8 and F400, respectively.

Table 4-4 Langmuir-Freundlich, Langmuir and Freundlich adsorption isotherms fitting parameters of atrazine on UiO-67, ZIF-8 and F400.

Isotherm Models	**Langmuir Parameters**			**Freundlich Parameters**			**Langmuir-Freundlich Parameters**			
Adsorbents	**Q_m (mg g^{-1})**	**K_L (L mg^{-1})**	**R^2**	**K_F (mg g^{-1} (L $mg^{-1})^{1/N}$**	**1/N**	**R^2**	**K_L (L mg^{-1})**	**Q_m (mg g^{-1})**	**N**	**R^2**
UiO-67	26	0.263	0.991	**4.82**	**0.72**	**0.997**	$9.15*10^{-4}$	4645	0.76	0.993
ZIF-8	14.77	0.18	0.88	2.03	0.70	0.811	**0.097**	**9.95**	**2.50**	**0.978**
F400	**26.7**	**1.82**	**0.995**	15.4	0.27	0.705	2.06	26.01	1.51	0.862

*Q_m (mg g^{-1}) maximum adsorption capacity, K_L (L mg^{-1}) Langmuir constant rate and K_F (mg g^{-1} (L $mg^{-1})^{1/N}$ Freundlich constant rate

**Experimental Data were fitted to Langmuir-Freundlich adsorption isotherm by using Origin Pro 9.1

4.3.6: Effect of pH on Adsorption of Atrazine

Table 4-5 shows the change in the amount of atrazine adsorbed with respect to varying pH which was obtained by 50 mg of each adsorbent added in to 25 mL atrazine solution at an initial concentration of 25 mg L^{-1}. It was found that the pH of the solution does not have a significant effect on atrazine adsorption. This may be due to the fact that the neutral form of atrazine in aqueous solution is dominant over the protonated form (Salvestrini et al., 2010). Overall the insensitivity of the atrazine adsorption to the changes in pH indicates that the adsorption of atrazine is not governed by electrostatic interaction, but rather hydrophobic interactions and π-π interactions between the heterocyclic rings of atrazine and the aromatic carbons in the ligands of ZIF-8 and UiO-66 and graphene layers of F400. In a similar experimental study of adsorption of micropollutants (including atrazine) in activated carbon, Nam et al. (2014) pointed out that hydrophobic interaction between micropollutants and activated carbon is the dominant mechanism of adsorption for hydrophobic compounds (Nam et al., 2014).

Table 4-5 The effect of pH on atrazine adsorption by the studied MOFs and F400.

pH	Adsorbed Amount (mg atrazine / g adsorbent)			
	ZIF-8	**UiO-66**	**UiO-67**	**F400**
2.8	6.27	2.69	10.45	12.28
4.5	6.28	2.02	11.87	12.09
6.9 (initial pH)	6.78	2.57	10.96	13.73
8.9	6.19	1.71	10.04	11.53
9.8	6.69	1.89	10.95	12.64

4.3.7: Regeneration and Stability of UiO-67

In order to probe its reusability, UiO-67 was regenerated by washing with copious acetone and stirring at 25°C and 250 rpm followed by heat activation at 90°C. Three consecutive atrazine adsorption/desorption cycles were conducted and regenerated UiO-67 showed no significant decrease in adsorption capacity compared to fresh UiO-67. At the end of the third adsorption cycle UiO-67 lost less than 10% of its original adsorption capacity **(Figure 4-11**). Upon regeneration of UiO-67, minimal loss of adsorption capacity was observed, affirming its effective use several times for atrazine removal from water. To further investigate the stability of regenerated UiO-67 to the process, N_2 adsorption-desorption isotherms of UiO-67 regenerated via washing with acetone were measured **(**

Figure 4-12**a).** As seen in

Figure 4-12**a,** the BET surface area was not significantly changed after regeneration in acetone indicating that adsorbed atrazine was successfully desorbed, and the textural properties were retained. PXRD pattern observed for atrazine adsorbed UiO-67 upon solvent exchange to acetone from water followed by thermal activation at 90°C was identical to the starting materials (Figure 12b). These results suggest that the crystallinity of UiO-67 was maintained under the conditions studied and for comparison, the simulated PXRD pattern of UiO-67 was also included. Moreover, SEM images of UiO-67 before adsorption of atrazine and regenerated UiO-67 in acetone after adsorption of atrazine confirms that no morphology change was observed in regenerated UiO-67 **(Figure 4-13).** Overall, the regenerated UiO-67`s crystallinity, textural properties and morphology were

pleasingly retained without collapsing the structure, which suggests that UiO-67 has potential for atrazine removal from water.

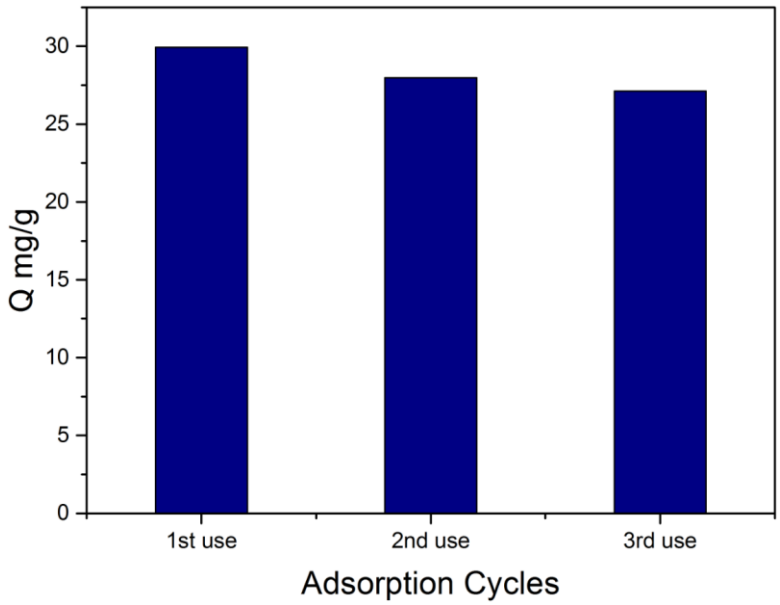

Figure 4-11 Reusability of UiO-67 for atrazine removal after acetone washing (Ci= 25 mg L^{-1} and 15 mg adsorbent)

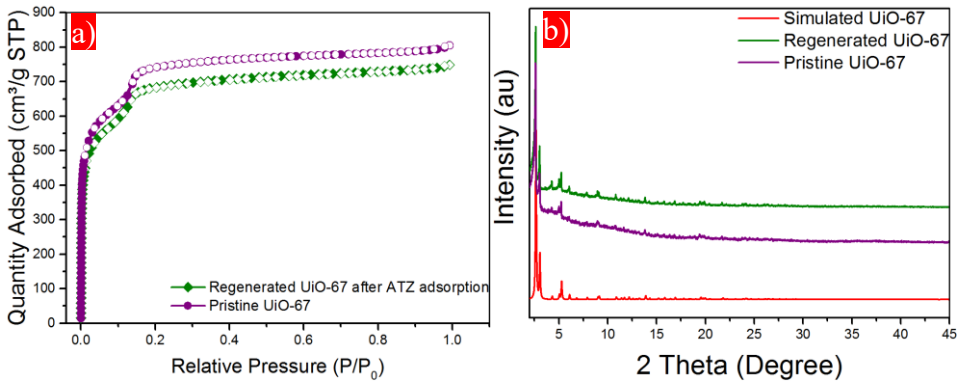

Figure 4-12 (a) N_2 adsorption-desorption isotherms of prepared UiO-67 and regenerated UiO-67 in acetone followed by thermally activated and (b) PXRD patterns of starting UiO-67 before adsorption of atrazine, regenerated after atrazine adsorption and the simulated PXRD pattern of UiO-67 is also included for comparison.

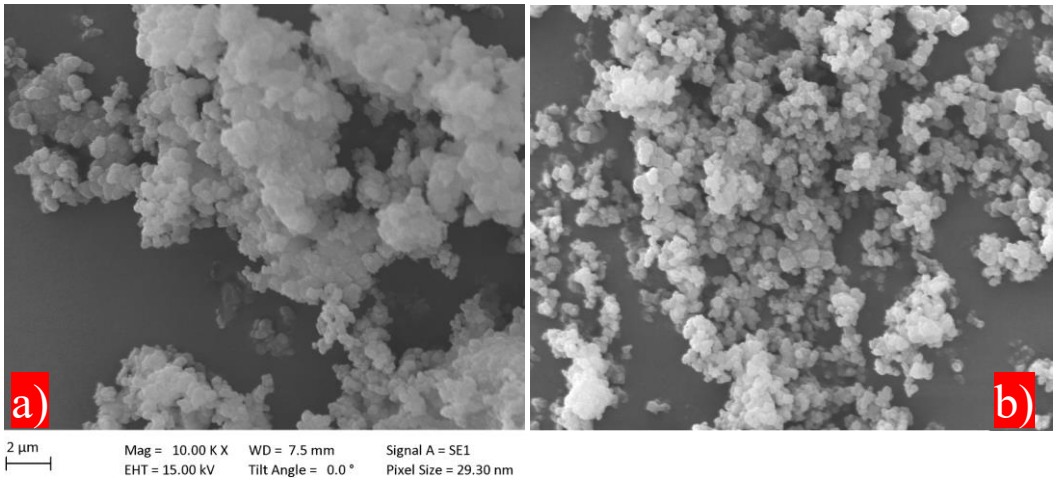

Figure 4-13 SEM images of (a) pristine UiO-67 before atrazine adsorption and (b) regenerated UiO-67 after atrazine adsorption

4.4: CONCLUSIONS

Three highly porous and water stable MOFs; ZIF-8, UiO-66 and UiO-67 and the most known HKUST-1 were explored for the adsorption of atrazine from water in comparison with a commercial activated carbon, F400. UiO-67 was found to exhibit the fastest rate of atrazine removal, and removed 98% of atrazine from water in just 2 min. In contrast, it took ZIF-8 40 min and F400 50 min to reach the same 98% removal of atrazine from water. Moreover, regenerated UiO-67 maintained most of its atrazine adsorption capacity after the third use. Considering its rapid atrazine uptake, comparable adsorption capacity to commercial F400 and its regenerability without significant loss of adsorption capacity, UiO-67 can be considered as a promising adsorbent for the removal of atrazine from water.

Chapter 5: RAPID AND EFFICIENT REMOVAL OF CARBAMAZEPINE FROM WATER BY UIO-67

5.1: INTRODUCTION

Carbamazepine, is known as 5H-dibenzo[b,f]azepine-5-carboxamid, has been extensively used as an antiepileptic and antipsychotic drug and detected in wastewater treatment effluents, surface waters, groundwater and drinking water.(Zhang et al., 2010) It is a persistent organic compound in the environment (Zhang et al., 2010) and toxic to the aquatic system (Zhang et al., 2008, Suriyanon et al., 2013, Wei et al., 2013, Domínguez-Vargas et al., 2013). It is resistant to biodegradation and barely removed during conventional and biological wastewater treatments (Gebhardt and Schroder, 2007, Clara et al., 2005, Kosjek et al., 2009).

Carbamazepine is also one of the six pharmaceuticals detected at high concentrations above the limit of detection (10-100 ng/L) in UK drinking water sources as well as in treated drinking water (Boxall et al., 2012). The maximum concentrations of carbamazepine measured in some European drinking water sources were reported as 20 ng/L (Germany), 70 ng/L (Finland), 75 ng/L (Austria), 78 ng/L (France) and 30-150 ng/L (Switzerland) ((WHO), 2012).

Advanced treatment technologies studied for carbamazepine removal from aqueous solution include ozonation (Ternes et al., 2002, McDowell et al., 2005), ultrafiltration (Clara et al., 2005)**,** oxidation (Hu et al., 2009) and photo catalytic degradation (Haroune et al., 2014). Photo catalysis and ozonation generate various byproducts and the effects of these derivatives are uncertain and they can be more persistent to biological degradation. (McDowell et al., 2005, Haroune et al., 2014).

Adsorption on porous materials is considered as an alternative technique in order to remove organic contaminants from water thanks to its low cost, ease of operation and practically no risk of releasing toxic byproducts to the environment.(Wang et al., 2015, Han et al., 2017) Clays, (Zhang et al., 2010), silica-based porous materials, (Bui and Choi, 2009, Suriyanon et al., 2013) carbon nanotubes, (Oleszczuk et al., 2010, Lerman et al., 2013, Wei et al., 2013) activated carbon, (Yu et al., 2008, Nielsen et al., 2014) mesoporous silica and functionalized polymers, (Dai et al., 2013) zeolites (Cabrera-Lafaurie et al., 2014) and biochar (Chen et al., 2017) are adsorbents which have been previously studied for carbamazepine removal from aqueous solutions with limited success. There has been much research over the last past several years have been assigned to the preparation of MOFs and their potential applications in many various areas such as gas storage, catalysis, sensing, the removal of hazardous organic compounds from air and water and drug delivery. MOFs have offered high adsorption capacity for the liquid phase adsorption (Khan et al., 2013b, Dias and Petit, 2015, Hasan and Jhung, 2015) due to active vacancy sites and tunable textural (i.e. surface area, porosity, pore size etc.) and chemical functionality properties. Therefore, the removal of a number of PPCPs were achieved by MOFs which makes MOFs to be considered as potential promising adsorbents (Hasan et al., 2012a, Hasan et al., 2013, Bhadra et al., 2017, Seo et al., 2016a, Hasan et al., 2016b, Wang et al., 2016a, Seo et al., 2017) herbicides and pesticides.(Zhu et al., 2015, Seo et al., 2015a, Wei et al., 2016).

In this chapter, two zirconium-based isostructural MOFs, UiO-66 and UiO-67, for carbamazepine removal from water owing to their exceptional chemical, thermal, and water stability (DeCoste et al., 2013, Mondloch et al., 2014, Howarth et al., 2016). Zr based MOFs, UiO-66 and UiO-67, and F400 were proposed to use

as adsorbents for the uptake of carbamazepine in aqueous media. Commercial granular activated carbon Filtrasorb 400 (F400) is used because it is commonly used for water treatment applications. In **Table 5-1**, chemical structure and physicochemical properties of carbamazepine are represented. Carbamazepine has a pKa of 13.9 and is found to be neutral in the range of pH 2-13.9. The octanol-water partitioning coefficient of carbamazepine is 2.45 showing that the degree hydrophobicity, hence carbamazepine is slightly soluble in water (112 mg L^{-1} at 25 ^{o}C). Octanol-water coefficient is slightly close to 2.5 indicating that carbamazepine tends to be adsorbed on the adsorbent.

Table 5-1 Chemical structure and physicochemical properties of carbamazepine

Compound	**Structure**	**Molecular Weight**	**Solubility in water at 25 ˚C [a]**	**LogKow [b]**	**pKa [c]**
Carbamazepine $C_{15}H_{12}N_2O$	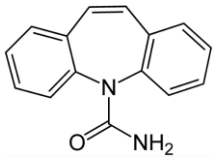	236.27	112	2.45	13.90

[a] carbamazepine solubility in water (Liu et al., 2014) [b] log-transformed octanol-water partition coefficient; [c] acid dissociation constant

5.2: EXPERIMENTAL METHODS

5.2.1: Materials

The materials used in this chapter are the same as those used in Chapter 3 (see section 3.1). Carbamazepine is purchased from Sigma Aldrich, UK and used as received.

5.2.2: Synthesis and Characterisation of adsorbents

The procedures of synthesis of MOFs, UiO-66 and UiO-67 are the same as described in detail in Chapter 3 (see section 3.2.2 and 3.2.3, respectively).

Powder X-Ray Diffraction (PXRD) patterns of the materials were obtained by a Stoe Stadi-P and the detail of measurements is given in section 3.3.1. PXRD was used to confirm the crystallinity of the synthesized isostructural UiO-66 and UiO-67 crystals and the stability of regenerated UiO-67.

In order to evaluate the BET surface areas, total pore volumes, micropore volumes and the pore size distributions, N_2 adsorption/desorption measurements of UiO-66 was performed on Quantachrome Autosorb IQ MP Physisorption analyzer and both UiO-67 and F400 were conducted on Micromeritics Tristar porosity analyzer at 77 K. Prior to analysis, UiO-66 was outgassed at 120 °C for 16 hours and UiO-67 and F400 were outgassed at 150 ºC overnight under vacuum. At least 70 mg of sample was used in measurements. The specific surface areas were calculated using BET method at the range of 0.005-0.2 relative pressure range. The pore size distributions of the adsorbents were derived by density functional theory (DFT) using the carbon slit pore N_2-DFT model. The micropore volumes of all materials were calculated using the t plot method from N_2 adsorption isotherm (Audu et al., 2016).

SEM images were recorded on a Zeiss evolution MA10 SEM to assess the morphology and particle size of adsorbents. Samples were firstly coated with a thin layer of gold for conductivity and then operated in beam mode at a 15kV of acceleration voltage.

5.2.3: Liquid phase adsorption experiments:

A 100 mg L^{-1} carbamazepine stock solution (Sigma Aldrich) was obtained by dissolving carbamazepine in ultrapure water (18 M.Ω.cm) by ultrasonication until completely dissolved. Initial concentrations have chosen based on their detection by analytical equipment before and after the uptake. Moreover, as a proof of concept, batch exposure experiments were started with the highest amount that can be soluble in water. Verification of the uptake by MOFs at even high concentrations can yield an insight to the adsorptive removal of various analytes. The working solution concentrations for batch adsorption experiments were obtained with diluting the carbamazepine stock solution with ultrapure water. The initial and equilibrium carbamazepine concentrations in solutions were measured using a UV-visible spectrophotometer (Perkin Elmer, Lambda 950) according to the maximum absorbance at 285 nm of wavelength.

5.2.4: Initial comparison of adsorbents for carbamazepine adsorption:

6 mg of UiO-66, UiO-67 and F400 were introduced separately in to 5 mL aqueous solutions of carbamazepine with 100 mg L^{-1} initial concentration. The carbamazepine solutions with adsorbents were shaken at 25°C at the speed of 250 rpm for 24 hours in an incubator shaker to ensure equilibrium was obtained. All experiments were performed in triplicate and the mean values are reported. Control experiments without adsorbents were also carried out to measure the initial concentration. The supernatants were separated from the adsorbents using a syringe filter (0.2 μm cellulose acetate membrane). The percentage removal of carbamazepine was calculated by using Equation 4-1.

5.2.5: Effect of adsorbent concentration on carbamazepine adsorption

The effect of adsorbent amount on the removal efficiency was studied by introducing 3 mg, 6 mg, 9 mg, 10 mg and 12 mg of adsorbents into 5 mL of aqueous solution with 100 mg L^{-1} carbamazepine concentration. Then the vials were placed in an incubator shaker and shaken at 250 rpm and 25°C for 24 hours. Control samples without adsorbents were also included.

5.2.6: Kinetics of carbamazepine adsorption:

The adsorption kinetic studies on the removal of carbamazepine from water were performed by placing 48 mg of adsorbents in 40 mL carbamazepine solutions with an initial concentration of 100 mg L^{-1}. Afterwards the solutions were shaken at 250 rpm at 25 °C. The supernatants were collected at predetermined time intervals using a syringe filter (0.2µm, cellulose acetate membrane). Kinetic experiments were carried out in triplicate and the results reported here are the mean values. The amount adsorbed (Qt) in mg of analyte per g of adsorbent as a function of time was calculated by using **Equation 3-8.**

The experimental data were fitted to Lagergren pseudo-first order (**Equation 3-11**) or pseudo-second order linear kinetic model (**Equation 3-12**) (Ho and McKay, 1999) to describe the kinetic rate constant of the system.

5.2.7: Adsorption isotherms of carbamazepine:

6 mg of UiO-67, UiO-66 and F400 were placed separately in contact with 5 mL of carbamazepine solutions with concentrations in the range of 5-100 mg L^{-1} and shaken at 250 rpm and 25°C for 24h. The supernatant was separated from

adsorbents by filtering off with 0.2µm cellulose acetate syringe filter. The adsorbed amounts of carbamazepine were calculated by using **Equation 3-1.**

Adsorption isotherm models Freundlich (Freundlich, 1906) and Langmuir (Langmuir, 1916) in their linearized forms were fitted to experimental data, which are given in **Equations 3-5 and 3-6.**

5.2.8: Effect of pH on carbamazepine adsorption:

To investigate the effect of pH on the adsorption of carbamazepine, 0.01 M hydrochloric acid (HCl, 36.5-38 %, Sigma Aldrich) or 0.01 M sodium hydroxide solution (NaOH, Sigma Aldrich) was used to adjust the pH of carbamazepine solutions. 6 mg of UiO-67 and UiO-66 were introduced to 5 mL of solutions with an initial concentration of 100 mg L^{-1} for 24 hours at 25 °C. The adsorption capacities of UiO-67 were recorded as a function of pH.

5.2.9: Regeneration of UiO-67

The spent UiO-67 was soaked in acetone and shaken at 25 °C for 6 h and then supernatant was removed and re-soaked in fresh acetone and re-shaken at 25 °C followed by removal of the acetone. Finally, the adsorbent was dried at 90°C overnight under vacuum. The regeneration of UiO-67 was repeated for at least six times following the above procedure prior to each adsorption.

5.3: RESULTS AND DISCUSSION

5.3.1: Characterisation of adsorbents:

Figure 5-1 shows that the PXRD patterns of the synthesized UiO-67 and UiO-66 are in good agreement with the simulated patterns which confirms the crystallinity. **Figure 5-2** shows the N_2 adsorption–desorption measurements in all adsorbents studied and their respective pore size distributions as a function of pore width. BET surface areas and pore volumes of UiO-67, UiO-66 and F400 are given in **Table 5-2**. UiO-67 has the highest specific surface area and the total pore volume among the three adsorbents, followed by UiO-66 and F400. UiO-67 and F400 possess both micropores and mesopores (i.e. > 20 Å), whereas UiO-66 has only micropores. Because UiO-66 and UiO-67 were synthesized with the missing linkers' route they both exhibit pores slightly larger compared to those found in the defect free UiO-66 and UiO-67 (Audu et al., 2016). Finally, according to the SEM images given in **Figure 5-3,** UiO-66 and UiO-67 have similar average particle sizes, 0.233 μm and 0.278 μm, respectively, whereas F400 has a much larger average particle size of around 24 μm (Figure 16c). The particle size analysis was obtained by using Image J analysis. At least 20 particles were selected, measured their particle size by using Image J and finally average particle size value of these chosen particles was reported here.

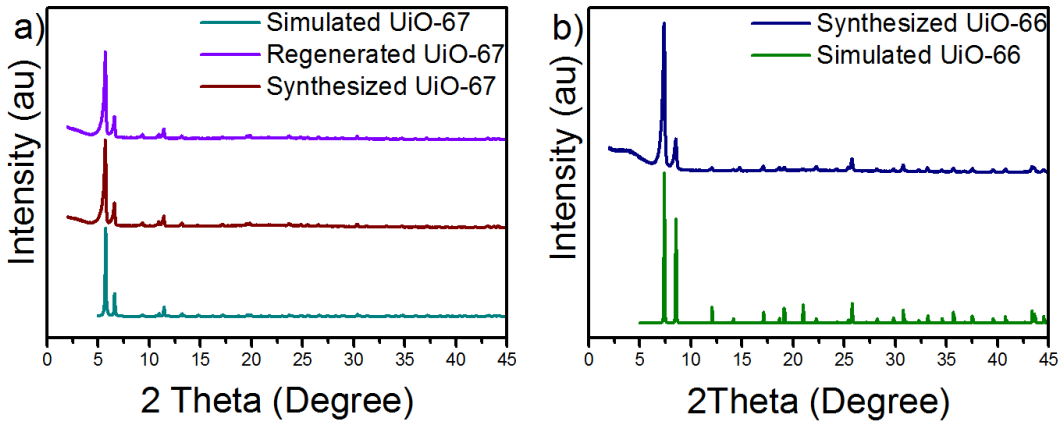

Figure 5-1 PXRD patterns of UiO-67 (a) and UiO-66 (b)

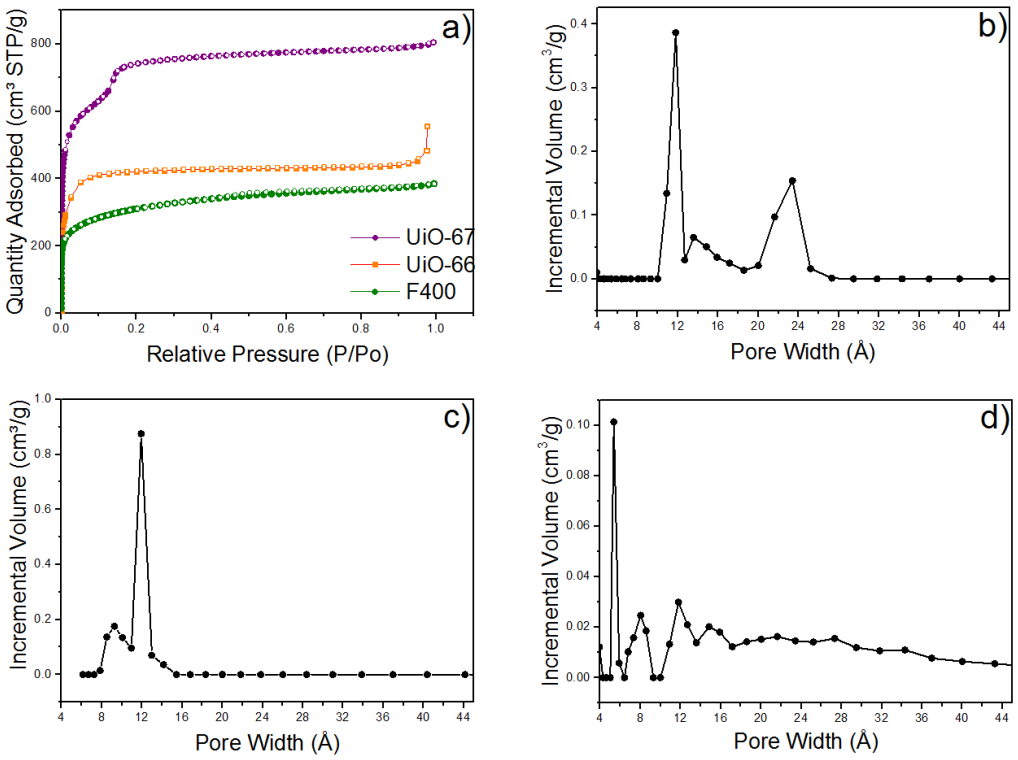

Figure 5-2 a) N_2 adsorption-desorption isotherms at 77 K for UiO-67, UiO-66 and F400 (filled and empty symbols are represented for adsorption and desorption, respectively) and pore size distribution and pore volumes of b) UiO-67, c) UiO-66, d) F400

Table 5-2 Surface area and pore volume properties of UiO-66, UiO-67 and F400.

Materials	Specific Surface Area, $m^2 g^{-1}$	Total Pore Volume, $cm^3 g^{-1}$	Micropore Volume $cm^3 g^{-1}$
UiO-67	2560	1.069	0.938
UiO-66	1640	0.656	0.621
F400	1135	0.485	0.241
Regenerated UiO-67	2300	1.005	0.885

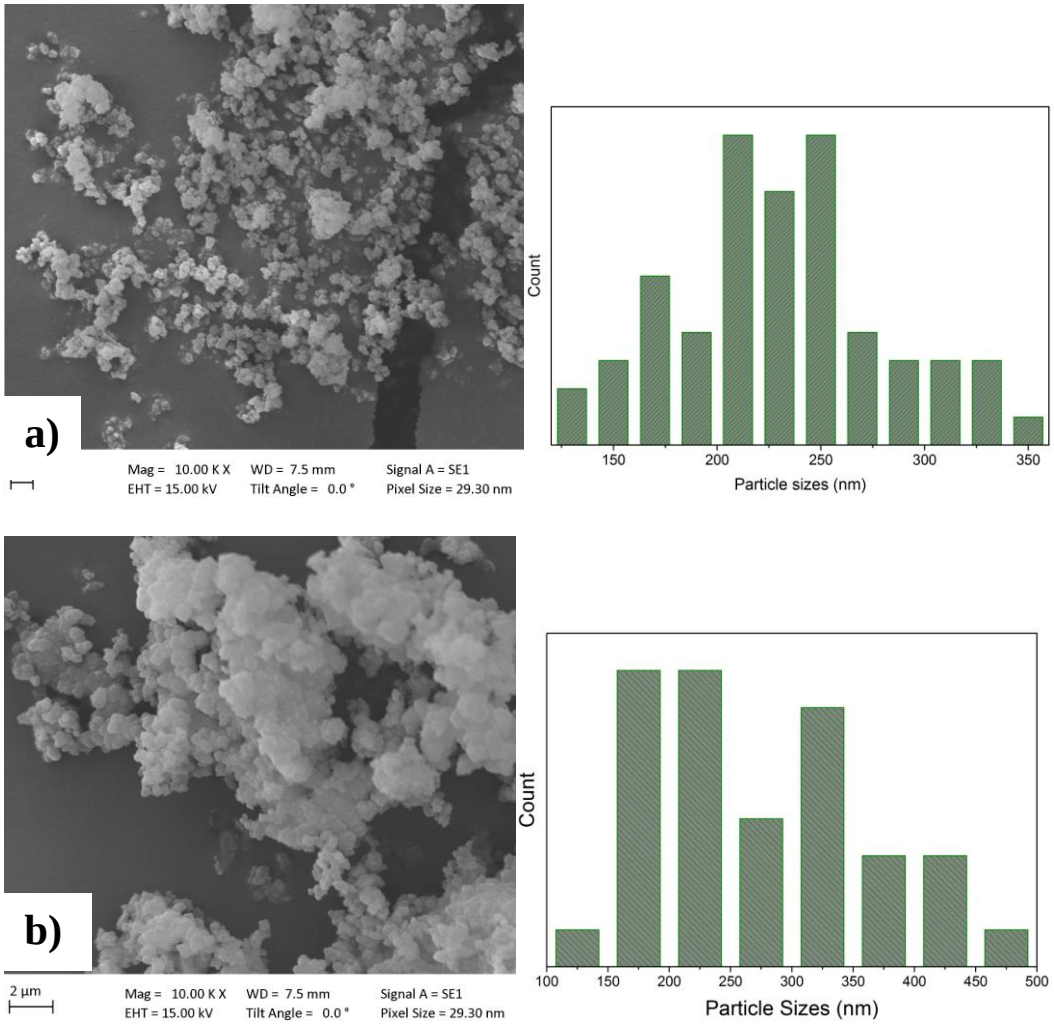

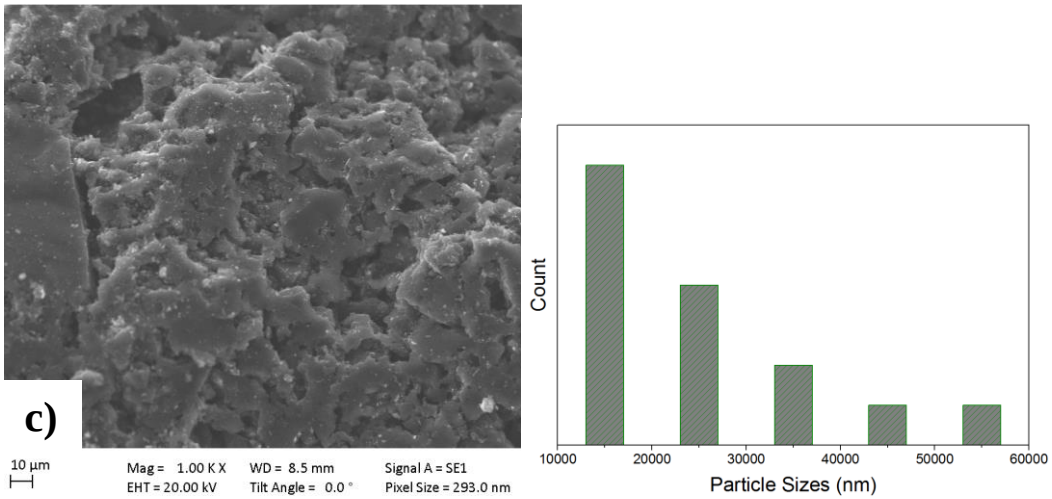

Figure 5-3 SEM images and particle size distributions of (a) UiO-66, (b) UiO-67 and (c) F400

5.3.2: Initial comparison of carbamazepine removal in UiO-67, UiO-66 and F400:

At first, the carbamazepine removal efficiency (%) of UiO-66, UiO-67 and F400 were compared by studying carbamazepine adsorption at two different initial carbamazepine concentrations, 10 and 100 mg L^{-1}, with the same amount of adsorbent concentration (1.2 mg mL^{-1}) **(Figure 5-4).** Removal efficiencies given in **Figure 5-4** show that UiO-67 and F400 removed around 95% and 85% of the carbamazepine initially present in the water at both concentrations studied. UiO-66 on the other hand, removed around 35% of the carbamazepine from water. The results clearly show that UiO-66 was found to be ineffective in the removal of carbamazepine and offer less adsorption capacity towards carbamazepine removal compared to activated carbon. This may be attributed to the narrow pore aperture (6 Å) (Kim and Cohen, 2012) and relatively smaller pore size of UiO-66 which prevent carbamazepine (kinetic diameter of 7.4 Å) (Cabrera-Lafaurie et al., 2014)

from being adsorbed in its pores. Given its poor performance for carbamazepine removal from water, UiO-66 was excluded from the rest of the adsorption experiments in this study.

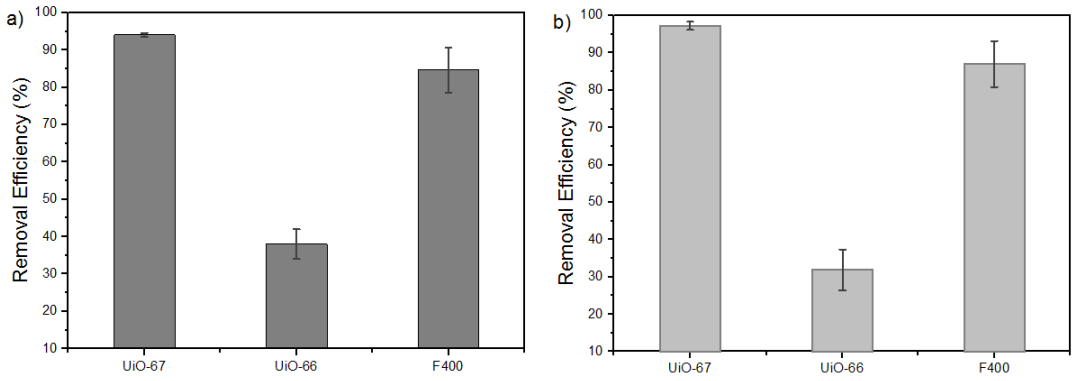

Figure 5-4. Removal efficiency of carbamazepine from water at initial carbamazepine concentrations of (a) 10 mg L^{-1} and b) 100 mg L^{-1}. Experiments were performed in triplicate, and the mean values are reported. Error bars correspond to standard deviation. (Adsorbent concentration 1.2 mg mL^{-1}).

5.3.3: The effect of adsorbent concentration:

Figure 5-5 shows the carbamazepine removal efficiency of UiO-66, UiO-67 and F400 as a function of adsorbent concentration. UiO-67 removed effectively most of carbamazepine (around 96 %) from water at a very small adsorbent concentration of 0.6 mg mL^{-1}, whereas F400 and UiO-66 removed about 52 % and 18 %, respectively at the same adsorbent concentration. For UiO-67 the increase in adsorbent concentration made only a small difference reaching to 98% within the range studied **(Figure 5-5)**. For F400, although the removal rate increased with increasing F400 concentration, the maximum carbamazepine removal efficiency observed was around 85%. In the case of UiO-66, only 50% removal of

carbamazepine was achieved even at high adsorbent concentration in which UiO-67 removed most of carbamazepine. These indicate that UiO-67 has a much better removal efficiency of carbamazepine compared to F400 and UiO-66.

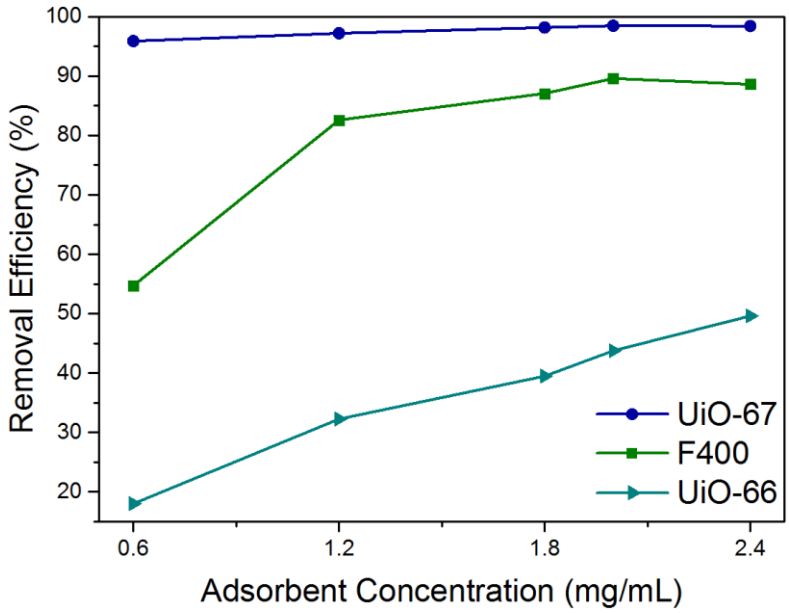

Figure 5-5. Effect of adsorbent concentration on carbamazepine removal. The initial carbamazepine concentration is 100 mg L^{-1}. Experiments were performed in triplicate and the mean values are reported. Errors are smaller than the symbols. The solid lines are given as guides to the eye. Adsorption isotherms:

Adsorption isotherms of carbamazepine in UiO-67 and F400 are given in **Figure 5-6**. The adsorption isotherms were fitted to the linearized forms of the Langmuir and Freundlich models **(Figure 5-7)** and the calculated Langmuir and Freundlich parameters are given in **Table 5-4** Even though both models gave good fits for UiO-67 and F400, the Freundlich isotherm was deemed to be more applicable since the isotherms did not approach saturation regime within the studied concentration range. Carbamazepine adsorption in UiO-67, in particular, shows almost a linear trend which indicates that UiO-67 can adsorb higher amounts with increasing

concentration of carbamazepine. Based on the greater K_F value, UiO-67 is predicted to have a carbamazepine adsorption capacity about 3 times larger than that of F400, which is in line with the pore volumes reported in **Table 5-2.** A comparison of the K_F values of carbamazepine by various adsorbents are given in **Table 5-3**, which shows that the adsorption capacity of UiO-67 is expected to be higher than those of other adsorbents including F400, mesoporous silicate, resin and polymer.

Table 5-3. Comparison of Freundlich rate constant values (K_F) for adsorption of carbamazepine by various adsorbents reported in the literature.

Adsorbent	**Carbamazepine- Freundlich Rate Constant**			
	pH	K_F (mg g^{-1}) (L mg^{-1})$^{1/N}$	N	Refs.
Hexagonal mesoporous silicate, HMS	7.0	0.113	0.835	(Suriyanon et al., 2013)
Mercapto-functionalized HMS, M-HMS	7.0	0.747	1.106	(Suriyanon et al., 2013)
Amine-functionalized HMS - (A-HMS)	7.0	0.047	1.106	(Suriyanon et al., 2013)
Mesoporous silicate SBA-15	7.0	0.206	0.885	(Suriyanon et al., 2013)
Mesoporous silicate MCM-41	7.0	0.143	0.860	(Suriyanon et al., 2013)
Powdered activated carbon	7.0	1.852	1.072	(Suriyanon et al., 2013)
Mesoporous silica SBA-15	5.0	1.10	1.34	(Bui and Choi, 2009)
Single-walled carbon nanotubes	n.a	62.5	0.35	(Lerman et al., 2013)
Molecularly imprinted polymer, MIP	n.a	28.7	0.38	(Dai et al., 2013)
Non-imprinted polymer, NIP	n.a	10.2	0.32	(Dai et al., 2013)
Y-zeolites modified with extra framework	6.0	Low loading n.a	-	(Cabrera-Lafaurie et al., 2014)

transition metal and surfactant cations				
Amberlite XAD-7 acrylic-ester-resin	7	5.56	0.744	(Domínguez et al., 2011)
Activated carbon/Fe_3O_4	6.0	63.2	4.44	(Shan et al., 2016)
Biochar/Fe_3O_4	6.0	23.1	3.73	(Shan et al., 2016)
Activated Carbon F400	5.0	6.6	0.55	This work
UiO-67	5.0	18.9	0.94	This work

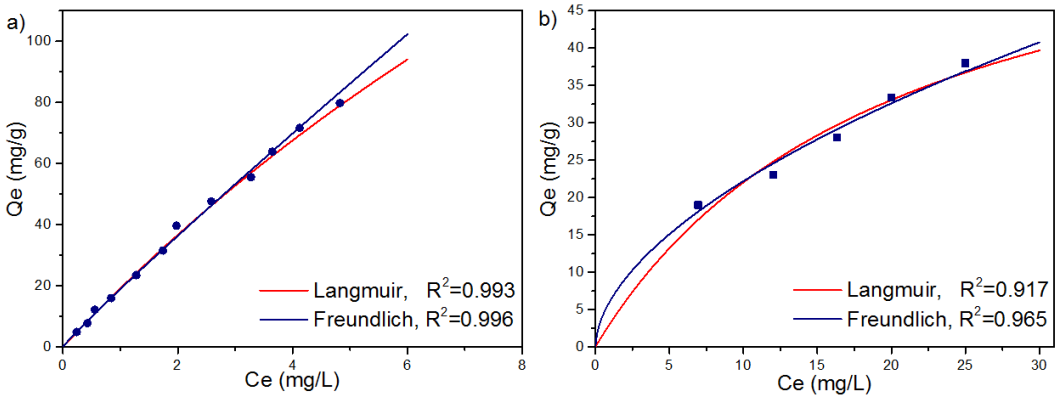

Figure 5-6. Adsorption isotherm of carbamazepine in (a) UiO-67 and b) F400. Solid lines show the Langmuir and Freundlich model fits. Experiments were performed in triplicate, and the mean values are reported. Errors are smaller than the symbols.

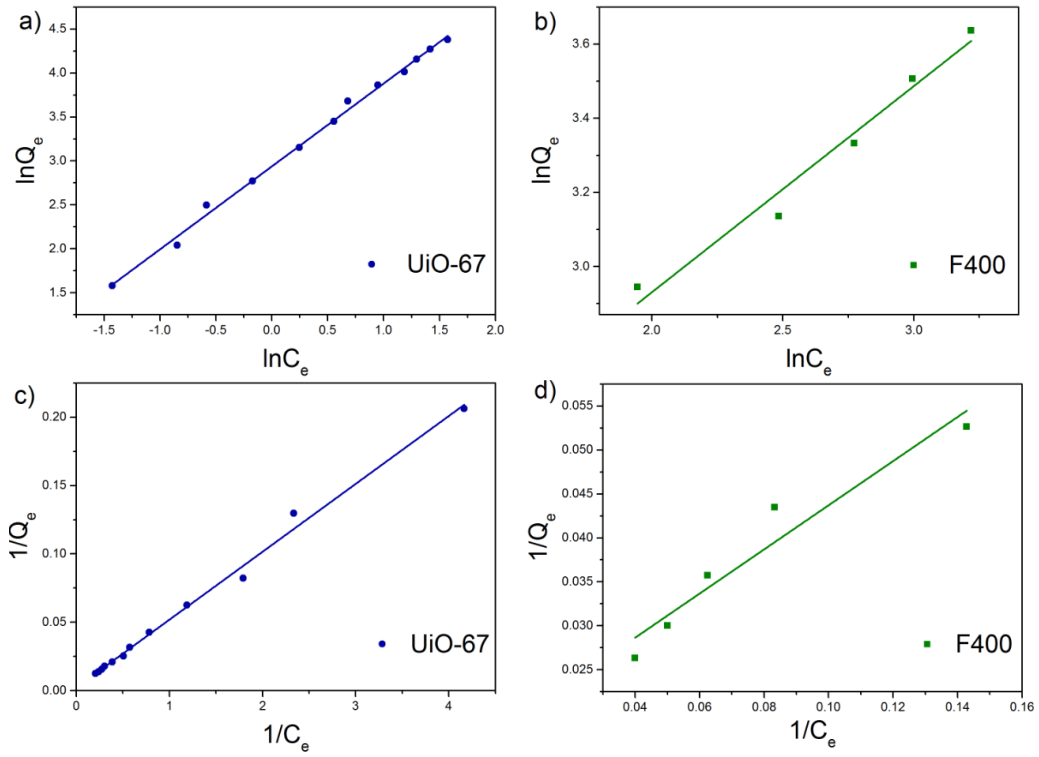

Figure 5-7 Freundlich adsorption isotherm model fittings of carbamazepine in (a) UiO-67 and (b) F400, and Langmuir adsorption isotherm model fittings of carbamazepine in (c) UiO-67 and (d) F400.

Table 5-4 Langmuir and Freundlich Adsorption Models Fitting Parameters.

Isotherm Models	**Langmuir Parameters**			**Freundlich Parameters**		
Adsorbents	Q_m (mg g^{-1})	K_L (L mg^{-1})	R^2	K_F (mg g^{-1}) (L mg^{-1})$^{1/N}$	N	R^2
UiO-67	427	0.047	0.994	18.9	0.94	0.996
F400	66.3	0.049	0.917	6.6	0.55	0.965

5.3.4: Adsorption Kinetics:

Figure 5-8a shows the adsorption of carbamazepine as a function of time with an initial carbamazepine concentration of 100 mg L^{-1}. After 2 hours, equilibrium uptake of carbamazepine was found to be 82.61 mg $g^{-1}$and 75 mg g^{-1} for UiO-67 and for F400, respectively, which correspond to 97 % removal efficiency for UiO-67 and 88.7% for F400. More importantly, UiO-67 removed 95% of carbamazepine in just 2 minutes. In contrast, F400 removed only 35% of the carbamazepine in the first 2 minutes. The faster removal rate of carbamazepine in UiO-67 in comparison to F400 can be ascribed to several reasons including the active adsorption sites created by the missing-linker defects, UiO-67's smaller particle size **(Figure 5-3b)**, higher surface area and pore volume.

To understand kinetic mechanism better, the pseudo first order and the pseudo second order kinetic models were considered to analyse the experimental kinetic data **(Figure 5-8 and Table 5-5)**. The adsorption kinetics of carbamazepine in both UiO-67 and F400 are well represented by the pseudo second order kinetic model. The pseudo second order rate constant (k_2) of carbamazepine adsorption in UiO-67 was calculated to be 0.04 mg g^{-1} min^{-1}, which is 27 times greater than that of for F400 (0.0015 mg g^{-1} min^{-1}).

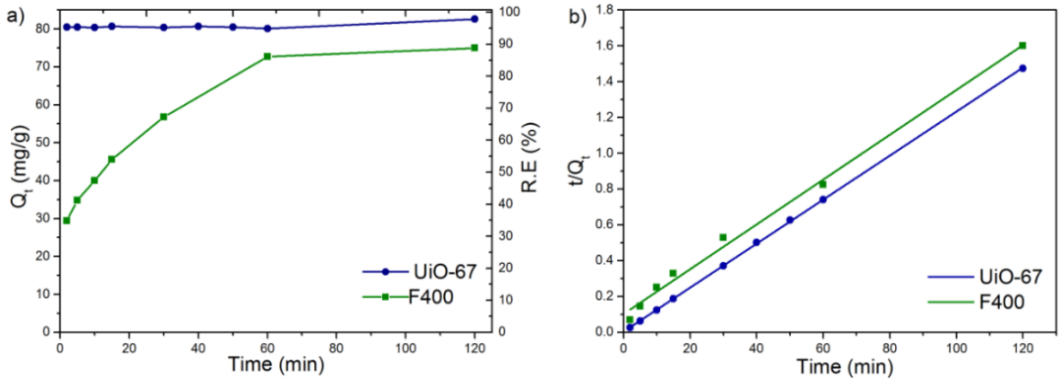

Figure 5-8. (a) Adsorption of carbamazepine in UiO-67 and F400 as a function of time and (b) The corresponding pseudo second order kinetic plots. Adsorbent concentration is 1.2 mg mL^{-1}. Experiments were performed in triplicate, and the mean values are reported. Errors are smaller than the symbols. Solid lines are given as guides to the eye.

Table 5-5. Pseudo first order and pseudo second order kinetic models fitting parameters.

Model	**Pseudo First Order Kinetic Model**			**Pseudo Second Order Kinetic Model**		
Adsorbent	Q_e (mg g^{-1})	k_1 (min^{-1})	R^2	Q_e (mg g^{-1})	k_2 (g mg^{-1} min^{-1})	R^2
UiO-67	2.9	0.0244	0.79	82.64	0.04	0.9998
F400	58.2	0.0511	0.967	80	0.0015	0.9946

5.3.5: Effect of pH:

The solution pH is a crucial parameter in practical water treatment which affects the adsorption capacity possibly by altering the electrostatic interactions between adsorbents and adsorbates. **Figure 5-9** shows the change in the adsorbed amount of carbamazepine with respect to varying pH. It was found that the amount of carbamazepine adsorbed did not significantly change within the pH range studied.

This may be attributed to carbamazepine exists almost exclusively as a neutral compound at pH 3.0- 9.0 since acid association constant (pKa) of carbamazepine is 13.9.

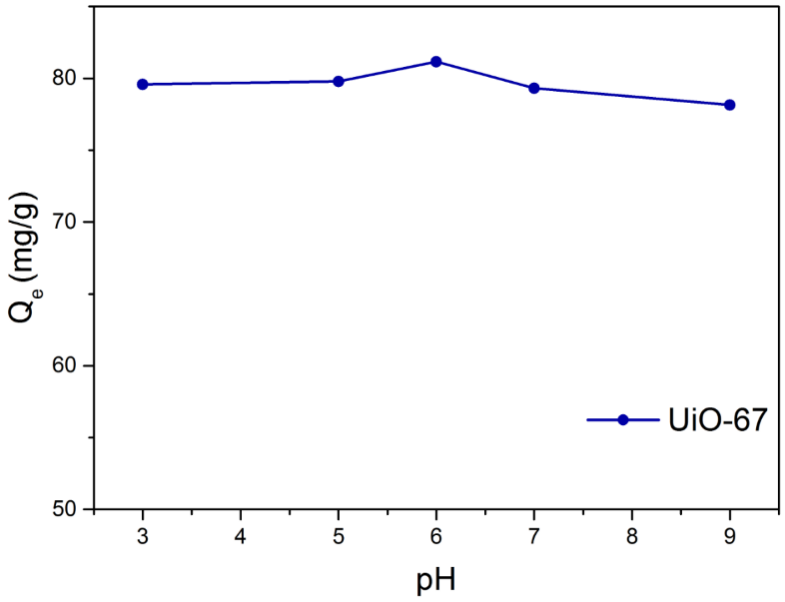

Figure 5-9. Effect of pH on adsorptive removal of carbamazepine. Experiments were performed in triplicate, and the mean values are reported. Errors are smaller than the symbols. The solid lines are guides to the eye.

5.3.6: Adsorption Mechanism:

Hydrogen bonding was previously used to explain the adsorptive removal of organic contaminants using MOFs (Seo et al., 2016a, Ahmed and Jhung, 2017). However, the insensitivity of carbamazepine adsorption in UiO-67 **(Figure 5-9)** with respect to varying pH values indicates that the electrostatic interactions do not play a significant role and the contribution of hydrogen bonding is expected to be negligible and that it is rather the hydrophobic and π-π interactions between the benzene rings of carbamazepine and the UiO-67 linkers which dominate.

Carbamazepine has amine group (-NH_2) that is a strong electron donating group (Wei et al., 2013), this electron-rich, π donor, benzene rings of carbamazepine can strongly bind with the electron acceptor, π acceptor, of the oxygen containing functional group on the surface of UiO-67. Similar interactions have been reported for carbamazepine adsorption in other adsorbents in the literature (Wei et al., 2013, Domínguez et al., 2011, Cai and Larese-Casanova, 2014).

5.3.7: Stability and Regeneration of UiO-67:

Regeneration of used adsorbents is of significant importance in terms of water remediation applications. The feasibility of regenerating UiO-67 was investigated using the solvent assisted desorption technique. UiO-67 was tested for the adsorption of carbamazepine after the spent adsorbent soaked in acetone, shaken at room temperature and re-activated under vacuum at 90˚C. This process was repeated five times and at the end of the 5th cycle, adsorption capacity of UiO-67 showed only an insignificant decrease **(Figure 5-10)**. The crystallinity the regenerated UiO-67 was also confirmed by XRD patterns **(Figure 5-1a)** indicating that UiO-67`s structure was not destroyed after soaking with acetone and reactivating at 90˚C. To further clarify the stability of UiO-67 to process and successfully achievement of desorption of adsorbed-carbamazepine, N_2 adsorption isotherm of regenerated UiO-67 was measured and given in **Figure 5-11**. This affirms the fact that the porosity of UiO-67 retained and the surface area remained almost the same as the surface area of pristine UiO-67 **(Table 5-6)** and adsorbed-carbamazepine was also effectively desorbed from the pores of UiO-67 (not much carbamazepine left in the pores). Pleasingly the crystallinity and textural properties of UiO-67 were maintained after regeneration process of UiO-67 by using acetone.

Overall, these prove that UiO-67 not only removes carbamazepine effectively and rapidly but also it is a durable adsorbent which can be used several times, which is absolutely a requirement for a practical and economical operation.

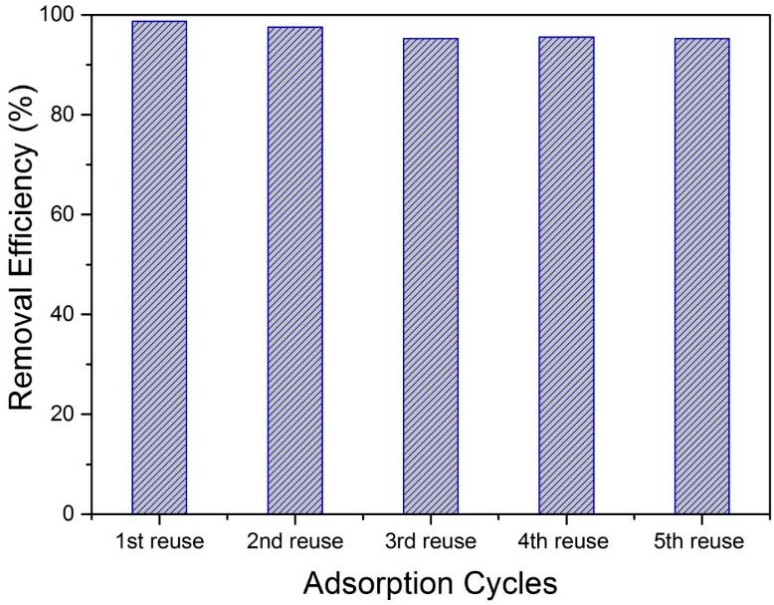

Figure 5-10. The adsorbed amount of carbamazepine by UiO-67 after consecutive regeneration cycles. (12 mg UiO-67 was in contact with 5 mL solution of 100 mg L^{-1} initial concentration)

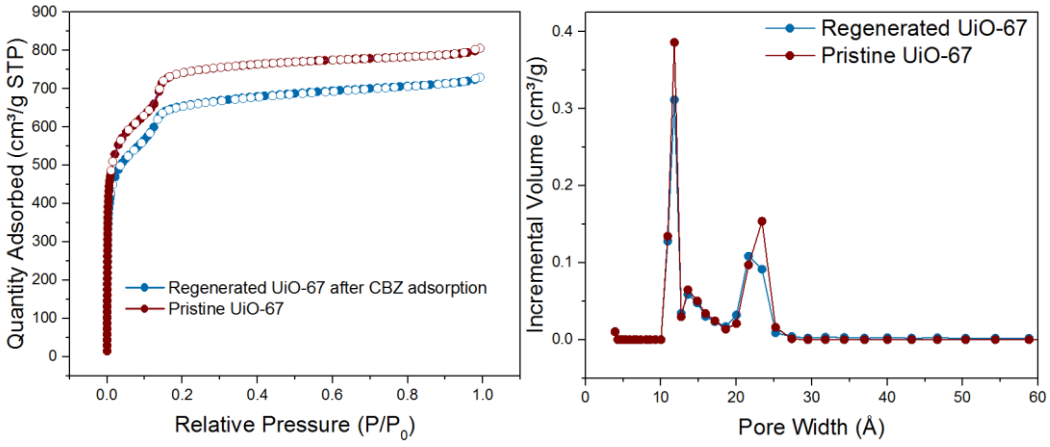

Figure 5-11 N_2 adsorption-desorption isotherms and pore size distributions of pristine UiO-67 and regenerated UiO-67 after carbamazepine adsorption (from left to right)

5.4: CONCLUSIONS

The removal of carbamazepine from water by using two water stable MOFs, UiO-66 and UiO-67 and a commercial activated carbon F400 was studied. UiO-67 showed superior performance in comparison to the other two adsorbents. The rapid and highly efficient removal of carbamazepine in UiO-67 has been attributed to the active adsorption sites formed by the missing linker defects, well defined crystalline particles which are relatively small in size and high surface area and pore volume. Carbamazepine adsorption was found to be independent of pH, therefore, not the electrostatic but the hydrophobic and π-π interactions were deemed to dominate the adsorption mechanism. Overall, fast adsorption kinetics, good solvent stability and reusability reveal that UiO-67 can be considered as a promising adsorbent for the carbamazepine removal from water.

Chapter 6: SIMULTANEOUS REMOVAL OF MIXTURE OF ANTIEPILEPTIC DRUG AND ENDOCRINE DISRUPTING COMPOUND BY A ZIRCONIUM BASED MOF-UIO-67

6.1: INTRODUCTION

The aim of this study is to investigate competitive/simultaneous adsorption between carbamazepine and atrazine in water. Based on the previous results on atrazine and carbamazepine removal from water by UiO-67, we decided to study the binary solute system of atrazine and carbamazepine in water in order to see the competitive adsorption in the presence of mixture of organic contaminants.

Persistent organic compounds and other pollutants such as heavy metals or other PPCPs are generally common in the environment (Lekkerkerker-Teunissen et al., 2012, Nam et al., 2014, Tan et al., 2016, Zhou et al., 2017, Sophia and Lima, 2018). Atrazine and carbamazepine, emerging contaminants, can be coexist in ground and surface waters. These emerging contaminants are persistent in the environment and also known potentially carcinogen (atrazine) (Zhou et al., 2017) and to have potential threaten to human health and ecological environment. Therefore, their removal from water before entering the environment are needed. As mentioned in the previous chapters, many treatment technologies include conventional (coagulation, precipitation), ozonation and advanced oxidation process, which have been implemented to remove these kinds of persistent organic pollutants from water. However, they may not be completely degraded or may be partially degraded by these treatment technologies. Adsorption-based technologies is considered as an effective, simple and inexpensive method for the PPCPs and EDCs removal in sole

and binary components. Many researches on the adsorption of these types of organic pollutants have been reported on pure components; however, these organic substances are generally present as a mixture in industrial effluents and real waters. The competitive adsorption in a binary system can lead to the decrease or increase in adsorption performance compared to adsorption performance in a sole system because the adsorbates will compete for the active sites of the adsorbent. We employed the simultaneous adsorption of atrazine and carbamazepine (as probe molecules) to demonstrate the effectiveness of UiO-67 for the uptake of multicomponent. We chose these probe molecules in a binary system since UiO-67`s superior performance (effective and rapid uptake) for atrazine and carbamazepine in a sole system was demonstrated in Chapter 4 and Chapter 5, respectively. Hence it is beneficial to elucidate the applicable of UiO-67 as an adsorbent for the adsorption of multicomponent since they are detected as a mixture in real waters. We also studied the adsorption behaviour of carbamazepine and atrazine in the presence of salts such calcium chloride and sodium chloride in water because there are many natural salts and ions occur in the real water and may affect the adsorption of analytes.

6.2: EXPERIMENTAL METHODS

6.2.1: Synthesis and characterisation of UiO-67:

The preparation of UiO-67 with missing linker was given in Chapter 3 (see section3.2.3). The crystallinity of the prepared UiO-67 crystals was confirmed by PXRD. PXRD patterns of the materials were recorded by a Stoe Seifert diffractometer and the detail was given in section3.3.1. The BET surface areas, total

pore volumes, micropore volumes and the pore size distributions, N_2 adsorption/desorption measurements of UiO-67 was performed on Micromeritics Tristar porosity analyzer at 77 K. Prior to analysis, UiO-67 was outgassed at 150 ºC overnight under vacuum. 110 mg of sample was used in measurements. The specific surface areas were calculated using BET method at the range of 0.005-0.2 relative pressure range. N_2-DFT model was used to calculate the pore size distributions of the UiO-67.

6.2.2: Liquid phase adsorption experiments:

An initial concentration 100 mg L^{-1} of carbamazepine stock solution (Sigma Aldrich) and 25 mg L^{-1} of atrazine stock solution were prepared by dissolving carbamazepine and atrazine as single components in ultrapure water (18 M.Ω.cm) until completely dissolved. The binary mixture of working solution concentrations of carbamazepine (20 mg L^{-1}) and atrazine (5 mg L^{-1}) were prepared in ultrapure water. These initial concentrations were selected based on their solubility in water.

For this purpose, 15 mg of UiO-67 was placed into 25 mL of mixture solution of 20 mg L^{-1} of carbamazepine and 5 mg L^{-1} of atrazine. Samples with adsorbent and control samples without adsorbent (25 mL of mixture of carbamazepine and atrazine solution) were placed in an incubator shaker at 250 rpm and 25°C for 24h. The presence of salts in atrazine and carbamazepine wastewater may affect the atrazine and carbamazepine adsorption. Hence, to investigate the interference effect of ionic strength on the adsorption of pure components and mixture of carbamazepine and atrazine, 0.1M sodium chloride and 0.1M calcium chloride were added to the both solutions. All experiments were performed five times and

the mean values are reported here. The solutions were separated from adsorbents by filtering off with a syringe filter (0.2 µ cellulose acetate syringe filter). The initial and equilibrium carbamazepine and atrazine concentrations in the stock solutions and in the filtrates, respectively were determined by comparing the obtained peak area corresponding to the calibration standards of carbamazepine and atrazine which were obtained on a HPLC (Shimadzu LC2010HT) with coupled with a UV-vis detector at 223 nm of wavelength. A single components and mixture of carbamazepine and atrazine were measured on the reversed phase C18 column (Hichrom, ACE 5 C18, 150 mm x 4.6 mm, 5 µm particle) with a 45:55% v/v of water/methanol mobile phase at a flow rate of 1 mL min^{-1} with 100µL of injection volume. The temperature of column set at 25°C. The amount of adsorbed carbamazepine atrazine (mg adsorbate per g of adsorbent) was calculated by using **Equation 3-1** and the removal efficiency (%) of these organic pollutants by the adsorbent was calculated by using **Equation 4-2.**

6.2.3: Regeneration of UiO-67:

25 mL of binary solutions with an initial concentration of 5 mg L^{-1} and 20 mg L^{-1} atrazine and carbamazepine as a mixture, respectively, were placed to be contact with 21 mg of UiO-67 adsorbent. The adsorbed carbamazepine and atrazine in UiO-67 was desorbed by soaking the spent UiO-67 in acetone and shaken at 25 °C for 6 h and then supernatant was removed and re-soaked in fresh acetone and re-shaken at 25 °C for overnight. Eventually, UiO-67 was dried at 90°C overnight under vacuum for the next adsorption. This adsorption-desorption cycle of UiO-67 was repeated for at least 6 times following the above procedure prior to each adsorption.

6.3: RESULTS AND DISCUSSION

6.3.1: Characterisation of UiO-67:

N_2 adsorption-desorption isotherms and powder X-ray diffraction were used to confirm the textural properties and crystallinity, respectively as shown in **Figure 6-1**. The apparent surface area and pore volume UiO-67 with defect were calculated to be of 2506 m^2 g^{-1} and 1.010 cm^3 g^{-1}, respectively, which is consistent with the literature (Audu et al., 2016). The mesoporous step at relative pressure of 0.05-0.2 was also clearly seen in **Figure 6-1 a**. Furthermore, X-ray diffraction patterns of the synthesised UiO-67 was matched very well with simulated patterns **(Figure 6 - 1c)**. These all characterisation results confirm that UiO-67 was successfully synthesised.

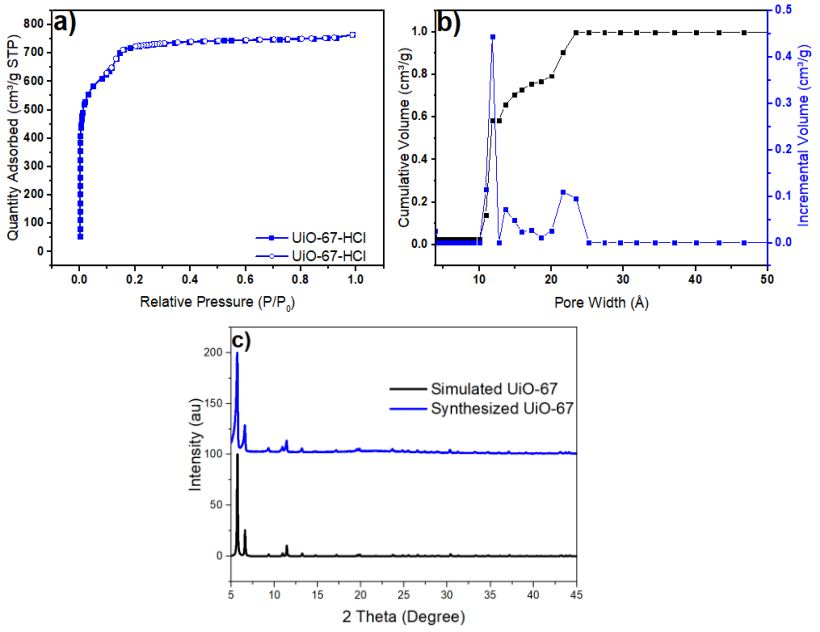

Figure 6-1 a) N_2 adsorption-desorption isotherms of UiO-67 (filled and empty symbols represent adsorption and desorption, respectively) and b) the pore volume and pore size distribution of UiO-67 and c) PXRD patterns of synthesized and simulated UiO-67

6.3.2: Calibration Curves of atrazine and carbamazepine:

Figure 6-2 shows the calibration curves of carbamazepine and atrazine in water as individual compounds with high correlation coefficient of 0.999. The chromatogram of binary mixture of carbamazepine (20mg L^{-1}) and atrazine (5 mg L^{-1}) was presented in **Figure 6-3**. The retention times are recorded as 8.02 min and 10.87 min for carbamazepine and atrazine, respectively.

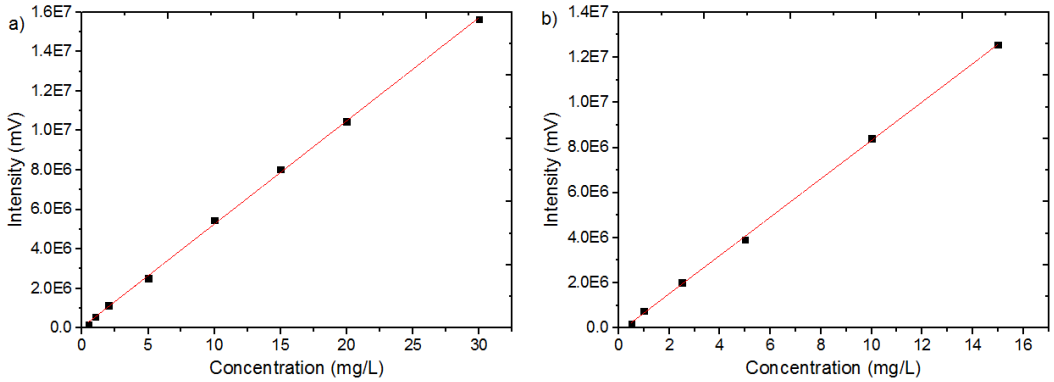

Figure 6-2 Calibration Curves of carbamazepine (a) and atrazine (b) in water

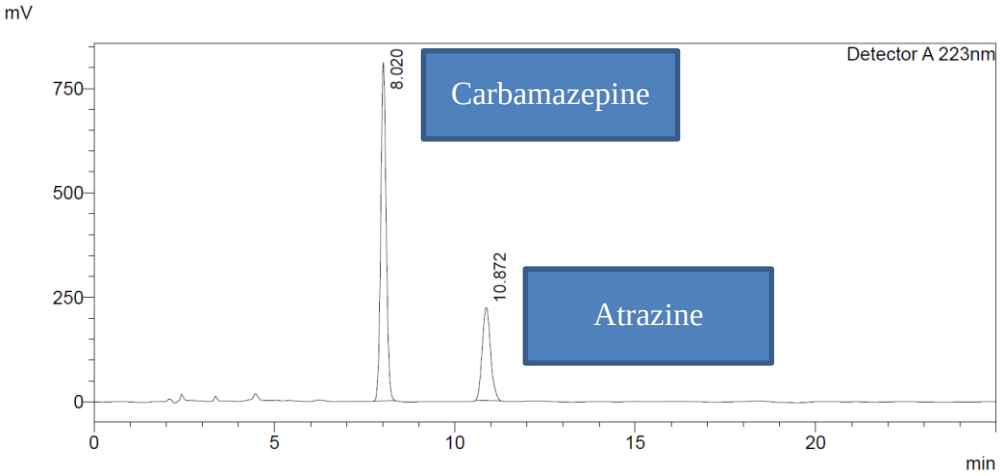

Figure 6-3 A representative chromatogram of binary mixture of carbamazepine and atrazine with initial concentrations of 20 mg L^{-1} and 5 mg L^{-1}, respectively.

6.3.3: The simultaneous adsorption of carbamazepine and atrazine in UiO-67

As can be seen in **Figure 6-4**, the carbamazepine and atrazine removal from binary mixture were not significantly decreased compared to individual removal of carbamazepine and atrazine. UiO-67 removed over 86 % of carbamazepine and 58 % of atrazine as individual components and showed close removal 83 % and 54% of carbamazepine and atrazine in the mixture, respectively. This indicates that UiO-67 can be considered as promising and efficient adsorbent to remove persistent organic compounds from mixtures in real waters without significant loss of efficiency.

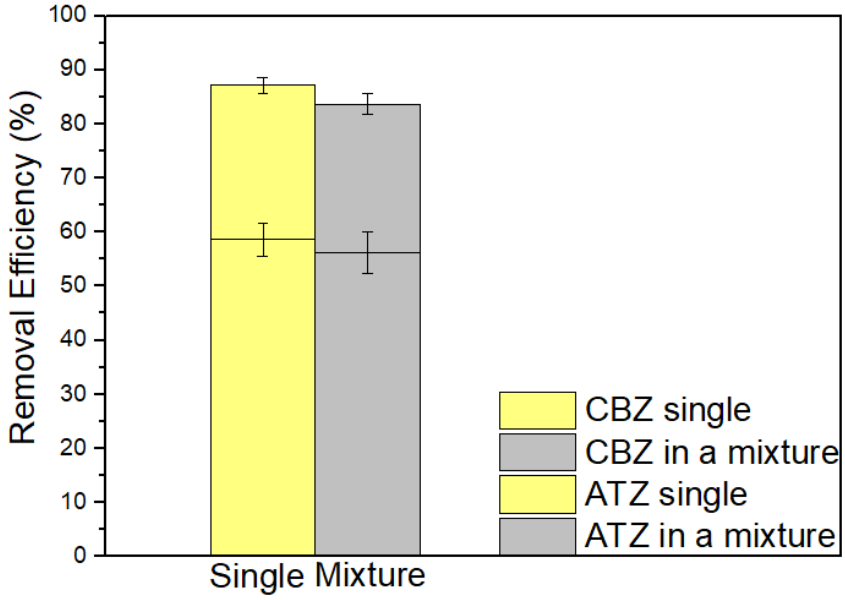

Figure 6-4 Removal Efficiency of carbamazepine and atrazine as pure components and as binary mixtures by UiO-67 (20 ppm carbamazepine and 5 ppm atrazine in binary mixture was contacted with 15 mg UiO-67 at 25 ˚C for 24 h.)

6.3.4: Kinetic Studies of UiO-67 for carbamazepine and atrazine mixture:

The required time is to reach saturation simultaneously is only 1min for carbamazepine and atrazine mixture **(Figure 6-5)** indicating that UiO-67 can remove two components very fast even they are found as a mixture in water. Furthermore, UiO-67 offered the similar uptake of carbamazepine and atrazine as pure components from water **(Figure 6-5).** The kinetics of the binary mixture of carbamazepine and atrazine adsorption in UiO-67 were analysed by pseudo-second order model **(Equation. 3-8)** in order to get better insight to the adsorption kinetic of UiO-67 for mixture of carbamazepine and atrazine. **Figure 6-6** shows the adsorption capacity of UiO-67 toward binary mixture of carbamazepine and atrazine as a function of time and the calculated data for pseudo-second kinetic model fitting are displayed in **Table 6-1**. **Figure 6-7** displays the pseudo-second order kinetic model fitting results for the binary mixture of carbamazepine and atrazine by plotting t/Q_t versus time to obtain intercept and slope for the calculation of model fittings. The calculated equilibrium adsorbed amounts of carbamazepine and atrazine in UiO-67 by pseudo-second order were calculated to be the same with the experimental adsorbed amount with high yield of 0.9999. Therefore, the kinetic experimental data were well described by the pseudo-second order kinetic model, implying that chemisorption was the rate-limiting step for the adsorption of mixture of carbamazepine and atrazine by UiO-67.

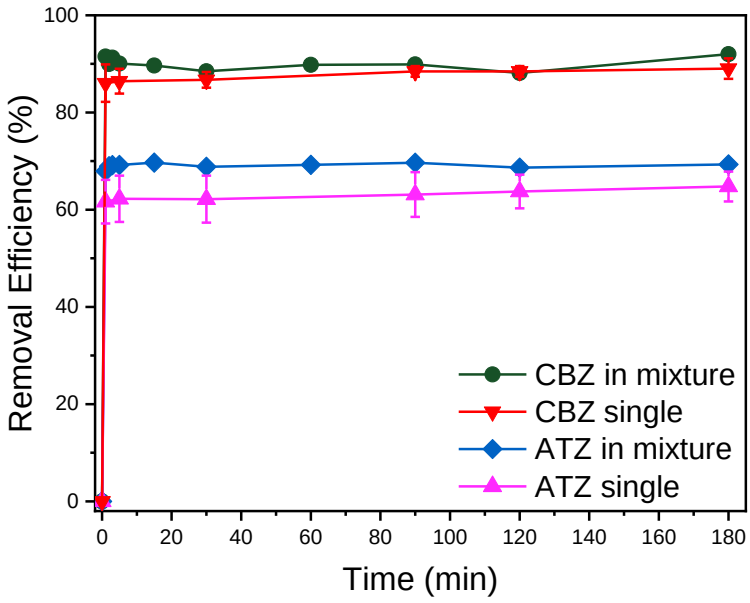

Figure 6-5 Removal Efficiency of UiO-67 for mixture of carbamazepine and atrazine with initial concentrations of 20 mg L^{-1} and 5 mg L^{-1} in a mixture, respectively and individually 20 mg L^{-1} of carbamazepine and 5 mg L^{-1} atrazine. Error bars represent standard deviation.

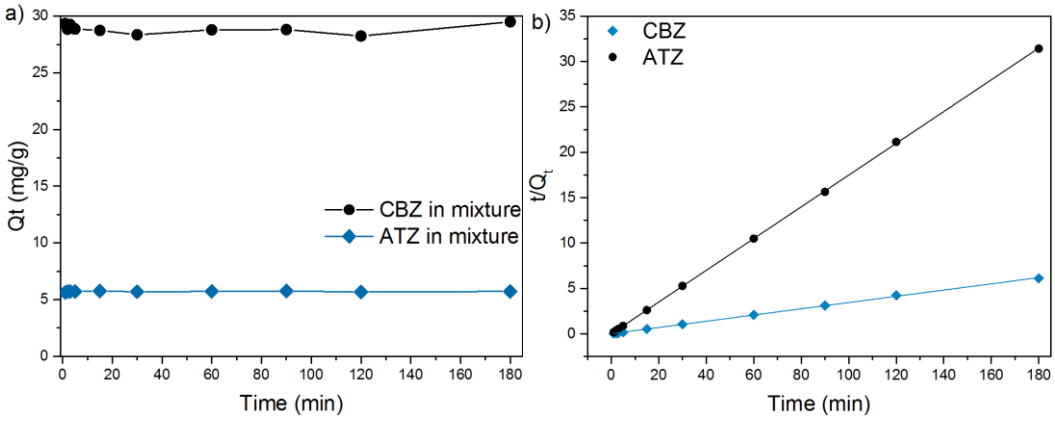

Figure 6-6 Adsorption capacity of UiO-67 for carbamazepine and atrazine mixture as a function of time (a) and pseudo second order fit for triclosan in UiO-67 (15 mg UiO-67 added into in 25 mL of solution with an initial concentration of 20 mg L^{-1} of carbamazepine and 5 mg L^{-1} of atrazine as binary mixture)

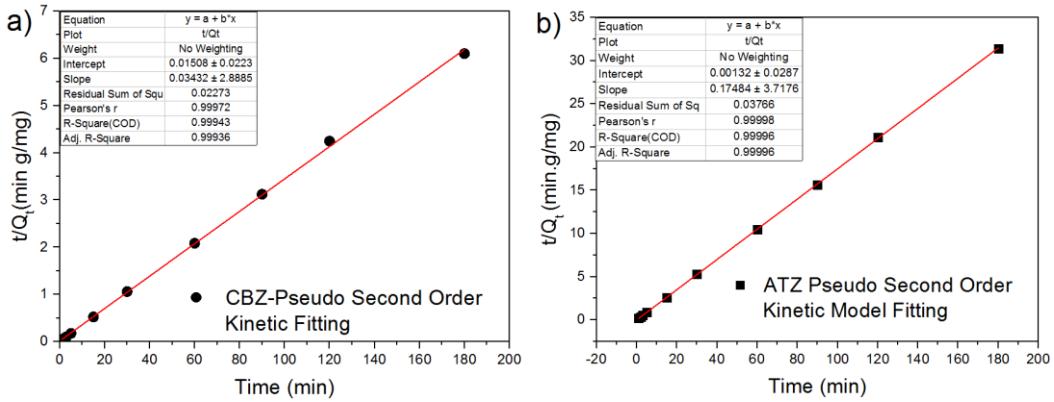

Figure 6-7 Pseudo Second Order Kinetic Fitting of mixture of carbamazepine (20 mg L^{-1}) and atrazine (5 mg L^{-1}).

Table 6-1 Pseudo Second Order Kinetic Model Parameter Fittings of UiO-67 towards mixture of carbamazepine and atrazine.

Organic Compounds	Qe exp. (mg g^{-1})	Qe cal. (mg g^{-1})	k_2 (g mg^{-1} min^{-1})	R^2
CBZ	29.5	29.14	0.078	0.999
ATZ	5.72	5.72	23.15	0.999

6.3.5: The effect of salt on the adsorption of carbamazepine and atrazine mixture

Figure 6-8 depicts the adsorbed amount of carbamazepine and atrazine in the presence of salt in water. The adsorbed amounts carbamazepine with an initial concentration of 20 mg L^{-1} were calculated to be around 29 and 27 mg of carbamazepine per g of UiO-67 as individual and in the mixture, respectively. On the other hand, the adsorbed amounts of carbamazepine with the presence of 0.1 M NaCl or $CaCl_2$ were found to be around 31 mg and 30 mg carbamazepine per g of UiO-67, respectively. Likewise, the adsorbed amounts of atrazine as pure and mixture were calculated to be 4.6 and 5 mg of atrazine per g of UiO-67, the presence

of 0.1 M NaCl or $CaCl_2$ does not affect the adsorbed amount and the adsorbed amounts of atrazine were found to be calculated the very close to the atrazine adsorbed amount from pure components. Therefore, the significant change in the adsorbed amounts of both carbamazepine and atrazine with the presence of salts in the water were not observed, indicates that UiO-67 can be used as promising adsorbents in the presence of salt ions in real water.

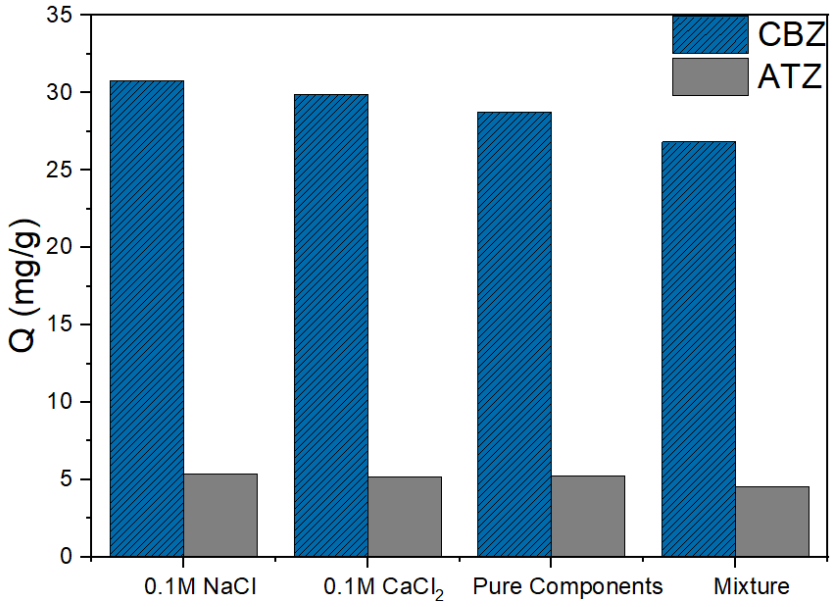

Figure 6-8 The effect of salt on the adsorption of carbamazepine and atrazine as pure components and mixture.

6.3.6: Regeneration of UiO-67 for the mixture of carbamazepine and atrazine

Regeneration is a significant parameter that needs to be taken into account in terms of industrial and practical applications. In this chapter, the spent UiO-67 was successfully regenerated with using mild acetone washing conditions at 25˚C and reusability for the mixture of carbamazepine and atrazine adsorption were repeated at least up to 6 times. The acetone was used for the regeneration of UiO-67 because

of high solubility of both carbamazepine and atrazine (31 g L^{-1} at 25 ˚C) in acetone as well as the structure of UiO-67 was proved to be retained after regenerating the UiO-67 spent for the adsorption carbamazepine and atrazine in acetone in the **Chapter 4 and 5.** Figure 6-9 shows that adsorbed carbamazepine and atrazine as a binary mixture in UiO-67 were effectively desorbed the adsorbed mixture and re-used the regenerated UiO-67 for the mixture of carbamazepine and atrazine removal for 6 times without significant amount of adsorption efficacy loss.

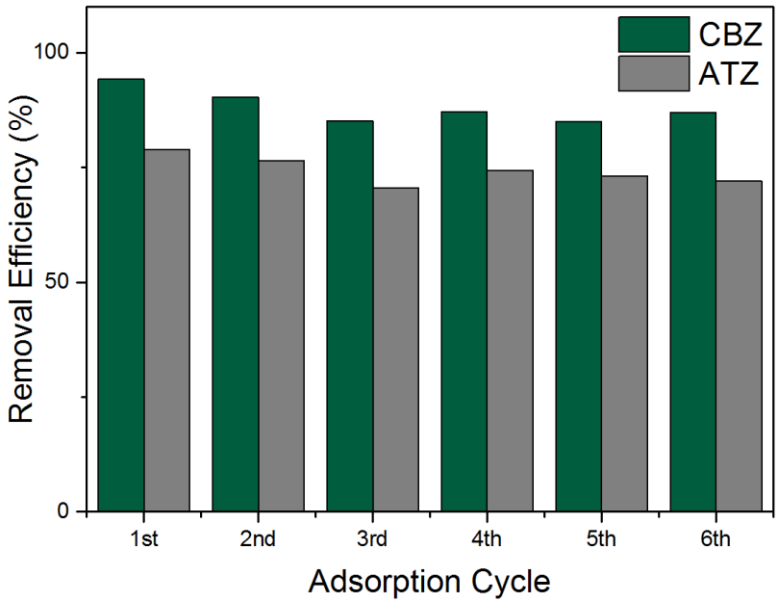

Figure 6-9 Regeneration of UiO-67 for adsorption of carbamazepine atrazine in binary mixture (30 mg of UiO-67 with an initial concentration of 20 mg L^{-1} of carbamazepine and 5 mg L^{-1} atrazine as a binary mixture).

6.4: CONCLUSION

Carbamazepine and atrazine adsorption from mixture was found to be simultaneous removal and insensitive to the presence of salt. Their adsorption uptake rate was determined to be very fast even they present in mixture. The

findings also pointed that UiO-67 can be regenerated by simply washing with acetone and re-used for the adsorption experiments of mixture components at least up to 6 times without adsorption capacity loss. Considering the efficient removal of carbamazepine and atrazine in a mixture when compared to individual components and as well as the salt ions presence under the same conditions, showing that UiO-67 have strong promising adsorbent for the removal of pharmaceuticals having comparable size.

Chapter 7: EFFECTIVE UPTAKE OF A PERSONAL CARE PRODUCT BY METAL-ORGANIC FRAMEWORKS

7.1: INTRODUCTION

Triclosan was first released into the market in 1964 and total annual production of triclosan exceeds about 1500 ton throughout the world and 96% of triclosan is released into the sewage system during normal use and then end up in aquatic environment. (Zhang et al., 2015) Triclosan (5-chloro-2-(2,4- dichlorophenoxy) phenol), a typical PPCPs, that is widely used as antimicrobial and antifungal agents in personal hygiene and consumer products such as liquid hand soap, detergents, shampoos, oral care products, deodorants and body washes. Plastic, polymer and textile industry also use triclosan as an additive. As a result of the widespread use of triclosan in various products, it is discharged into wastewater treatment plants and then transported into surface water by means of human excretion and wastewater treatment effluents. (Behera et al., 2010, Tong et al., 2016) Triclosan is found to be highly toxic to certain aquatic organisms (green algae). Moreover, triclosan have been reported to have an effect indirectly on aquatic organisms by blocking enzyme carrying proteins, which might develop bacterial resistance in these organisms and to produce more toxic by-products such as dioxin and endocrine disrupting chemicals. (Behera et al., 2010, Zhu et al., 2014) Triclosan showed presence in human milk as well as it is detected in surface water and waste water treatment plants. Therefore, its increasing occurrence in variety of sources has raised concern about threaten to the aquatic organisms and human health. (Behera et al., 2010)

Triclosan is also relatively hydrophobic compound with log Kow of 4.76 (indicator of hydrophobicity of compounds) despite having hydroxyl functional group (**Table 7-1)** and is not readily soluble in water (Sw=10 mg L^{-1}). (Cho et al., 2011) Triclosan is exclusively presented highly hydrophobic even in an ionized state due to its strong hydrophobic nature. Its high octanol water partition coefficient may result in sorption to particles. (Behera et al., 2010)

The incomplete removal of triclosan from drinking water and wastewater through conventional treatment methods was observed by using the conventional treatment method. Advanced tertiary treatment methods such as advanced oxidation, UV treatment and membrane filtration can successfully eliminate the micropollutants; however, these methods may require high infrastructure and operational costs. (Tong et al 2016). For example, biologic degradation and photo catalytic degradation were reported to be effective methods for the removal of triclosan; however, these methods suffer from slow degradation rate and long biodegradation half-life. High operational cost and its uncertain degradation products (could be more toxic) make these methods limited to practical use.(Zhang et al., 2015) In order to effectively remove such organic compounds for a sustainable healthy environment, exploring or improving technologies is still of great importance. (Behera et al., 2010)

Adsorption method can be deemed as promising method for the batch treatment of water samples, which has received a considerable deal of attention to remove triclosan due to many reasons including but not limited to the requirement of uncomplicated design, economically feasible and the ability to use for the removal of compounds at very low concentrations. (Behera et al., 2010) In the adsorption

technologies, adsorbents are very significant because adsorption is a surface process. Activated carbon`s pore structure and functional groups on the surface and high surface area make it applicable for removing small organic compounds by adsorption. (Behera et al., 2010) However, due to difficulty in regeneration and using activated carbon in ionizable compounds and ill-defined structures, the promising and efficient adsorbents are still needed. In the last past decades, a new class of hybrid organic inorganic crystalline nanoporous/microporous materials, MOFs, are found to be effective for the trace level contaminants from water.

In this chapter, adsorption of triclosan by two zirconium-based metal-organic frameworks of UiO-66 and UiO-67and other selected MOFs that are MIL-100(Fe) and HKUST-1 was investigated. Activated carbon Filtrasorb® 400 (F400) was also used for the comparison purpose. The physicochemical properties of triclosan (**Figure 7-1)** is represented in Table 7-1. As given in Table 7-1, triclosan has a pK_a of 7.9-8.14. The octanol-water partitioning coefficient of triclosan is 4.76 which is related to the degree hydrophobicity of the triclosan so the solubility of triclosan is very low. Additionally, the higher log K_{ow} of 4.76 than log K_{ow} of 2.5 demonstrates that triclosan is more likely to be adsorbed on the adsorbents.

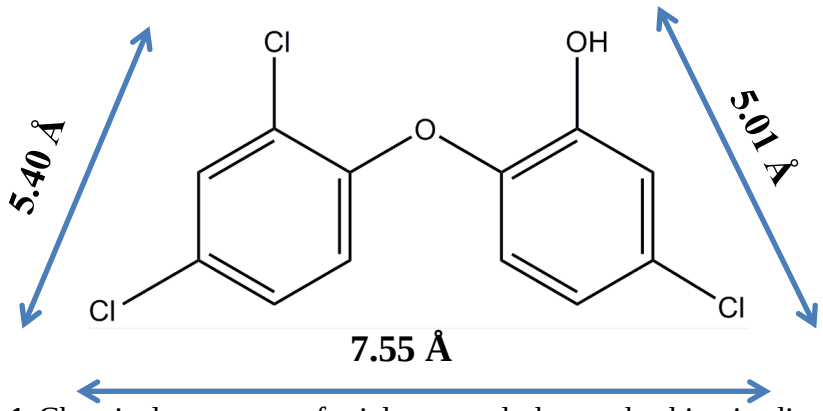

Figure 7-1 Chemical structure of triclosan and shows the kinetic diameters of triclosan in width, length and depth.

Table 7-1 Physicochemical properties of triclosan.

Compound	Molecular Weight ($g\ mol^{-1}$)	Solubility in water at 20 ˚C ($mg\ L^{-1}$)	$logK_{ow}$	pK_a*
Triclosan	289.54	10	4.76	7.9 -8.14

*(Behera et al., 2010, Cho et al., 2011)

7.1.1: Preparation and characterisation of adsorbents:

UiO-66, UiO-67 and MIL-100(Fe) were prepared according to the procedure given in detail in Chapter 3: (see section 3.2.2:,3.2.3: and 3.2.4:). HKUST-1 and activated carbon were received from Sigma Aldrich and Chemviron Calgon, UK, respectively. All chemicals were used as received without further activation (see Chapter 3, section 3.1). To confirm the successful synthesis and the characteristic properties of adsorbents studied here, powder X-ray diffraction for the crystallinity, surface area measurements by N_2 adsorption and desorption isotherms for the textural properties and SEM for the morphology and particle size distribution were performed. The detail of the conditions and equipment detail were provided in Chapter 3: (see section 3.3:). The phase and chemical composites of UiO-66, UiO-67, MIL-100(Fe) and HKUST-1 were recorded on a Stoe Seifert diffractometer (MoKα radiation source). N_2 adsorption-desorption measurements of the MOFs and F400 were obtained on a surface area/porosity analyser (Micromeritics, Tristar II 3020) after activating at 150°C overnight under vacuum.

Zeta potentials of the UiO-66 and UiO-67 was given in section 3.3.4. Both UiO-66 and UiO-67 were first dispersed in ultrapure water and the pH values of the two

solutions were adjusted by adding small volumes of 0.01 M HCl or 0.01M NaOH aqueous solutions.

7.2: MATERIALS AND METHODS

7.2.1: Triclosan batch adsorption experiments:

A stock solution of triclosan was typically dissolved by ultrasonication in ultrapure water followed by magnetic stirrer. Stock solutions with desired concentrations of triclosan were prepared before adsorption experiments. The triclosan concentrations of stock, control and equilibrium were determined with using HPLC. Chromatograms were obtained using mobile phase of methanol and water (90:10 % v/v) at flow rate 1 mL min^{-1} with 50 µL injection volume. The column temperature was kept constant at 25 °C and the UV-vis detector was set at a wavelength of 290 nm. A calibration curve for triclosan was obtained from by plotting the area of the standard triclosan solution versus the known concentrations range of 1-10 mg L^{-1}.

All adsorbents were activated at 100 ˚C prior to the liquid phase adsorption experiments. To test the performance of MOFs towards the triclosan adsorption, the batch adsorption experiments were first conducted with the selected MOFs in glass vials. 1 and 5 mg of each of activated MOFs, UiO-66, UiO-67, MIL-100(Fe) and HKUST-1 and activated carbon F400 were added as solids to 5 mL and 25 mL triclosan solutions, respectively, containing an initial concentration of 10 mg L^{-1} without pH adjustments. The glass vials were capped and stirred by using an incubator shaker (SCiQuid) at 250 rpm speed and constant temperature of 25 ˚C ± 1 for 24-hour contact time. Control samples without solid adsorbents were also

shaken under the same conditions to check the triclosan concentration change in the solution over time. The supernatants were taken using disposable syringes and filtered through 0.45 µm PTFE syringe filter (VWR international, UK) in order to separate the solutions from the solid adsorbents. The liquid samples were then directly added to into HPLC vials for the determination of triclosan concentrations. Control samples were also passed through 0.45 µm PTFE syringe filter before HPLC analysis. The adsorbed amount of triclosan is calculated by the difference between the triclosan amount in the control samples and the amount remained in the supernatant solution. The pH of triclosan solution was measured and adjusted to pH 3, 5, 7 and 9 using 0.01M aqueous solutions of NaOH and HCl in order to study the pH effects on adsorption of triclosan. The adsorbed amount of triclosan on different adsorbents and removal efficiency were calculated using **Equation 3-1 and Equation 4-2.**

To construct adsorption isotherm experiments, the pH of the solution was adjusted to 7 and 25 mL solutions with various initial triclosan concentrations ranging from 1 to 10 mg L^{-1} were prepared. Finally, 25 mL of triclosan solutions with different concentrations samples were exposed to 5 mg of each of adsorbents and agitated in an incubator shaker at 250 rpm for 24 h. For the kinetic adsorption experiments, 5 mg of UiO-66 and UiO-67 were added to 25 mL of solutions containing two different initial concentrations of 2 and 5 mg L^{-1} for each predetermined time interval from 1 min to 2 hours and each vial was shaken until a predetermined amount of time under the aforementioned experimental conditions. Control samples of 25 mL triclosan solutions without adsorbents were also

collected at specified time interval (1 min to 2 h) to monitor any change in the control samples during adsorption experiments.

7.2.2: Stability of the regenerated MOFs under batch adsorption experiments conditions:

100 mg of UiO-67 was added to 25 mL of triclosan solution with an initial concentration 9 mg L^{-1} and control samples without adding adsorbents were agitated 24 h under the given experimental conditions above. The spent UiO-67 and acetone was mixed in an incubator shaker for 6 h and replenished with fresh acetone for further stirring overnight followed by thermally activation at 90 °C under vacuum overnight. Regeneration of the spent of UiO-67, 21 mg of UiO-67 was stirred with acetone in an incubator shaker for 6 h at 25 °C and then replenished with fresh acetone and left to be soaked in acetone overnight. The supernatant was removed and then the solid was activated at 90 °C overnight under vacuum for the next adsorption cycles of triclosan. The spent UiO-67 was regenerated by using this method and reused for adsorption of triclosan up to 5 times. The regenerated of UiO-67 upon exchange to acetone followed by heating activation was examined by XRD and BET.

7.3: RESULTS AND DISCUSSION

7.3.1: Characterisation of adsorbents:

The phase purity was confirmed by PXRD patterns of UiO-66, UiO-67, HKUST-1 and MIL-100(Fe) which match very well with the simulated corresponding PXRD patterns of all MOFs **Figure 7-2**. The apparent surface areas, pore volumes

and micropore volumes are given in **Table 7-2**. Zeta potentials of UiO-66 and UiO-67 at various pH (2, 3, 4, 5, 6, 7, 8, 8.7,9 and 10) are given in **Figure 7-3**, the surface of both UiO-67 and UiO-66 negatively charged above pH 3.

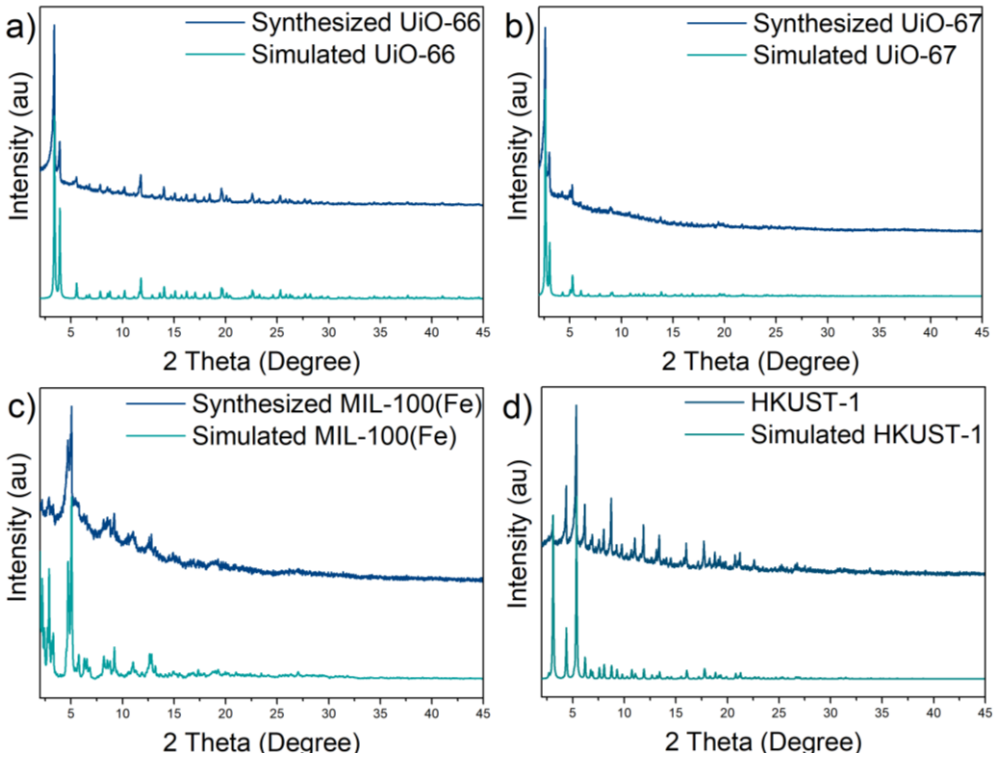

Figure 7-2 Structural analysis for the synthesized MOFs.

Table 7-2 Textural Properties of the studied MOFs in this study

MOFs	Surface area (m^2 g^{-1})	Total Pore Volume (cm^3 g^{-1})	Micropore Volume (cm^3 g^{-1})
UiO-66	1665	0.691	0.570
UiO-67	2510	1.053	0.916
MIL-100(Fe)	1645	0.828	0.533
HKUST-1	825	0.506	0.281
Regenerated UiO-67	2230	1.037	0.978

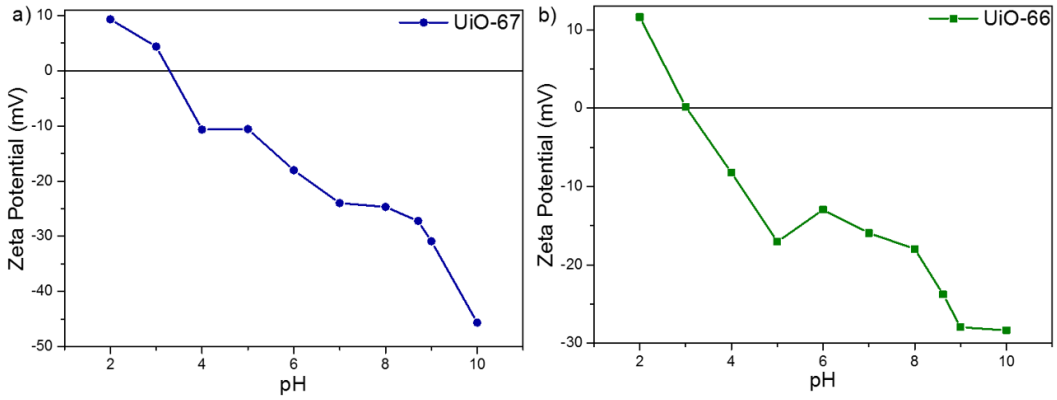

Figure 7-3 Zeta Potential of a) UiO-67and b) UiO-66

7.3.2: Adsorptive removal of hydrophobic triclosan using MOFs and activated carbon (F400):

In this chapter, the performance of MOFs in the adsorption of hydrophobic triclosan from water was elucidated. The adsorption rate of triclosan from aqueous solution onto various adsorbents at two different adsorbents concentrations are shown in **Figure 7-4.** UiO-67 has the highest surface and exhibited the highest the adsorption capacity compared to all adsorbents studied in this chapter. The adsorption capacity of triclosan is found in the order UiO-67 > UiO-66 > F400 which is in the same order of surface area of adsorbents (UiO-67 > UiO-66 > F400). The removal efficiency for triclosan in UiO-67 was calculated to be over 92 % and 98 % by exposing with 1 mg and 5 mg of UiO-67, respectively. These values are comparable to the removal efficiency was achieved by 1 mg and 5 mg of UiO-66 (89 % and 96 %, respectively). On the other hand, MIL-100(Fe) and HKUST-1 removed a small amount of triclosan from water which was calculated to be less than 20 % and about 20 % by each of 1 mg and 5 mg of MIL-100(Fe) and HKUST-1, respectively. In the case of F400, the adsorption capacity was found to be around

40 % and over 60 % by exposing the solution to 1 mg and 5 mg of F400, respectively. The removal efficiency by F400 at both adsorbent concentration was calculated to be less than that of UiO-66 and UiO-67, however, higher than that of MIL-100(Fe) and HKUST-1. Also, the adsorption capacity of HKUST-1 is lower than other MOFs and F400, which is consistent with the surface area calculated by N_2 adsorption-desorption isotherm **(Table 7-2).**

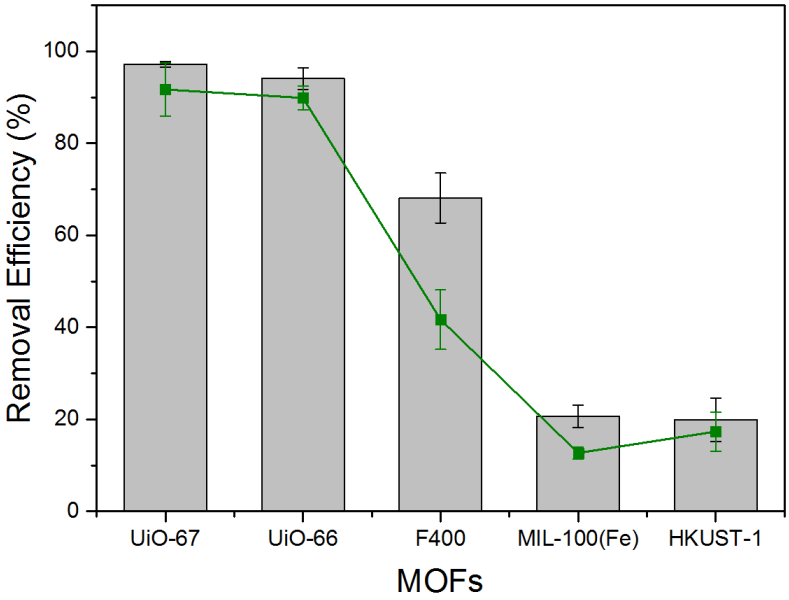

Figure 7-4 Removal Efficiency of triclosan on different adsorbents by adding various amounts of adsorbents. (Column bar represent for 5 mg and green line represents 1 mg of each of adsorbents).

7.3.3: Adsorption Kinetics of UiO-66 and UiO-67:

To compare the performance of UiO-66 and UiO-67 kinetically for the adsorption of triclosan from water, batch exposure experiments were monitored at two various initial concentrations of 2 and 5 mg L^{-1} at predetermined interval time (ranging from 1 min to 2 h) (**Figure 7-5**). The adsorption capacities for triclosan with UiO-66 and UiO-67 at initial concentrations of 2 mg L^{-1} and 5 mg L^{-1} increased rapidly during

the first 5 min and reached the maximum capacities within around 10 min at both concentrations **(Figure 7-5c)**. The initial fast removal rate of triclosan was probably attributed to the availability of unoccupied adsorption active sites. These available adsorption sites were occupied by triclosan after a while, thus a decrease in the adsorption rate was observed. At higher concentration (5 mg L^{-1}), more time was required to reach maximum adsorption capacity (within 30 min.). The increased amount of adsorbed triclosan was experimented with increasing the initial concentration indicating that UiO-67 and UiO-66 offers a favourable adsorption of triclosan at high concentration. It also revealed that both adsorbents captured effectively most of triclosan from water within 5 min at low concentration of 2 mg L^{-1}. The fast uptake of triclosan by UiO-66 was also observed, however, adsorption capacity is less than that of UiO-67, which might be attributed to the lower surface area and pore aperture of UiO-66 compared to UiO-67.

To gain better insight into the adsorption kinetics, the amount of adsorbed triclosan corresponding to the time were fitted to a pseudo-second order kinetic model (**Equation 3-12**). Pseudo second order kinetic model **(Figure 7-5b)** describes well the time dependent adsorption of triclosan in both UiO-67 and UiO-66 with high yield of correlation coefficients of 0.999 at both concentrations, respectively. Moreover, the calculated equilibrium adsorption capacity from fitting results were found to be almost the same as experimental equilibrium adsorption capacity **(Table 7-3).** When the initial concentration of triclosan increased, the pseudo second order kinetic rate constant (k_2) decreased from 0.134 to 0.055 for UiO-66 and 0.105 to 0.053 for UiO-67 at 2 and 5 mg L^{-1} **(Table 7-3),** implying that the chemisorption process plays significant role in the rate limiting step, involving

valency forces via sharing or exchange of electrons between adsorbate (triclosan) and adsorbents (UiO-67 and UiO-66). (Jiang et al., 2013, Zhu et al., 2015)

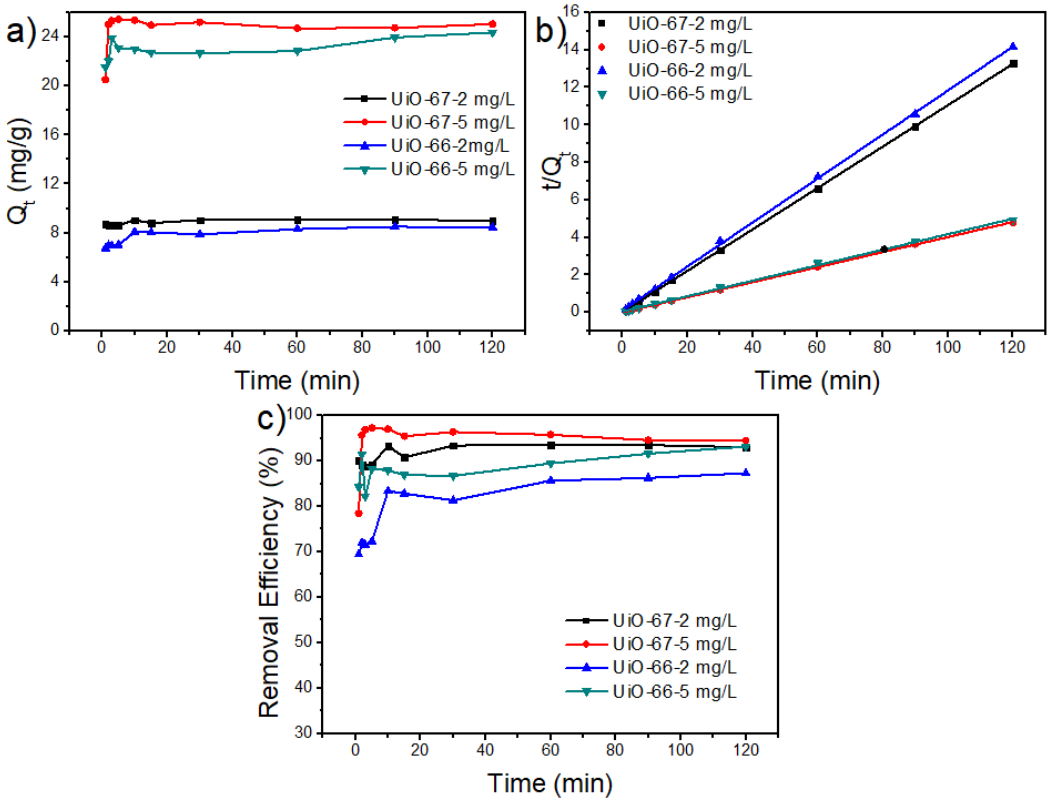

Figure 7-5 The adsorbed amount of mg of triclosan per g of UiO-66 and UiO-67 (a), pseudo second order plot for triclosan on UiO-66 and UiO-67 and removal efficiency (in %) of triclosan by UiO-66 and UiO-67 at two different concentrations as a function of time. (The data are reported as the mean of duplicate experiments).

Table 7-3 Pseudo Second Order Fitting for triclosan on UiO-67 and UiO-66

Model		**Pseudo Second Order Model**				
Adsorbents	**pH**	**Conc. (mg L^{-1})**	**Q_e (exp) (mg g^{-1})**	**Q_e (cal) (mg g^{-1})**	**k_2 (g mg^{-1} min^{-1})**	**R^2**
UiO-67	n. a	2	9.026	9.1	0.105	0.999

	n. a	5	25.05	25	0.053	0.999
UiO-66	n. a	2	8.47	8.5	0.134	0.999
	n. a	5	24.3	24.2	0.055	0.999

n.a. not adjusted

7.3.4: Zeta Potential measurements and pH effect on triclosan adsorption:

The pH of a solution is particularly necessary to understand adsorption mechanism in the aqueous solution. The protonation or dissociation of functional groups on the surface with the pH of the solution can lead to the change in the surface properties of the adsorbent and adsorbate. Since surface charges of adsorbents play a key role in adsorbing and separating charged contaminants, the zeta potential characteristics of UiO-66 and UiO-67 were performed. The zeta potentials of both UiO-66 and UiO-67 display negative above pH 3 owing to the presence of carboxylic acid (pK_a = 2.97) as expected (**Figure 7-6).** The dispersion of both UiO-66 and UiO-67 did not remain stable through the worked pH range, the surface charge might be affected by the protonation/deprotonation of the -OH groups. The difference in surface charge properties of UiO-66 and UiO-67 was not distinctive since they have the same functional groups. The zeta potentials of UiO-66 and UiO-67 were positive at pH range 2-3, respectively. However, both zeta potentials of UiO-66 and UiO-67 were negative mostly throughout the experimental pH conditions with the maximum value -28 mV for UiO-66 and -45 mV for UiO-67 at pH 10.

Batch adsorption experiments were conducted to demonstrate the adsorption mechanism over UiO-66 and UiO-67 and the effects of pH solution on the

adsorption behaviour. **Figure 7-6** shows the adsorption capacity of UiO-67 and UiO-66 corresponding to the solution pH (3, 5, 7 and 9). The increase in the amounts of adsorbed triclosan by both UiO-67 and UiO-66 was observed at the pH value from 3 and 7. However, as seen in **Figure 7-6,** the amount of adsorbed triclosan slightly decreased above pH 7 on both UiO-66 and UiO-67. Considering the pKa of triclosan, most of triclosan was found as the deprotonated form and became negatively charged at the solution of pH 8 (above the pKa of triclosan 7.9). Negative zeta potentials of both UiO-67 and UiO-66 and negatively charged triclosan above pH 8 leads to slightly lower uptake in UiO-67 and UiO-66. Therefore, electrostatic repulsion interaction between the triclosan and adsorbents can be considered as the potential adsorption mechanism. Although the adsorbed amount slightly decreased with exceeding pH from 8, the adsorbed amount seems quite stable; this might be the favourable contribution of H-bonding to triclosan adsorption. H-bonding can be considered as a plausible interaction because the O^- on triclosan after deprotonation and the functional groups on MOFs. These observations also revealed that both MOFs can be used for the removal of triclosan at natural waters at pH 7 because the adsorption capacity was not significantly affected by changing pH values.

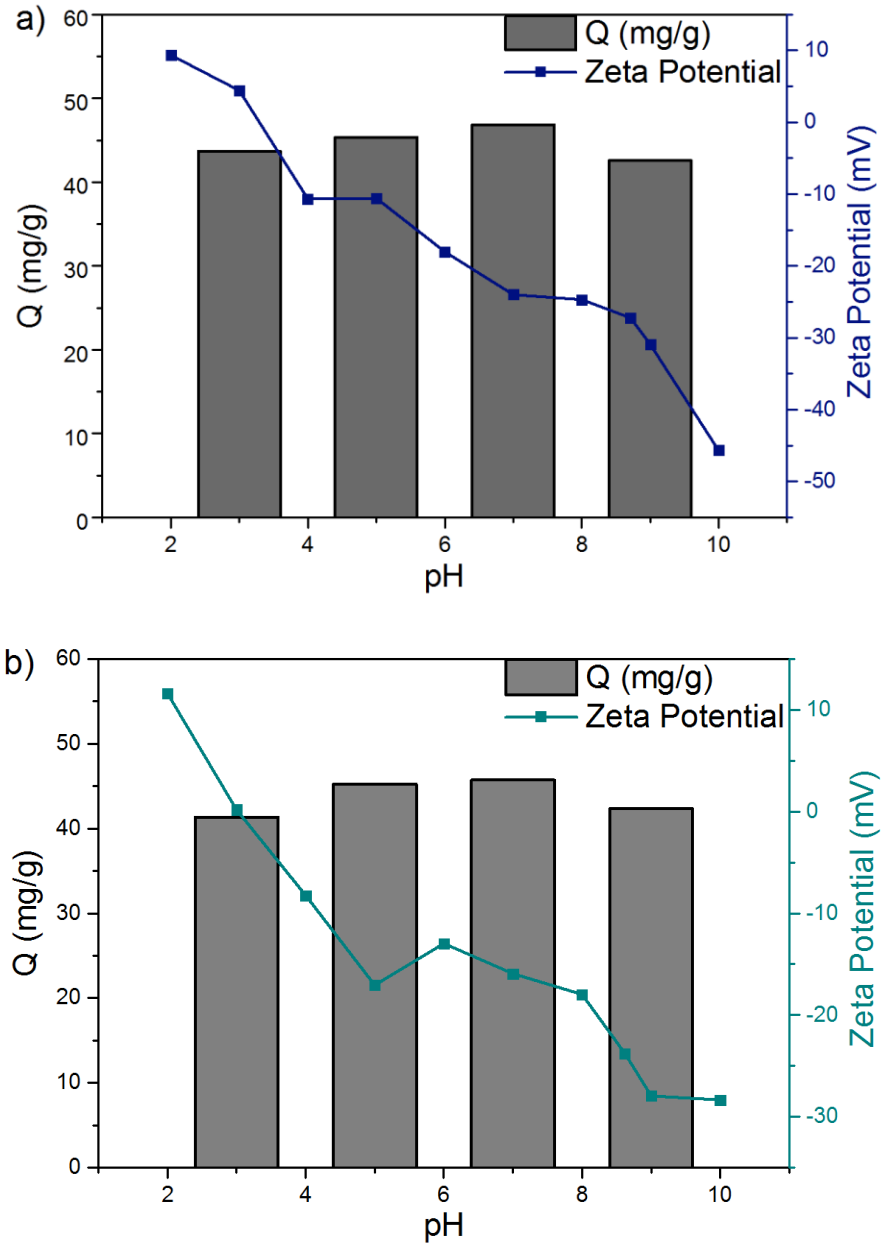

Figure 7-6 Effect of solution pH on triclosan adsorption on UiO-67 (a) and UiO-66(b) (initial concentration of triclosan was 9 mg L^{-1} contacting with 5 mg of each adsorbents for 24 h at 25 ˚C) and the zeta potential of UiO-67 (navy line, a) and UiO-66 (green line, b).

7.3.5: Adsorption isotherms for triclosan

Triclosan adsorption was conducted at some different initial concentrations ranging from 1 mg L^{-1} to 10 mg L^{-1} at pH 7 to demonstrate the maximum adsorption capacity of UiO-66 and UiO-67. The adsorption time was 24 hours to ensure adsorption equilibrium. The adsorption isotherms for triclosan over UiO-67 and UiO-66 in the basis of the unit weight of MOFs were shown in **Figure 7-7.** The tendency of **Figure 7-7** is good agreement in the results of kinetics at 1 mg L^{-1} and 5 mg L^{-1} of **Figure 7-5.** The isotherms were fitted into Langmuir-Freundlich isotherm (Equation 3-4), as shown in **Figure 7-7 a and b** and the obtained maximum adsorption capacity values, constant and correlation coefficient was tabulated in **Table 7-4**. Correlation coefficients were calculated to be very low by fitting the experimental data to other isotherm models; therefore, Langmuir-Freundlich isotherm model was chosen as it defined the adsorption very well with high yield of 96.70 % and 98.74 % for UiO-66 and UiO-67, respectively. Langmuir-Freundlich model was fitted by entering the code in Origin Pro 9.1 and the parameters were calculated. The maximum calculated adsorption capacities of UiO-66 and UiO-67 demonstrated to be comparable, however, UiO-67 gave higher maximum adsorption capacity than that of UiO-66 as expected. Therefore, it can be concluded that UiO-67 can be used as promising adsorbents for the removal of triclosan from water.

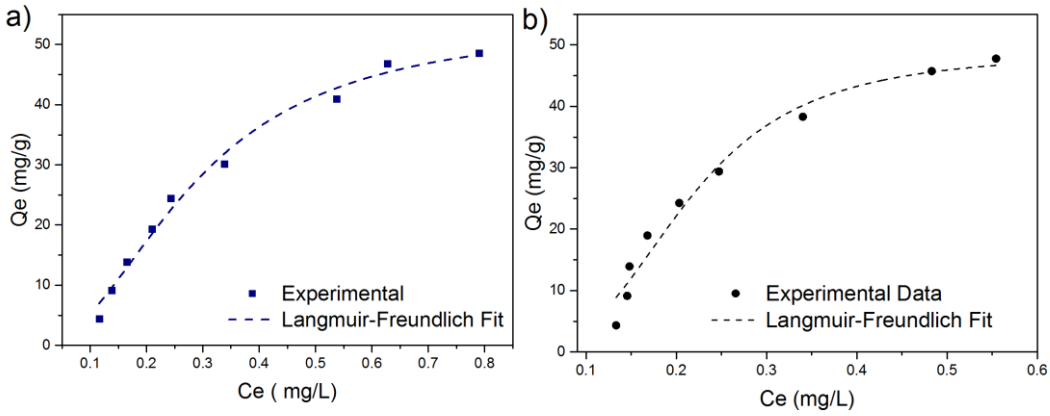

Figure 7-7 Langmuir-Freundlich fitting of triclosan on UiO-67 (a) and UiO-66 (b)

Table 7-4 Langmuir-Freundlich isotherm model fitting parameters

Adsorbents	**K_L (L mg^{-1})**	**Q_m (mg g^{-1})**	**N**	**R^2**
UiO-66	155	48.69	3.24	0.9670
UiO-67	14.68	53.84	2.13	0.9874

*Q_m maximum adsorption capacity, K_L Langmuir constant rate, N the intensity of the heterogeneity

**Experimental Data were fitted to Langmuir-Freundlich adsorption isotherm by using Origin Pro 9.1.

7.3.6: Adsorption mechanism

In general, adsorption of an adsorbate on a porous adsorbent depends on the porosity of adsorbent and the results obtained for triclosan adsorption indicate that the amount of adsorbed triclosan on MOFs and F400 can be correlated with their surface areas **(Table 7-2)** which follows the order of UiO-67> UiO-66> F400. Another possible mechanism used for the explanation of adsorption mechanism undergone in aqueous solution is hydrophobic and π-π interactions between phenyl rings of UiO-66 and UiO-67 and triclosan. In the literature, H-bonding was also

proposed to explain the adsorptive removal of organic contaminants using MOFs.(Seo et al., 2016a, Song and Jhung, 2017, Ahmed and Jhung, 2017) The presence of μ_3-OH groups in both UiO-66 and UiO-67 and O^- in triclosan above pK_a of triclosan, thus, H-bonding could play a significant role in the adsorption process. Triclosan act as H acceptor, UiO-67 and UiO-66 can act as H donor to form hydrogen bond between O^- in triclosan and μ_3-OH groups in MOFs. Finally, H-bonding can be proposed to explain the enhanced adsorption efficiency of UiO-66 and UiO-67.

7.3.7: Regeneration and Stability

Adsorptive removal of compounds relies on the reusability and regenerability of an adsorbent in commercial applications point of view. Particularly, the regenerability of an adsorbent lead to the improvement in the competitiveness of the adsorption process because it plays a necessarily key role in the adsorption in terms of reducing the cost and generating the less sludge after the treatment process. The reusability and stability of UiO-67 after regenerating the spent UiO-67 with acetone was investigated. As seen in **Figure 7-8 a,** a considerable decrease in the performance of the spent UiO-67 after acetone washing was not observed at least up to 5 times. The adsorption capacity was dropped from around 21 mg g^{-1} to around 19 mg g^{-1}, suggesting that UiO-67 is strong candidate for the adsorptive removal of triclosan from water. Furthermore, in order to study the stability of UiO-67 before and after the adsorption-desorption of triclosan, the phase purity, the surface area measurements and the phase changes were confirmed by means of XRD (**Figure 7-8 b**) and BET, respectively. **Figure 7-9** shows the N_2 adsorption-desorption isotherms of UiO-67 and regenerated UiO-67 after triclosan adsorption

confirming that the surface area and pore volume did not significantly change and also the phase crystallinity was conserved. These results revealed that the intact structure of the regenerated UiO67 confirmed by XRD, BET. Overall, just 2 % drop in the adsorption capacity and the structure stability point out that UiO-67 is strong candidate adsorbent material for the adsorptive removal of triclosan from water and can also offer potential applications in environmental water remediation.

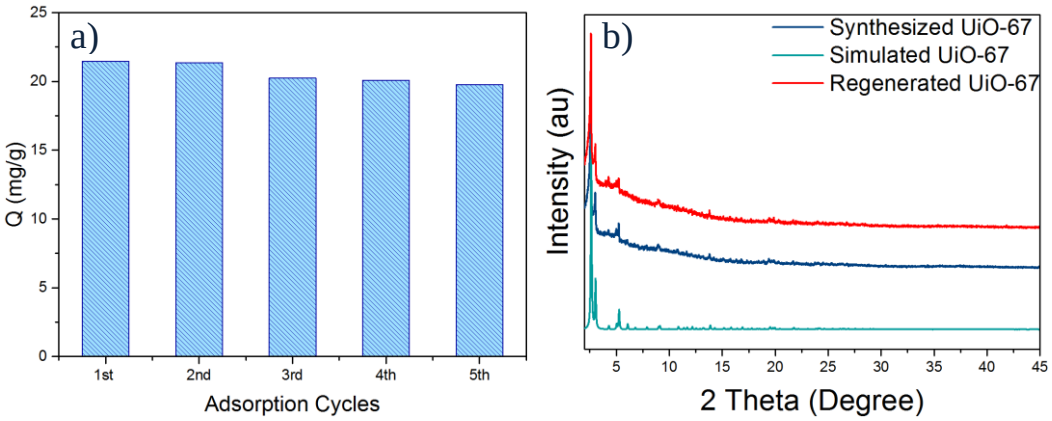

Figure 7-8 a) Adsorption Cycles of UiO-67 in the adsorption and b)XRD patterns of pristine UiO-67 and regenerated UiO-67.

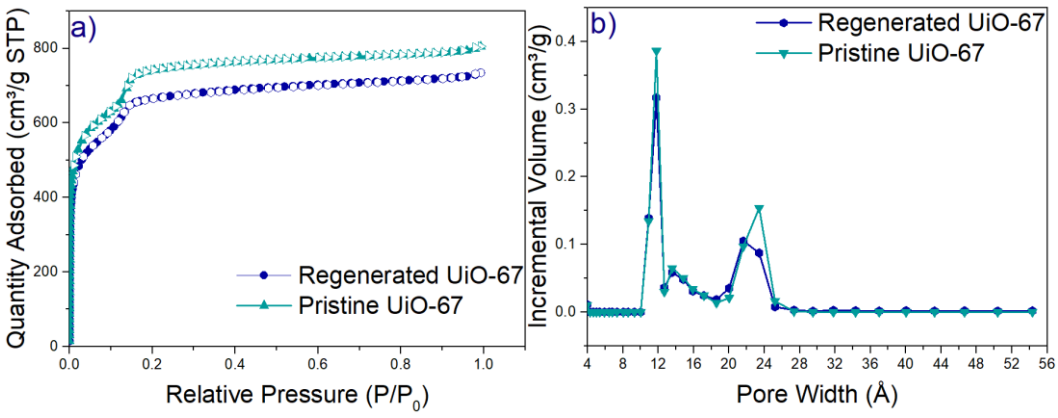

Figure 7-9 a) N_2 adsorption-desorption isotherms and b) pore size distributions of pristine UiO-67 and regenerated UiO-67 after triclosan adsorption (filled circle and empty circle represent adsorption and desorption, respectively).

7.4: CONCLUSION

Both UiO-66 and UiO-67 offered higher adsorption capacity towards triclosan adsorption when compared to F400, however, UiO-67 showed a little greater adsorption capacity than that of UiO-66. It is worth noting that F400 was not applicable for ionisable compounds adsorption (Behera et al., 2010, Domínguez et al., 2011). The adsorption capacity calculated by adsorption isotherm and kinetic experiments fittings confirm that surface area and pore volume play important role in the adsorption. Furthermore, electrostatic interactions maybe one mechanism that can be used to explain to the decrease in the adsorption capacity above pH 7 because pK_a of triclosan is 7.9 after which triclosan is deprotonated. UiO-66 and UiO-67 are negatively charged above pH 3. Therefore, where electrostatic repulsion takes place can explain the decrease in adsorption capacity between triclosan and both adsorbents. In line with the high adsorption capacity by UiO-67, the regeneration and reusability test applied to UiO-67 at least 5 times. According to the results observed in this chapter, UiO-67 can be successfully regenerated by soaking in acetone for 5 times (for one and half days) followed by re-activating at 90 ˚C for further adsorption experiments. The regenerated UiO-67 was re-used for adsorption batch experiments up to 5 times by repeating this adsorption-desorption cycle washing methods. Furthermore, the stability of UiO-67 to the adsorption process upon regeneration was elucidated by the crystallinity through PXRD and the N_2 adsorption isotherms. Hence, PXRD patterns and BET surface area results confirm that the structure of UiO-67 was unaltered after regenerated in acetone. These all observations affirm that UiO-67 can be determined as promising adsorbents for the removal of hydrophobic and ionisable compound from water.

Chapter 8: CONCLUDING REMARKS and FUTURE RECOMMENDATIONS

The main aim of the thesis was to evaluate the adsorption performance of crystalline materials, particularly, metal-organic frameworks (MOFs) in water purification applications. These hybrid materials with permanent porosity have attracted widespread attention and have been used in a wide range of applications due to their intriguing properties, including, but not to limited to, their tunable structure (i.e., pore size, porosity etc) (Furukawa et al., 2013b) and chemical features (i.e., functional groups etc.). Recently, the use of MOFs as adsorbents has been demonstrated in the liquid phase, for water purification applications involving the removal of contaminants such as volatile organic compounds, PPCPs, EDCs and nerve agent. The outcomes of the previous research presented exciting potential for use in treating contaminated water. These results prompted this thesis, which focussed on investigating the use of selected exceptionally chemical stable MOFs for the removal of persistent organic compounds from water. This research gives insight to design and development of efficient adsorbents for the effective and sustainable removal of emerging trace levels of organic contaminants such PPCPs, EDCs and other analytes.

The key findings of the research are given as follows:

Chapter 4 concentrated on the uptake of atrazine (pesticide) from water using various MOFs with having different pore sizes, apertures and surface areas. Additionally, the adsorption ability of the selected MOFs was elucidated by comparing the performance of MOFs with commercially available granular

activated carbon Filtrasorb 400 (F400). UiO-67 offered greater affinity for atrazine and more importantly exhibited fast uptake kinetic (98 % of atrazine removed) in less than 5 min. Therefore, UiO-67 surpassed activated carbon, ZIF-8, UiO-66, and HKUST-1. This greater adsorption capacity and fast uptake of UiO-67 are ascertained to UiO-67`s high surface area and pore size. Another significant parameter for industrial scale applications is regenerability of adsorbents, thus, UiO-67 was successively regenerated and re-used for the adsorption of atrazine through 3 cycles.

Chapter 5 investigated the applicability of MOFs for the uptake of carbamazepine. UiO-67 exhibited higher adsorption capacity and rapid uptake kinetic. UiO-67 removed 95% of carbamazepine in only 2 min, which might be due to the small particle size, pore volume and available active sites of UiO-67. The higher surface area of UiO-67 and active sites induced by missing linker leads to specific interaction with carbamazepine resulting in enhanced adsorption capacity of carbamazepine. Furthermore, the regenerability and the retainability of the structure after regeneration was verified.

Giving the promising results obtained in Chapter 4 and Chapter 5 of the thesis, Chapter 6 focused on the performance of the UiO-67 for the adsorptive removal of a binary mixture of carbamazepine and atrazine. Additionally, the interference effect of salts on the uptake of binary mixture in water investigated. The uptake of carbamazepine and atrazine as a mixture reached equilibrium in less than 2 min and the change in the uptake was not observed in the presence of salt. Furthermore, the spent UiO-67 was easily regenerated through 6 cycles. The key findings of this

chapter (superior capacity in the presence of salts and rapid uptake for the mixture of carbamazepine and atrazine) enlightened its potential in real water samples.

In the last chapter of this research demonstrated the hydrophobic antibacterial personal care product, UiO-66 and UiO-67, two zirconium-based MOFs, offered higher adsorption capacity compared to commercially available activated carbon. Although it is known that activated carbon shows greater adsorption capacity towards hydrophobic compound, MOFs outperformed activated carbons. This may be correlated with their higher surface areas and pore apertures which are large enough to accommodate triclosan in the pores. Furthermore, specific interaction, such as hydrogen bonding and π-π stacking interaction, may also contribute to the higher adsorption capacity. This chapter outlined the development of potent adsorbent that revealed a greater adsorption capacity of triclosan.

Overall, the faster uptake kinetics, regenerability of UiO-67 and stability of UiO-67 after the uptake of analytes (atrazine, carbamazepine, mixture of carbamazepine and triclosan) demonstrated that UiO-67 can be a promising adsorbent and applicable in full-scale industrial purification projects.

8.1: GENERAL CONCLUSION-COST ANALYSIS

MOF with exciting potential in water purification applications can offer unique structural and chemical properties that can be beneficial for an industrial application. This thesis particularly concentrated on demonstrating that MOFs as adsorbents are a better alternative to activated carbons to remove organic pollutants from water. Activated carbons suffer from slow analyte uptake (hours) and poor removal of hydrophilic micropollutants. Moreover, regenerating the spent activated

carbons needs for re-heating at 500-900 ºC resulting in high energy consumption and does not entirely recovered (de Andrade et al., 2018). This thermal activation can cause to weight loss and destroy the porous structure of activated carbons. The harsh regeneration increases the cost of adsorption process using activated carbons and encumbers the use in large scale. In the case of MOF crystalline materials, the results obtained in this thesis demonstrated that MOFs can be easily regenerated by simply soaking in an organic solvent (i.e., acetone) followed by drying in vacuum heating. The used acetone can also be recovered by distillation, suggesting that the use of MOF as an adsorbent is more advantageous than activated carbons. Additionally, a less amount of MOF can remove almost all the analytes (in percent) from water in the order of minutes whereas activated carbon can remove the same amount of analyte (in percent) as MOF removed in the order of hours. These makes adsorption using MOFs feasible in large scale applications.

Furthermore, MOFs synthesis protocol can be improved and can be easily scaled up to afford multigram scale, which is vital for industrial application projects. In scale up production, metal salts such as (hydr)oxides and sulphates are effortlessly available and their cost is also the lowest. Only organic linker molecules' cost is a requisite part of the raw material costs for MOF synthesis. Organic linkers include carboxylic acids (i.e., terephthalic, isophthalic, and formic acid, are more preferable in comparison to complex linkers (Yilmaz et al., 2012). The carboxylic acids are usually available at reasonable price in industrial scale.

The cost of adsorption processes is calculated to be approximately from US $10 to $200 per million litres, which is dependent on the type of adsorbent. However, advanced treatment technologies include reverse osmosis, ion exchange,

electrodialysis, and electrolysis increase the cost to US $450 per million litres (Ali, 2014). Capital and operational costs are the costs for an adsorption plant. The capital cost is related to an essential cost of the adsorbent price, which is dependent on the adsorbent capacity. The operational cost is the cost of the amount of energy needed for the process. An enhanced uptake capacity and faster uptake kinetic can lead to a decrease in the capital and operational costs. The following process variables for the total process cost are given (**Figure 8-1**) (https://jclfss.weebly.com/design-and-cost.html).

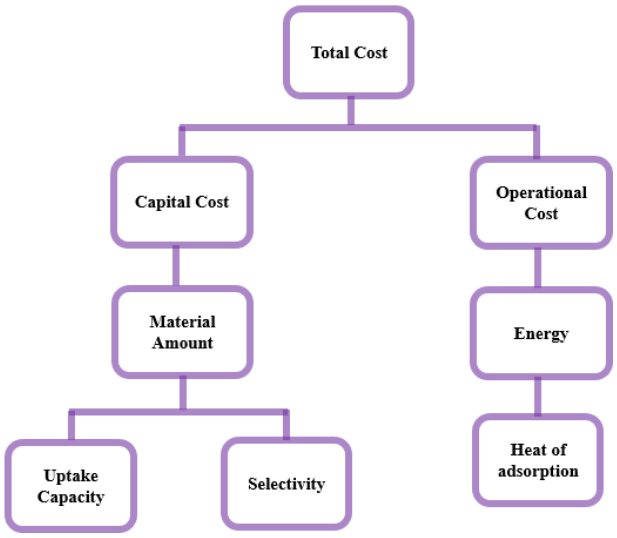

Figure 8-1 Flow chart of the total process cost

Concluding, easy regeneration and scaled up of MOF materials, larger uptake capacity and cost assessment affirms that MOF seems to be strong alternative candidate for industrial application compared to activated carbon.

FUTURE RECOMMENDATIONS

From the research conducted in the development of this thesis, it has been concluded that MOFs have enormous potential for use in various adsorption related applications, particularly those involving water purification. It is anticipated that there is significant scope for further progress in this field. To expedite this progress, the following recommendations with respect to this future work are given:

1. Design and develop MOF composites (i.e., MOF/graphene oxide composite) in various applications such as removal of heavy metal ions and persistent organic compounds.
2. Investigate the synergistic effect of drugs and metal ions in MOFs. To elucidate the effect of metal ions on the adsorption, a variety of MOFs having various metal ions such as zirconium, zinc, aluminium, iron, chromium and copper-based MOFs can be chosen, and screening test can be applied in one pharmaceutical and expand to mixture of drugs to investigate the selectivity.
3. Expand the investigation of multicomponent adsorption using MOFs. MOF materials can be engineered to different defect densities, thus, the effect of defect on the adsorption capacity of the MOFs is studied.
4. Synthesise MOFs having different functional groups and pyrene core to further investigate the nature of the prevalent adsorption forces such as H-bonding and π-π stacking, which governs the uptake of analytes.
5. Additionally, investigate the effects of incorporating only various functional groups in MOFs on adsorption of analytes.

Chapter 9: APPENDICES

9.1: APPENDIX I: Calibration Curves in Chapter 4

9.1.1: Atrazine Calibration Curve in Water

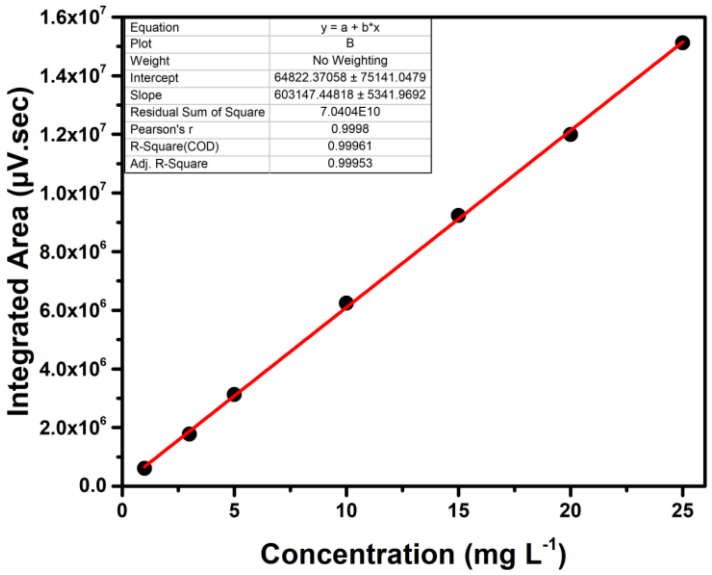

Figure 9-1 Atrazine Calibration Curve obtained by HPLC at pH 6.9

9.1.2: Atrazine calibration curves in water for pH effect Study

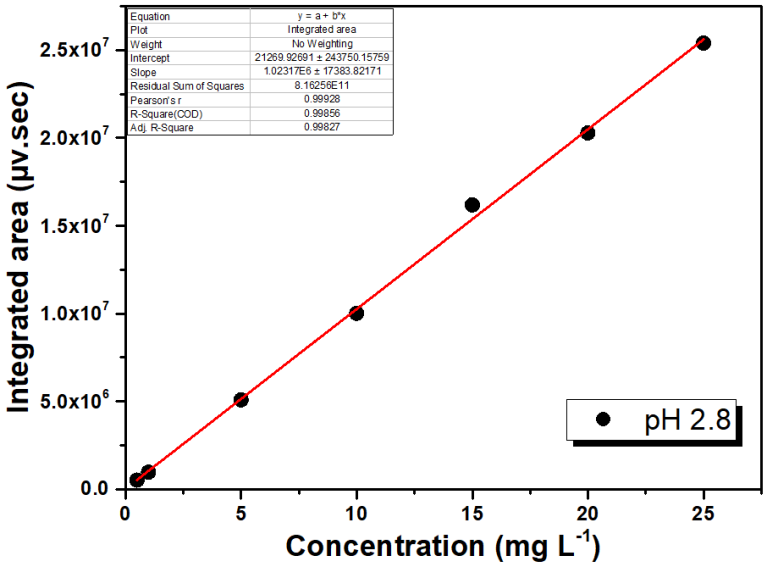

Figure 9-2 Atrazine Calibration Curve obtained by HPLC at pH 2.8

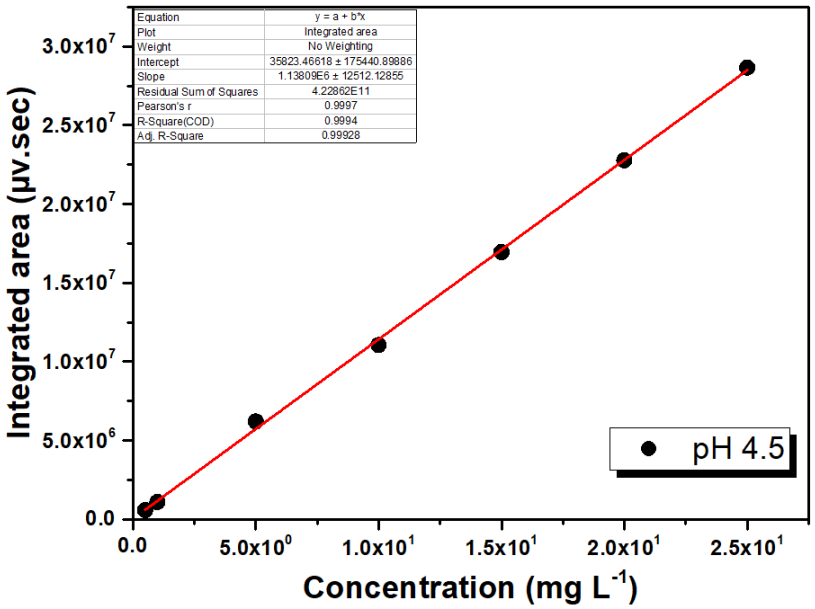

Figure 9-3 Atrazine Calibration Curve obtained by HPLC at pH 4.5

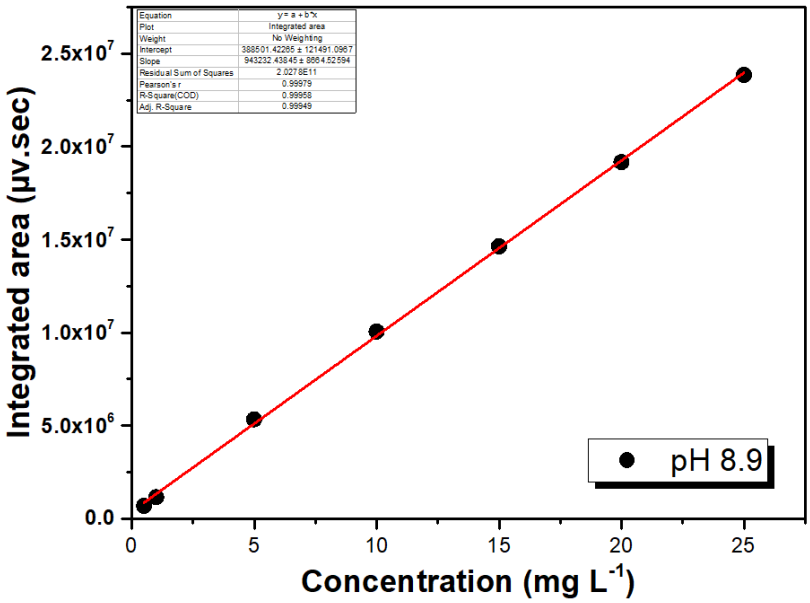

Figure 9-4 Atrazine Calibration Curve obtained by HPLC at pH 8.9

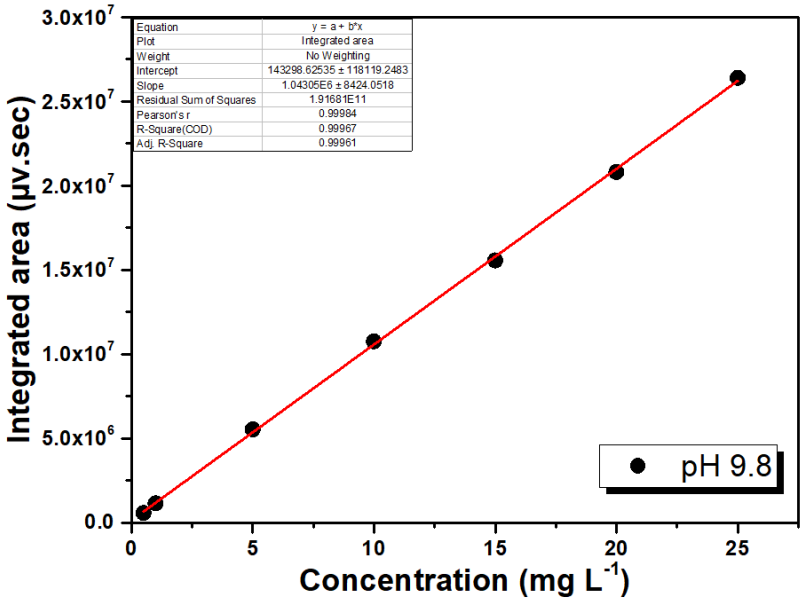

Figure 9-5 Atrazine Calibration Curve obtained by HPLC at pH 9.8

9.2: APPENDIX II: Calibration Curves in Chapter 5

9.2.1: Carbamazepine calibration curve in water

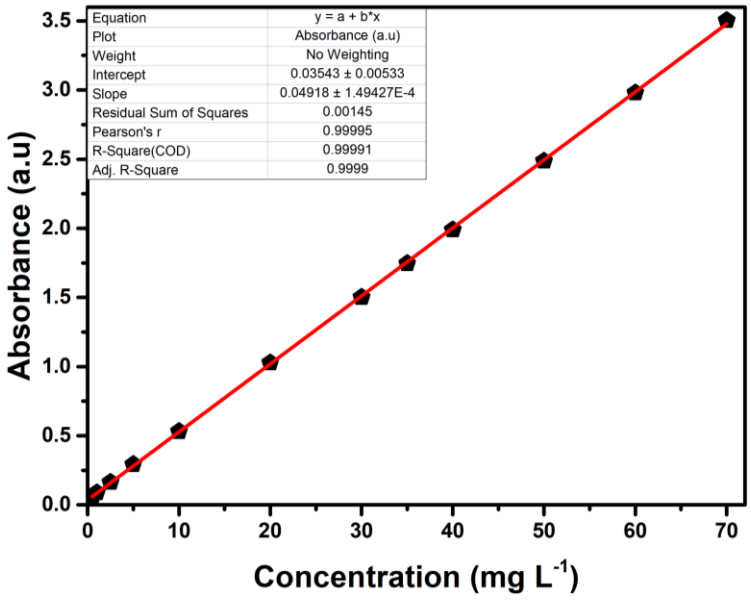

Figure 9-6 Carbamazepine Calibration Curve obtained by UV-vis at pH 5

9.2.2: Carbamazepine calibration curves in water for pH effect Study

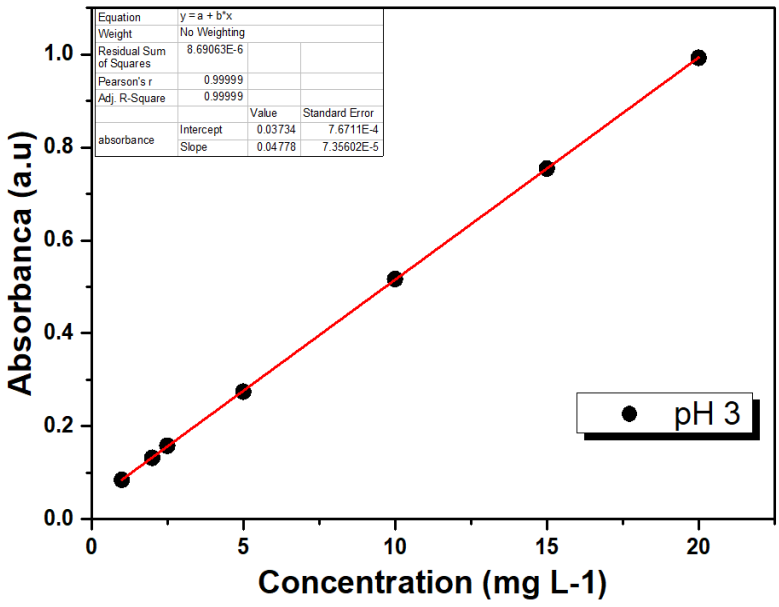

Figure 9-7 Carbamazepine Calibration Curve obtained by UV-vis at pH 3

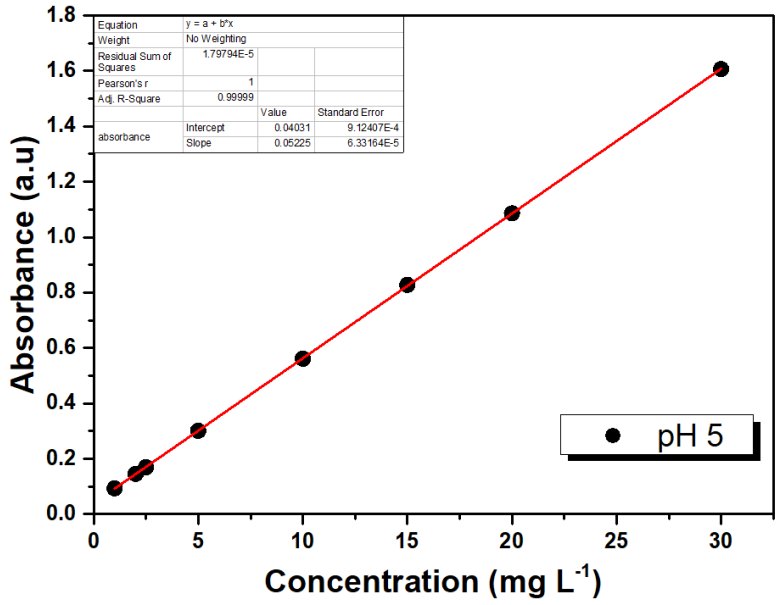

Figure 9-8 Carbamazepine Calibration Curve obtained by UV-vis at pH 5

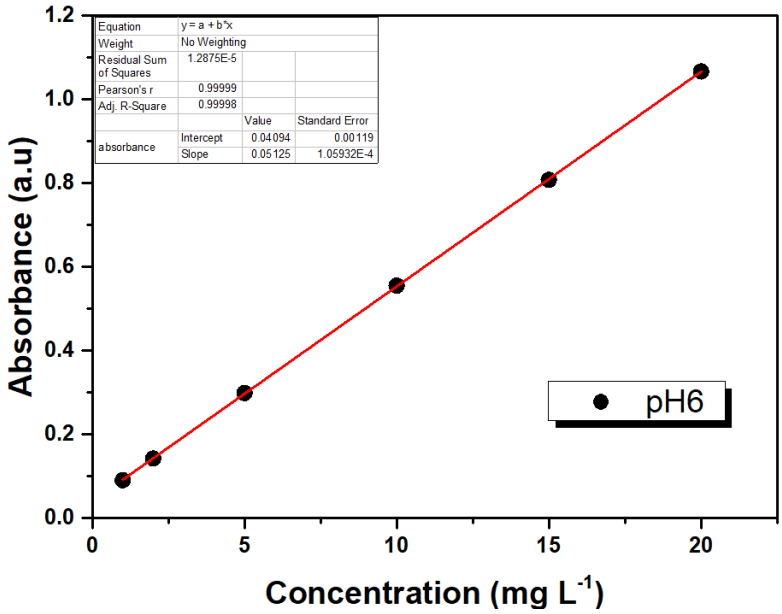

Figure 9-9 Carbamazepine Calibration Curve obtained by UV-vis at pH 6

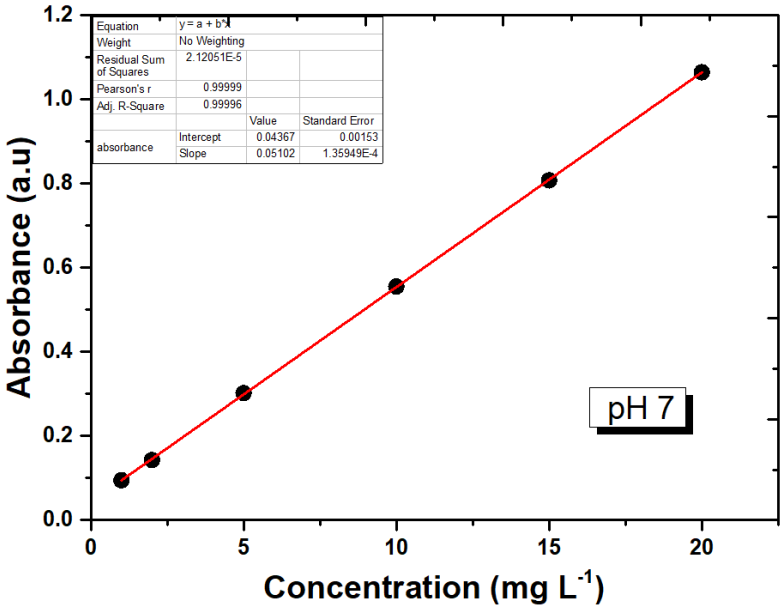

Figure 9-10 Carbamazepine Calibration Curve obtained by UV-vis at pH 7

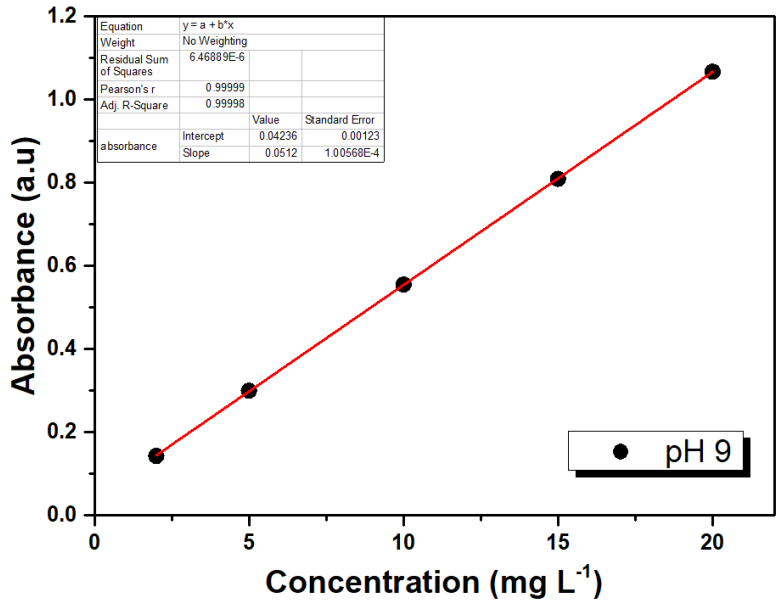

Figure 9-11 Carbamazepine Calibration Curve obtained by UV-vis at pH 9

9.3: APPENDIX II: Calibration Curves in Chapter 7

9.3.1: Triclosan Calibration Curve in Water

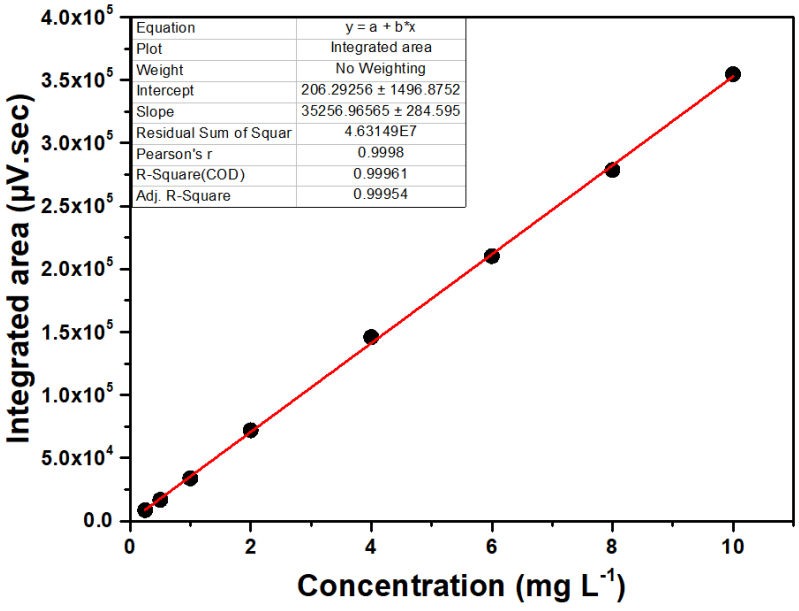

Figure 9-12 Triclosan Calibration Curve at pH 7

9.3.2: Triclosan calibration curves in water for pH effect Study

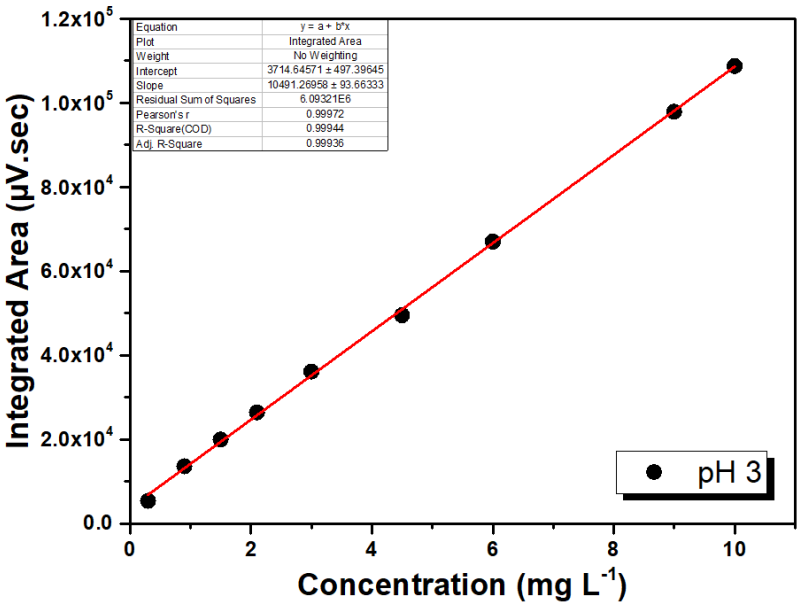

Figure 9-13 Triclosan Calibration Curve obtained by HPLC-UV at pH 3

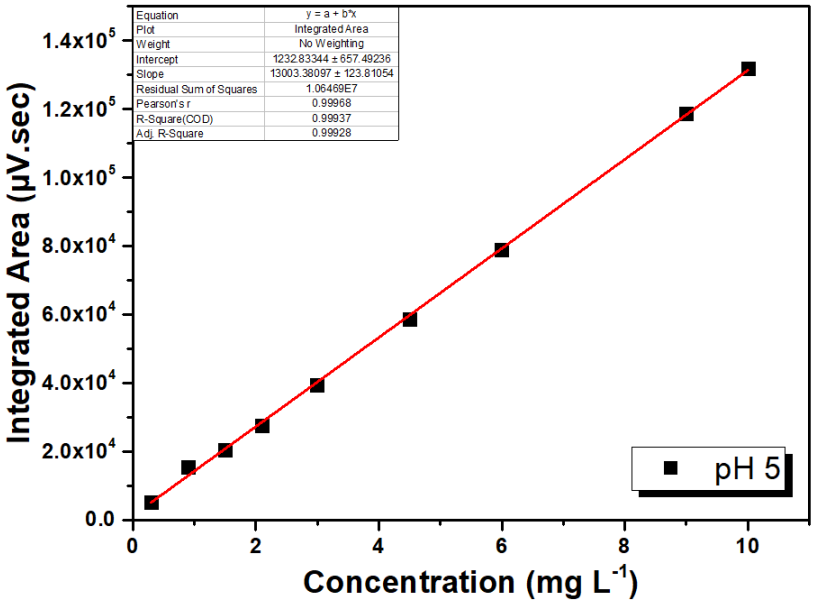

Figure 9-14 Triclosan Calibration Curve obtained by HPLC-UV at pH 5

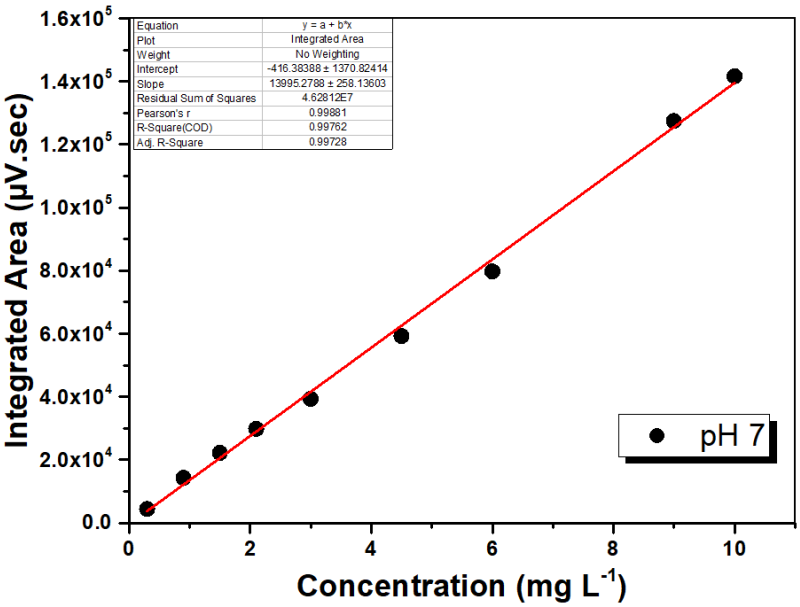

Figure 9-15 Triclosan Calibration Curve obtained by HPLC-UV at pH 7

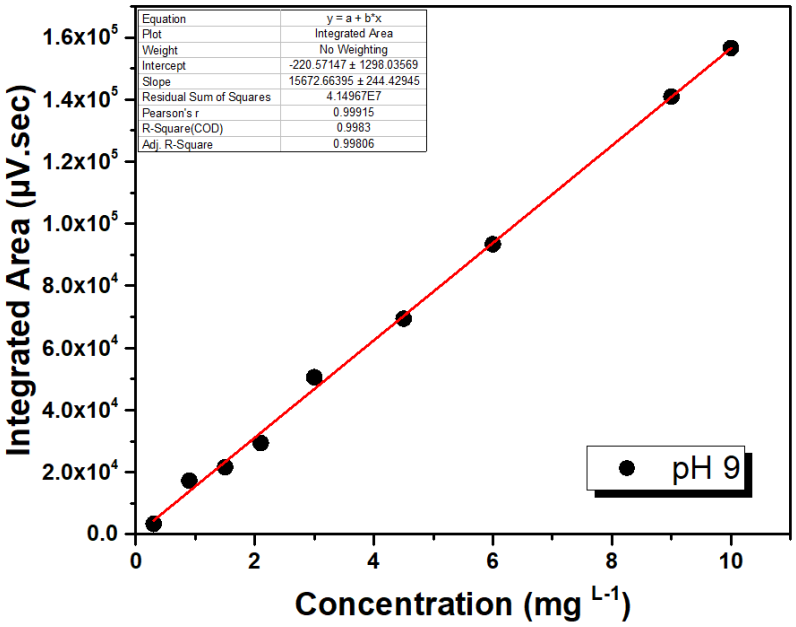

Figure 9-16 Triclosan Calibration Curve obtained by HPLC-UV at pH 9

RERERENCES

1. (WHO), W. H. O. 2012. *Pharmaceuticals in drinking-water* [Online]. Available: http://www.who.int/water_sanitation_health/publications/2012/pharmaceuticals/en/ [Accessed 10 Feb 2018 2018].
2. ABNEY, C. W., GILHULA, J. C., LU, K. & LIN, W. 2014. Metal-organic framework templated inorganic sorbents for rapid and efficient extraction of heavy metals. *Adv Mater,* 26**,** 7993-7.
3. ADAMS, C., WANG, Y., LOFTIN, K. & MEYER, M. 2002. Removal of Antibiotics from Surface and Distilled Water in Conventional Water Treatment Processes. *Journal of Environmental Engineering,* 128**,** 253-260.
4. AHMED, I. & JHUNG, S. H. 2016. Adsorptive desulfurization and denitrogenation using metal-organic frameworks. *J Hazard Mater,* 301**,** 259-76.
5. AHMED, I. & JHUNG, S. H. 2017. Applications of metal-organic frameworks in adsorption/separation processes via hydrogen bonding interactions. *Chemical Engineering Journal,* 310**,** 197-215.
6. AL-KUTUBI, H., GASCON, J., SUDHÖLTER, E. J. R. & RASSAEI, L. 2015. Electrosynthesis of Metal-Organic Frameworks: Challenges and Opportunities. *ChemElectroChem,* 2**,** 462-474.
7. ALI, I. 2014. Water Treatment by Adsorption Columns: Evaluation at Ground Level. *Separation & Purification Reviews,* 43**,** 175-205.
8. ALSBAIEE, A., SMITH, B. J., XIAO, L., LING, Y., HELBLING, D. E. & DICHTEL, W. R. 2016. Rapid removal of organic micropollutants from water by a porous β-cyclodextrin polymer. *Nature,* 529**,** 190-194.
9. ALTMANN, J., RUHL, A. S., ZIETZSCHMANN, F. & JEKEL, M. 2014. Direct comparison of ozonation and adsorption onto powdered activated carbon for micropollutant removal in advanced wastewater treatment. *Water Res,* 55**,** 185-93.
10. AUDU, C. O., NGUYEN, H. G. T., CHANG, C.-Y., KATZ, M. J., MAO, L., FARHA, O. K., HUPP, J. T. & NGUYEN, S. T. 2016. The dual capture of AsVand AsIIIby UiO-66 and analogues. *Chem. Sci.,* 7**,** 6492-6498.
11. AZHAR, M. R., ABID, H. R., PERIASAMY, V., SUN, H., TADE, M. O. & WANG, S. 2017. Adsorptive removal of antibiotic sulfonamide by UiO-66 and ZIF-67 for wastewater treatment. *J Colloid Interface Sci,* 500**,** 88-95.
12. BAERLOCHER, C., MCCUSKER, L. B. & OLSON, D. H. 2007. *Atlas of zeolite framework types*, Elsevier.
13. BANG, J. H. & SUSLICK, K. S. 2010. Applications of ultrasound to the synthesis of nanostructured materials. *Adv Mater,* 22**,** 1039-59.
14. BÁRCIA, P. S., GUIMARÃES, D., MENDES, P. A. P., SILVA, J. A. C., GUILLERM, V., CHEVREAU, H., SERRE, C. & RODRIGUES, A. E. 2011. Reverse shape selectivity in the adsorption of hexane and xylene isomers in MOF UiO-66. *Microporous and Mesoporous Materials,* 139**,** 67-73.

15. BAREA, E., MONTORO, C. & NAVARRO, J. A. 2014. Toxic gas removal--metal-organic frameworks for the capture and degradation of toxic gases and vapours. *Chem Soc Rev,* 43**,** 5419-30.
16. BARRETT, E. P., JOYNER, L. G. & HALENDA, P. P. 1951. The Determination of Pore Volume and Area Distributions in Porous Substances. I. Computations from Nitrogen Isotherms. *Journal of the American Chemical Society,* 73**,** 373-380.
17. BEHERA, S. K., OH, S. Y. & PARK, H. S. 2010. Sorption of triclosan onto activated carbon, kaolinite and montmorillonite: effects of pH, ionic strength, and humic acid. *J Hazard Mater,* 179**,** 684-91.
18. BHADRA, B. N., AHMED, I., KIM, S. & JHUNG, S. H. 2017. Adsorptive removal of ibuprofen and diclofenac from water using metal-organic framework-derived porous carbon. *Chemical Engineering Journal,* 314**,** 50-58.
19. BHADRA, B. N. & JHUNG, S. H. 2017. A remarkable adsorbent for removal of contaminants of emerging concern from water: Porous carbon derived from metal azolate framework-6. *J Hazard Mater,* 340**,** 179-188.
20. BOBBITT, N. S., MENDONCA, M. L., HOWARTH, A. J., ISLAMOGLU, T., HUPP, J. T., FARHA, O. K. & SNURR, R. Q. 2017. Metal-organic frameworks for the removal of toxic industrial chemicals and chemical warfare agents. *Chem Soc Rev,* 46**,** 3357-3385.
21. BOXALL, A., MONTEIRO, S. C., FUSSELL, R., WILLIAMS, R. J., BRUEMER, J., GREENWOOD, R. & BERSUDER, P. 2012. Targeted monitoring for human pharmaceuticals in vulnerable source and final waters.
22. BRENNER, H. 2013. *Adsorption Calculations and Modelling*, Elsevier.
23. BRITT, D., FURUKAWA, H., WANG, B., GLOVER, T. G. & YAGHI, O. M. 2009. Highly efficient separation of carbon dioxide by a metal-organic framework replete with open metal sites. *Proc Natl Acad Sci U S A,* 106**,** 20637-40.
24. BRITT, D., TRANCHEMONTAGNE, D. & YAGHI, O. M. 2008. Metal-organic Frameworks with High Capacity and Selectivity for Harmful Gases. *Proc. Natl. Acad. Sci. U. S. A.,* 105**,** 11623.
25. BROSEUS, R., VINCENT, S., ABOULFADL, K., DANESHVAR, A., SAUVE, S., BARBEAU, B. & PREVOST, M. 2009. Ozone oxidation of pharmaceuticals, endocrine disruptors and pesticides during drinking water treatment. *Water Res,* 43**,** 4707-17.
26. BROWN, N. W., ROBERTS, E. P., CHASIOTIS, A., CHERDRON, T. & SANGHRAJKA, N. 2004. Atrazine removal using adsorption and electrochemical regeneration. *Water Res,* 38**,** 3067-74.
27. BRUNAUER, S., EMMETT, P. H. & TELLER, E. 1938. Adsorption of Gases in Multimolecular Layers. *Journal of the American Chemical Society,* 60**,** 309-319.
28. BUI, T. X. & CHOI, H. 2009. Adsorptive removal of selected pharmaceuticals by mesoporous silica SBA-15. *J Hazard Mater,* 168**,** 602-8.
29. BURTCH, N. C., JASUJA, H. & WALTON, K. S. 2014. Water stability and adsorption in metal-organic frameworks. *Chem Rev,* 114**,** 10575-612.

30. CABRERA-LAFAURIE, W. A., ROMÁN, F. R. & HERNÁNDEZ-MALDONADO, A. J. 2014. Removal of salicylic acid and carbamazepine from aqueous solution with Y-zeolites modified with extraframework transition metal and surfactant cations: Equilibrium and fixed-bed adsorption. *Journal of Environmental Chemical Engineering,* 2**,** 899-906.
31. CAI, N. & LARESE-CASANOVA, P. 2014. Sorption of carbamazepine by commercial graphene oxides: a comparative study with granular activated carbon and multiwalled carbon nanotubes. *J Colloid Interface Sci,* 426**,** 152-61.
32. CALISTO, V., FERREIRA, C. I., OLIVEIRA, J. A., OTERO, M. & ESTEVES, V. I. 2015. Adsorptive removal of pharmaceuticals from water by commercial and waste-based carbons. *J Environ Manage,* 152**,** 83-90.
33. CAMPBELL, C. G., BORGLIN, S. E., GREEN, F. B., GRAYSON, A., WOZEI, E. & STRINGFELLOW, W. T. 2006. Biologically directed environmental monitoring, fate, and transport of estrogenic endocrine disrupting compounds in water: A review. *Chemosphere,* 65**,** 1265-80.
34. CARVALHO, F. P. 2017. Pesticides, environment, and food safety. *Food and Energy Security,* 6**,** 48-60.
35. CASTRO, C. S., GUERREIRO, M. C., GONCALVES, M., OLIVEIRA, L. C. & ANASTACIO, A. S. 2009. Activated carbon/iron oxide composites for the removal of atrazine from aqueous medium. *J Hazard Mater,* 164**,** 609-14.
36. CAVKA, J. H. 2008. A New Zirconium Inorganic Building Brick Forming Metal Organic Frameworks with Exceptional Stability. *J. Am. Chem. Soc.,* 130**,** 13850-13851.
37. CHAE, H. K., SIBERIO-PEREZ, D. Y., KIM, J., GO, Y., EDDAOUDI, M., MATZGER, A. J., O'KEEFFE, M. & YAGHI, O. M. 2004. A route to high surface area, porosity and inclusion of large molecules in crystals. *Nature,* 427**,** 523-527.
38. CHAPARADZA, A. & HOSSENLOPP, J. M. 2012. Adsorption kinetics, isotherms and thermodynamics of atrazine removal using a banana peel based sorbent. *Water Sci Technol,* 65**,** 940-7.
39. CHAVAN, S., VITILLO, J. G., GIANOLIO, D., ZAVOROTYNSKA, O., CIVALLERI, B., JAKOBSEN, S., NILSEN, M. H., VALENZANO, L., LAMBERTI, C., LILLERUD, K. P. & BORDIGA, S. 2012. H2 storage in isostructural UiO-67 and UiO-66 MOFs. *Phys Chem Chem Phys,* 14**,** 1614-26.
40. CHEN, C., YANG, S., GUO, Y., SUN, C., GU, C. & XU, B. 2009. Photolytic destruction of endocrine disruptor atrazine in aqueous solution under UV irradiation: products and pathways. *J Hazard Mater,* 172**,** 675-84.
41. CHEN, G.-C., SHAN, X.-Q., WANG, Y.-S., PEI, Z.-G., SHEN, X.-E., WEN, B. & OWENS, G. 2008. Effects of Copper, Lead, and Cadmium on the Sorption and Desorption of Atrazine onto and from Carbon Nanotubes. *Environmental Science & Technology,* 42**,** 8297-8302.
42. CHEN, J., ZHANG, D., ZHANG, H., GHOSH, S. & PAN, B. 2017. Fast and slow adsorption of carbamazepine on biochar as affected by carbon structure and mineral composition. *Sci Total Environ,* 579**,** 598-605.

43. CHINGOMBE, P., SAHA, B. & WAKEMAN, R. J. 2006. Sorption of atrazine on conventional and surface modified activated carbons. *J Colloid Interface Sci,* 302**,** 408-16.
44. CHO, H. H., HUANG, H. & SCHWAB, K. 2011. Effects of solution chemistry on the adsorption of ibuprofen and triclosan onto carbon nanotubes. *Langmuir,* 27**,** 12960-7.
45. CHUI, S. S.-Y., LO, S. M.-F., CHARMANT, J. P. H., ORPEN, A. G. & WILLIAMS, I. D. 1999. A Chemically Functionalizable Nanoporous Material [Cu₃(TMA)₂(H₂O)₃]_n. *Science,* 283**,** 1148-1150.
46. CLARA, M., STRENN, B., GANS, O., MARTINEZ, E., KREUZINGER, N. & KROISS, H. 2005. Removal of selected pharmaceuticals, fragrances and endocrine disrupting compounds in a membrane bioreactor and conventional wastewater treatment plants. *Water Res,* 39**,** 4797-807.
47. CORCORAN, J., WINTER, M. J. & TYLER, C. R. 2010. Pharmaceuticals in the aquatic environment: a critical review of the evidence for health effects in fish. *Crit Rev Toxicol,* 40**,** 287-304.
48. D'ALESSANDRO, D. M., SMIT, B. & LONG, J. R. 2010. Carbon dioxide capture: prospects for new materials. *Angew Chem Int Ed Engl,* 49**,** 6058-82.
49. DAI, C. M., ZHANG, J., ZHANG, Y. L., ZHOU, X. F., DUAN, Y. P. & LIU, S. G. 2013. Removal of carbamazepine and clofibric acid from water using double templates-molecularly imprinted polymers. *Environ Sci Pollut Res Int,* 20**,** 5492-501.
50. DAUGHTON, C. G. & TERNES, T. A. 1999. Pharmaceuticals and Personal Care Products in the Environment : Agents of subtle Change? *Environmental Health Perspectives,* 107**,** 907–942.
51. DAVIS, M. E. 2002. Ordered porous materials for emerging applications. *Nature,* 417**,** 813-821.
52. DE ANDRADE, J. R., OLIVEIRA, M. F., DA SILVA, M. G. C. & VIEIRA, M. G. A. 2018. Adsorption of Pharmaceuticals from Water and Wastewater Using Nonconventional Low-Cost Materials: A Review. *Industrial & Engineering Chemistry Research,* 57**,** 3103-3127.
53. DE BOER, J. H., LIPPENS, B. C., LINSEN, B. G., BROEKHOFF, J. C. P., VAN DEN HEUVEL, A. & OSINGA, T. J. 1966. Thet-curve of multimolecular N2-adsorption. *Journal of Colloid and Interface Science,* 21**,** 405-414.
54. DECOSTE, J. B. & PETERSON, G. W. 2014. Metal-organic frameworks for air purification of toxic chemicals. *Chem Rev,* 114**,** 5695-727.
55. DECOSTE, J. B., PETERSON, G. W., SCHINDLER, B. J., KILLOPS, K. L., BROWE, M. A. & MAHLE, J. J. 2013. The effect of water adsorption on the structure of the carboxylate containing metal–organic frameworks Cu-BTC, Mg-MOF-74, and UiO-66. *Journal of Materials Chemistry A,* 1**,** 11922.
56. DENG, S. 2006. Sorbent technology. *Encyclopedia of Chemical Processing***,** 2825-2845.
57. DIAS, E. M. & PETIT, C. 2015. Towards the use of metal–organic frameworks for water reuse: a review of the recent advances in the field of

organic pollutants removal and degradation and the next steps in the field. *J. Mater. Chem. A,* 3**,** 22484-22506.
58. DO, D. D. 1998. *Adsorption Analysis: Equilibria and Kinetics:(With CD Containing Computer Matlab Programs)*, World Scientific.
59. DO, J. L. & FRISCIC, T. 2017. Mechanochemistry: A Force of Synthesis. *ACS Cent Sci,* 3**,** 13-19.
60. DOMÍNGUEZ-VARGAS, J. R., GONZALEZ, T., PALO, P. & CUERDA-CORREA, E. M. 2013. Removal of Carbamazepine, Naproxen, and Trimethoprim from Water by Amberlite XAD-7: A Kinetic Study. *CLEAN - Soil, Air, Water,* 41**,** 1052-1061.
61. DOMÍNGUEZ, J. R., GONZÁLEZ, T., PALO, P. & CUERDA-CORREA, E. M. 2011. Removal of common pharmaceuticals present in surface waters by Amberlite XAD-7 acrylic-ester-resin: Influence of pH and presence of other drugs. *Desalination,* 269**,** 231-238.
62. DUBININ, M. I. 1975. Physical adsorption of gases and vapors in micropores. *Progress in surface and membrane science,* 9**,** 1-70.
63. EBRAHIM, A. M., LEVASSEUR, B. & BANDOSZ, T. J. 2013. Interactions of NO2 with Zr-based MOF: effects of the size of organic linkers on NO2 adsorption at ambient conditions. *Langmuir,* 29**,** 168-74.
64. EDDAOUDI, M., KIM, J., ROSI, N., VODAK, D., WACHTER, J., O'KEEFFE, M. & YAGHI, O. M. 2002. Systematic design of pore size and functionality in isoreticular MOFs and their application in methane storage. *Science,* 295**,** 469-72.
65. ENVIRONMENTAL PROTECTION AGENCY, U. S. 2015. *EDSP: Weight of Evidence Analysis of Potential Interaction with The Estrogen, Androgen or Thyroid Pathyways* [Online]. Available: https://www.epa.gov/endocrine-disruption/endocrine-disruptor-screening-program-tier-1-screening-determinations-and [Accessed 14 November 2016 2016].
66. ESPLUGAS, S., BILA, D. M., KRAUSE, L. G. & DEZOTTI, M. 2007. Ozonation and advanced oxidation technologies to remove endocrine disrupting chemicals (EDCs) and pharmaceuticals and personal care products (PPCPs) in water effluents. *J Hazard Mater,* 149**,** 631-42.
67. EUROPEAN PARLIAMENT, C. O. T. E. U. 2013. *Directive 2013/39/EU of the European Parliament and of the council* [Online]. Available: http://eur-lex.europa.eu/legal-content/EN/ALL/?uri=CELEX%3A32013L0039 [Accessed 10 March 2018 2018].
68. FARHA, O. K., ERYAZICI, I., JEONG, N. C., HAUSER, B. G., WILMER, C. E., SARJEANT, A. A., SNURR, R. Q., NGUYEN, S. T., YAZAYDIN, A. O. & HUPP, J. T. 2012. Metal-organic framework materials with ultrahigh surface areas: is the sky the limit? *J Am Chem Soc,* 134**,** 15016-21.
69. FENG, Y., JIANG, H., LI, S., WANG, J., JING, X., WANG, Y. & CHEN, M. 2013. Metal–organic frameworks HKUST-1 for liquid-phase adsorption of uranium. *Colloids and Surfaces A: Physicochemical and Engineering Aspects,* 431**,** 87-92.
70. FOO, K. Y. & HAMEED, B. H. 2010. Insights into the modeling of adsorption isotherm systems. *Chemical Engineering Journal,* 156**,** 2-10.

71. FREUNDLICH, H. 1906. Over the adsorption in solution. *J. Phys. Chem,* 57**,** 385-470.
72. FROST, H., DÜREN, T. & SNURR, R. Q. 2006. Effects of Surface Area, Free Volume, and Heat of Adsorption on Hydrogen Uptake in Metal−Organic Frameworks. *The Journal of Physical Chemistry B,* 110**,** 9565-9570.
73. FU, Y. Y., YANG, C. X. & YAN, X. P. 2013. Fabrication of ZIF-8@SiO2 core-shell microspheres as the stationary phase for high-performance liquid chromatography. *Chemistry,* 19**,** 13484-91.
74. FURUKAWA, H., CORDOVA, K. E., O'KEEFFE, M. & YAGHI, O. M. 2013a. The chemistry and applications of metal-organic frameworks. *Science,* 341**,** 1230444.
75. FURUKAWA, H., CORDOVA, K. E., O'KEEFFE, M. & YAGHI, O. M. 2013b. The Chemistry and Applications of Metal-Organic Frameworks. *Science,* 341**,** 1230444.
76. FURUKAWA, S., REBOUL, J., DIRING, S., SUMIDA, K. & KITAGAWA, S. 2014. Structuring of metal-organic frameworks at the mesoscopic/macroscopic scale. *Chem Soc Rev,* 43**,** 5700-34.
77. GALHETAS, M., ANDRADE, M. A., MESTRE, A. S., KANGNI-FOLI, E., VILLA DE BRITO, M. J., PINTO, M. L., LOPES, H. & CARVALHO, A. P. 2015. The influence of the textural properties of activated carbons on acetaminophen adsorption at different temperatures. *Phys Chem Chem Phys,* 17**,** 12340-9.
78. GAO, Y. & DESHUSSES, M. A. 2011. Adsorption of clofibric acid and ketoprofen onto powdered activated carbon: Effect of natural organic matter. *Environmental Technology,* 32**,** 1719-1727.
79. GEBHARDT, W. & SCHRODER, H. F. 2007. Liquid chromatography-(tandem) mass spectrometry for the follow-up of the elimination of persistent pharmaceuticals during wastewater treatment applying biological wastewater treatment and advanced oxidation. *J Chromatogr A,* 1160**,** 34-43.
80. GHOSH, P., COLON, Y. J. & SNURR, R. Q. 2014. Water adsorption in UiO-66: the importance of defects. *Chem Commun (Camb),* 50**,** 11329-31.
81. GOMEZ-GUALDRON, D. A., MOGHADAM, P. Z., HUPP, J. T., FARHA, O. K. & SNURR, R. Q. 2016. Application of Consistency Criteria To Calculate BET Areas of Micro- And Mesoporous Metal-Organic Frameworks. *J Am Chem Soc,* 138**,** 215-24.
82. GRUNDGEIGER, E., LIM, Y. H., FROST, R. L., AYOKO, G. A. & XI, Y. 2015. Application of organo-beidellites for the adsorption of atrazine. *Applied Clay Science,* 105-106**,** 252-258.
83. HAILIAN LI, M. E., M. O`KEEFFE & O.M. YAGHI 1999. Design and synthesis of an exceptionally stable and highly porous metal-organic framework. *Nature,* 402**,** 276-279.
84. HAN, S., LIU, K., HU, L., TENG, F., YU, P. & ZHU, Y. 2017. Superior Adsorption and Regenerable Dye Adsorbent Based on Flower-Like Molybdenum Disulfide Nanostructure. *Sci Rep,* 7**,** 43599.
85. HAN, Y., LI, W., ZHANG, J., MENG, H., XU, Y. & ZHANG, X. 2015. Adsorption behavior of Rhodamine B on nanoporous polymers. *RSC Adv.,* 5**,** 104915-104922.

86. HAROUNE, L., SALAUN, M., MENARD, A., LEGAULT, C. Y. & BELLENGER, J. P. 2014. Photocatalytic degradation of carbamazepine and three derivatives using TiO(2) and ZnO: effect of pH, ionic strength, and natural organic matter. *Sci Total Environ,* 475**,** 16-22.
87. HASAN, Z., CHOI, E.-J. & JHUNG, S. H. 2013. Adsorption of naproxen and clofibric acid over a metal–organic framework MIL-101 functionalized with acidic and basic groups. *Chemical Engineering Journal,* 219**,** 537-544.
88. HASAN, Z., JEON, J. & JHUNG, S. H. 2012a. Adsorptive removal of naproxen and clofibric acid from water using metal-organic frameworks. *J. Hazard. Mater.,* 209**,** 151-157.
89. HASAN, Z., JEON, J. & JHUNG, S. H. 2012b. Adsorptive removal of naproxen and clofibric acid from water using metal-organic frameworks. *J Hazard Mater,* 209-210**,** 151-7.
90. HASAN, Z. & JHUNG, S. H. 2015. Removal of hazardous organics from water using metal-organic frameworks (MOFs): plausible mechanisms for selective adsorptions. *J Hazard Mater,* 283**,** 329-39.
91. HASAN, Z., KHAN, N. A. & JHUNG, S. H. 2016a. Adsorptive Removal of Diclofenac Sodium from Water with Zr-based Metal–organic Frameworks. *Chem. Eng. J.,* 284**,** 1406.
92. HASAN, Z., KHAN, N. A. & JHUNG, S. H. 2016b. Adsorptive removal of diclofenac sodium from water with Zr-based metal–organic frameworks. *Chemical Engineering Journal,* 284**,** 1406-1413.
93. HEINEMANN, H. 1981. Technological Applications of Zeolites in Catalysis. *Catalysis Reviews,* 23**,** 315-328.
94. HO, Y. S. & MCKAY, G. 1998. A Comparison of Chemisorption Kinetic Models Applied to Pollutant Removal on Various Sorbents. *Process Safety and Environmental Protection,* 76**,** 332-340.
95. HO, Y. S. & MCKAY, G. 1999. Pseudo-second order model for sorption processes. *Process Biochemistry,* 34**,** 451-465.
96. HOIGNÉ, J. 1998. Chemistry of Aqueous Ozone and Transformation of Pollutants by Ozonation and Advanced Oxidation Processes. *In:* HRUBEC, J. (ed.) *Quality and Treatment of Drinking Water II.* Berlin, Heidelberg: Springer Berlin Heidelberg.
97. HORCAJADA, P., GREF, R., BAATI, T., ALLAN, P. K., MAURIN, G., COUVREUR, P., FEREY, G., MORRIS, R. E. & SERRE, C. 2012. Metal-organic frameworks in biomedicine. *Chem Rev,* 112**,** 1232-68.
98. HORCAJADA, P., SERRE, C., VALLET-REGÍ, M., SEBBAN, M., TAULELLE, F. & FÉREY, G. 2006. Metal–Organic Frameworks as Efficient Materials for Drug Delivery. *Angewandte Chemie,* 118**,** 6120-6124.
99. HOSKINS, B. F. & ROBSON, R. 1989. Infinite Polymeric Frameworks Consisting of Three Dimensionally Linked Rod-like Segments.pdf>. *American Chemical Society* [Online], 111.
100. HOSKINS, B. F. & ROBSON, R. 1990. Design and Construction of a New Class of Scaffolding-like Materials Comprising Infinite Polymeric Frameworks of 3D-Linked Molecular Rods. A Reappraisal of the Zn(CN)2 and Cd(CN)2 Structures and the Synthesis and Structure of the Diamond-Related Frameworks [N(CH3)4][Cu1Zn11(CN)4]and CUI[4,4”4”,4”’-

tetracyanotetraphenylmethane] BF4~xC6H5NO. *American Chemical Society Journal,* 112**,** 1546-1554.
101. HOWARTH, A. J., LIU, Y., HUPP, J. T. & FARHA, O. K. 2015. Metal–organic frameworks for applications in remediation of oxyanion/cation-contaminated water. *CrystEngComm,* 17**,** 7245-7253.
102. HOWARTH, A. J., LIU, Y., LI, P., LI, Z., WANG, T. C., HUPP, J. T. & FARHA, O. K. 2016. Chemical, thermal and mechanical stabilities of metal–organic frameworks. *Nature Reviews Materials,* 1**,** 15018.
103. HOWARTH, A. J., PETERS, A. W., VERMEULEN, N. A., WANG, T. C., HUPP, J. T. & FARHA, O. K. 2017. Best Practices for the Synthesis, Activation, and Characterization of Metal–Organic Frameworks. *Chemistry of Materials,* 29**,** 26-39.
104. HU, L., MARTIN, H. M., ARCE-BULTED, O., SUGIHARA, M. N., KEATING, K. A. & STRATHMANN, T. J. 2009. Oxidation of Carbamazepine by Mn(VII) and Fe(VI): Reaction Kinetics and Mechanism. *Environmental Science & Technology,* 43**,** 509-515.
105. HU, Y., SONG, C., LIAO, J., HUANG, Z. & LI, G. 2013. Water stable metal-organic framework packed microcolumn for online sorptive extraction and direct analysis of naproxen and its metabolite from urine sample. *J Chromatogr A,* 1294**,** 17-24.
106. HUA, W., BENNETT, E. R. & LETCHER, R. J. 2006. Ozone treatment and the depletion of detectable pharmaceuticals and atrazine herbicide in drinking water sourced from the upper Detroit River, Ontario, Canada. *Water Res,* 40**,** 2259-66.
107. HUXFORD, R. C., DELLA ROCCA, J. & LIN, W. 2010. Metal-organic frameworks as potential drug carriers. *Curr Opin Chem Biol,* 14**,** 262-8.
108. ISLAMOGLU, T., ATILGAN, A., MOON, S.-Y., PETERSON, G. W., DECOSTE, J. B., HALL, M., HUPP, J. T. & FARHA, O. K. 2017. Cerium(IV) vs Zirconium(IV) Based Metal–Organic Frameworks for Detoxification of a Nerve Agent. *Chemistry of Materials,* 29**,** 2672-2675.
109. JENSEN, N. K., RUFFORD, T. E., WATSON, G., ZHANG, D. K., CHAN, K. I. & MAY, E. F. 2012. Screening Zeolites for Gas Separation Applications Involving Methane, Nitrogen, and Carbon Dioxide. *Journal of Chemical & Engineering Data,* 57**,** 106-113.
110. JIANG, J.-Q. & ASHEKUZZAMAN, S. M. 2012. Development of novel inorganic adsorbent for water treatment. *Current Opinion in Chemical Engineering,* 1**,** 191-199.
111. JIANG, J. Q., YANG, C. X. & YAN, X. P. 2013. Zeolitic imidazolate framework-8 for fast adsorption and removal of benzotriazoles from aqueous solution. *ACS Appl Mater Interfaces,* 5**,** 9837-42.
112. JONES, O. A., VOULVOULIS, N. & LESTER, J. N. 2001. Human pharmaceuticals in the aquatic environment a review. *Environmental Technology,* 22**,** 1383-1394.
113. JOSS, A., ZABCZYNSKI, S., GOBEL, A., HOFFMANN, B., LOFFLER, D., MCARDELL, C. S., TERNES, T. A., THOMSEN, A. & SIEGRIST, H. 2006. Biological degradation of pharmaceuticals in municipal wastewater treatment: proposing a classification scheme. *Water Res,* 40**,** 1686-96.

114. JUNG, B. K., HASAN, Z. & JHUNG, S. H. 2013. Adsorptive removal of 2,4-dichlorophenoxyacetic acid (2,4-D) from water with a metal–organic framework. *Chemical Engineering Journal,* 234**,** 99-105.
115. JUNG, B. K., JUN, J. W., HASAN, Z. & JHUNG, S. H. 2015. Adsorptive removal of p-arsanilic acid from water using mesoporous zeolitic imidazolate framework-8. *Chemical Engineering Journal,* 267**,** 9-15.
116. KATZ, M. J., BROWN, Z. J., COLON, Y. J., SIU, P. W., SCHEIDT, K. A., SNURR, R. Q., HUPP, J. T. & FARHA, O. K. 2013. A facile synthesis of UiO-66, UiO-67 and their derivatives. *Chem Commun (Camb),* 49**,** 9449-51.
117. KHAN, N. A., HASAN, Z. & JHUNG, S. H. 2013a. Adsorptive removal of hazardous materials using metal-organic frameworks (MOFs): A review. *J. Hazard. Mater.,* 244**,** 444-456.
118. KHAN, N. A., HASAN, Z. & JHUNG, S. H. 2013b. Adsorptive removal of hazardous materials using metal-organic frameworks (MOFs): a review. *J Hazard Mater,* 244-245**,** 444-56.
119. KHAN, N. A. & JHUNG, S. H. 2015. Synthesis of metal-organic frameworks (MOFs) with microwave or ultrasound: Rapid reaction, phase-selectivity, and size reduction. *Coordination Chemistry Reviews,* 285**,** 11-23.
120. KHAN, N. A., JUNG, B. K., HASAN, Z. & JHUNG, S. H. 2015. Adsorption and removal of phthalic acid and diethyl phthalate from water with zeolitic imidazolate and metal-organic frameworks. *J Hazard Mater,* 282**,** 194-200.
121. KHETAN, S. K. & COLLINS, T. J. 2007. Human Pharmaceuticals in the Aquatic Environment: A Challenge to Green Chemistry. *Chemical Reviews,* 107**,** 2319-2364.
122. KIM, M. & COHEN, S. M. 2012. Discovery, development, and functionalization of Zr(iv)-based metal–organic frameworks. *CrystEngComm,* 14**,** 4096-4104.
123. KLAVARIOTI, M., MANTZAVINOS, D. & KASSINOS, D. 2009. Removal of residual pharmaceuticals from aqueous systems by advanced oxidation processes. *Environ Int,* 35**,** 402-17.
124. KLINOWSKI, J., PAZ, F. A., SILVA, P. & ROCHA, J. 2011. Microwave-assisted synthesis of metal-organic frameworks. *Dalton Trans,* 40**,** 321-30.
125. KOBLE, R. A. & CORRIGAN, T. E. 1952. ADSORPTION ISOTHERMS FOR PURE HYDROCARBONS. *Industrial & Engineering Chemistry,* 44**,** 383-387.
126. KOMTCHOU, S., DIRANY, A., DROGUI, P., DELEGAN, N., EL KHAKANI, M. A., ROBERT, D. & LAFRANCE, P. 2016. Degradation of atrazine in aqueous solution with electrophotocatalytic process using TiO2-x photoanode. *Chemosphere,* 157**,** 79-88.
127. KOSJEK, T., ANDERSEN, H. R., KOMPARE, B., LEDIN, A. & HEATH, E. 2009. Fate of Carbamazepine during Water Treatment. *Environmental Science & Technology,* 43**,** 6256-6261.

128. KRYSTL, V., HRADIL, J., BERNAUER, B. & KOČIŘíK, M. 2001. Heterogeneous membranes based on zeolites for separation of small molecules. *Reactive and Functional Polymers,* 48**,** 129-139.
129. KUPPLER, R. J., TIMMONS, D. J., FANG, Q.-R., LI, J.-R., MAKAL, T. A., YOUNG, M. D., YUAN, D., ZHAO, D., ZHUANG, W. & ZHOU, H.-C. 2009. Potential applications of metal-organic frameworks. *Coordination Chemistry Reviews,* 253**,** 3042-3066.
130. KYRIAKOPOULOS, G. & DOULIA, D. 2006. Adsorption of Pesticides on Carbonaceous and Polymeric Materials from Aqueous Solutions: A Review. *Separation & Purification Reviews,* 35**,** 97-191.
131. KYZAS, G. Z., KOLTSAKIDOU, A., NANAKI, S. G., BIKIARIS, D. N. & LAMBROPOULOU, D. A. 2015. Removal of beta-blockers from aqueous media by adsorption onto graphene oxide. *Sci Total Environ,* 537**,** 411-20.
132. LANGMUIR, I. 1916. The Constitution and Fundamental Properties of Solids and Liquids. *American Chemical Society,* 38**,** 2221-2295.
133. LANGMUIR, I. 1918. THE ADSORPTION OF GASES ON PLANE SURFACES OF GLASS, MICA AND PLATINUM. *Journal of the American Chemical Society,* 40**,** 1361-1403.
134. LEE, J., FARHA, O. K., ROBERTS, J., SCHEIDT, K. A., NGUYEN, S. T. & HUPP, J. T. 2009. Metal-organic framework materials as catalysts. *Chem Soc Rev,* 38**,** 1450-9.
135. LEE, Y.-R., KIM, J. & AHN, W.-S. 2013. Synthesis of metal-organic frameworks: A mini review. *Korean Journal of Chemical Engineering,* 30**,** 1667-1680.
136. LEKKERKERKER-TEUNISSEN, K., J. BENOTTI, M., SNYDER, S. & DIJK, J. 2012. *Transformation of atrazine, carbamazepine, diclofenac and sulfamethoxazole by low and medium pressure UV and UV/H2O2 treatment*.
137. LEMIC, J., KOVACEVIC, D., TOMASEVIC-CANOVIC, M., KOVACEVIC, D., STANIC, T. & PFEND, R. 2006. Removal of atrazine, lindane and diazinone from water by organo-zeolites. *Water Res,* 40**,** 1079-85.
138. LERMAN, I., CHEN, Y., XING, B. & CHEFETZ, B. 2013. Adsorption of carbamazepine by carbon nanotubes: effects of DOM introduction and competition with phenanthrene and bisphenol A. *Environ Pollut,* 182**,** 169-76.
139. LI, J. R., KUPPLER, R. J. & ZHOU, H. C. 2009. Selective gas adsorption and separation in metal-organic frameworks. *Chem Soc Rev,* 38**,** 1477-504.
140. LI, J. R., SCULLEY, J. & ZHOU, H. C. 2012. Metal-organic frameworks for separations. *Chem Rev,* 112**,** 869-932.
141. LI, P., VERMEULEN, N. A., MALLIAKAS, C. D., GÓMEZ-GUALDRÓN, D. A., HOWARTH, A. J., MEHDI, B. L., DOHNALKOVA, A., BROWNING, N. D., O'KEEFFE, M. & FARHA, O. K. 2017. Bottom-up construction of a superstructure in a porous uranium-organic crystal. *Science,* 356**,** 624-627.

142. LI, Z.-Q., YANG, J.-C., SUI, K.-W. & YIN, N. 2015. Facile synthesis of metal-organic framework MOF-808 for arsenic removal. *Materials Letters,* 160**,** 412-414.
143. LIMA, D. L., ERNY, G. L. & ESTEVES, V. I. 2009. Application of MEKC to the monitoring of atrazine sorption behaviour on soils. *J Sep Sci,* 32**,** 4241-6.
144. LIPPENS, B., LINSEN, B. & DE BOER, J. 1964. Studies on pore systems in catalysts I. The adsorption of nitrogen; apparatus and calculation. *Journal of Catalysis,* 3**,** 32-37.
145. LIPPENS, B. C. & DE BOER, J. 1965. Studies on pore systems in catalysts: V. The t method. *Journal of Catalysis,* 4**,** 319-323.
146. LIU, F. F., ZHAO, J., WANG, S., DU, P. & XING, B. 2014. Effects of solution chemistry on adsorption of selected pharmaceuticals and personal care products (PPCPs) by graphenes and carbon nanotubes. *Environ Sci Technol,* 48**,** 13197-206.
147. LU, G. & ZHAO, X. S. 2004. *Nanoporous materials: science and engineering,* World Scientific.
148. MARTENS, J. & JACOBS, P. 1987. *Synthesis of high-silica aluminosilicate zeolites,* Elsevier.
149. MARTUCCI, A., PASTI, L., MARCHETTI, N., CAVAZZINI, A., DONDI, F. & ALBERTI, A. 2012. Adsorption of pharmaceuticals from aqueous solutions on synthetic zeolites. *Microporous and Mesoporous Materials,* 148**,** 174-183.
150. MASON, J. A., VEENSTRA, M. & LONG, J. R. 2014. Evaluating metal–organic frameworks for natural gas storage. *Chem. Sci.,* 5**,** 32-51.
151. MATITO-MARTOS, I., MARTIN-CALVO, A., GUTIERREZ-SEVILLANO, J. J., HARANCZYK, M., DOBLARE, M., PARRA, J. B., ANIA, C. O. & CALERO, S. 2014. Zeolite screening for the separation of gas mixtures containing SO2, CO2 and CO. *Phys Chem Chem Phys,* 16**,** 19884-93.
152. MCCUSKER, L., LIEBAU, F. & ENGELHARDT, G. 2001. Nomenclature of structural and compositional characteristics of ordered microporous and mesoporous materials with inorganic hosts (IUPAC Recommendations 2001). *Pure and Applied Chemistry,* 73**,** 381-394.
153. MCDONALD, T. M., MASON, J. A., KONG, X., BLOCH, E. D., GYGI, D., DANI, A., CROCELLA, V., GIORDANINO, F., ODOH, S. O., DRISDELL, W. S., VLAISAVLJEVICH, B., DZUBAK, A. L., POLONI, R., SCHNELL, S. K., PLANAS, N., LEE, K., PASCAL, T., WAN, L. F., PRENDERGAST, D., NEATON, J. B., SMIT, B., KORTRIGHT, J. B., GAGLIARDI, L., BORDIGA, S., REIMER, J. A. & LONG, J. R. 2015. Cooperative insertion of CO2 in diamine-appended metal-organic frameworks. *Nature,* 519**,** 303-8.
154. MCDOWELL, D. C., HUBER, M. M., WAGNER, M., VON GUNTEN, U. & TERNES, T. A. 2005. Ozonation of Carbamazepine in Drinking Water: Identification and Kinetic Study of Major Oxidation Products. *Environmental Science & Technology,* 39**,** 8014-8022.
155. MEEK, S. T., GREATHOUSE, J. A. & ALLENDORF, M. D. 2011. Metal-organic frameworks: a rapidly growing class of versatile nanoporous materials. *Adv Mater,* 23**,** 249-67.

156. MESTRE, A. S., MARQUES, S. C. R. & CARVALHO, A. P. 2012. Effect of the Alcohol Cosolvent in the Removal of Caffeine by Activated Carbons. *Industrial & Engineering Chemistry Research,* 51**,** 9850-9857.
157. MESTRE, A. S., NABIÇO, A., FIGUEIREDO, P. L., PINTO, M. L., SANTOS, M. S. C. S. & FONSECA, I. M. 2016. Enhanced clofibric acid removal by activated carbons: Water hardness as a key parameter. *Chemical Engineering Journal,* 286**,** 538-548.
158. MESTRE, A. S., PIRES, R. A., AROSO, I., FERNANDES, E. M., PINTO, M. L., REIS, R. L., ANDRADE, M. A., PIRES, J., SILVA, S. P. & CARVALHO, A. P. 2014. Activated carbons prepared from industrial pre-treated cork: Sustainable adsorbents for pharmaceutical compounds removal. *Chemical Engineering Journal,* 253**,** 408-417.
159. MITTAL, G., DHAND, V., RHEE, K. Y., PARK, S.-J. & LEE, W. R. 2015. A review on carbon nanotubes and graphene as fillers in reinforced polymer nanocomposites. *Journal of Industrial and Engineering Chemistry,* 21**,** 11-25.
160. MOGHADAM, P. Z., LI, A., WIGGIN, S. B., TAO, A., MALONEY, A. G. P., WOOD, P. A., WARD, S. C. & FAIREN-JIMENEZ, D. 2017. Development of a Cambridge Structural Database Subset: A Collection of Metal–Organic Frameworks for Past, Present, and Future. *Chemistry of Materials,* 29**,** 2618-2625.
161. MOHAN, D. & PITTMAN, C. U., JR. 2006. Activated carbons and low cost adsorbents for remediation of tri- and hexavalent chromium from water. *J Hazard Mater,* 137**,** 762-811.
162. MOMPELAT, S., LE BOT, B. & THOMAS, O. 2009. Occurrence and fate of pharmaceutical products and by-products, from resource to drinking water. *Environ Int,* 35**,** 803-14.
163. MONDLOCH, J. E., KATZ, M. J., PLANAS, N., SEMROUNI, D., GAGLIARDI, L., HUPP, J. T. & FARHA, O. K. 2014. Are Zr(6)-based MOFs water stable? Linker hydrolysis vs. capillary-force-driven channel collapse. *Chem Commun (Camb),* 50**,** 8944-6.
164. MOON, S. Y., WAGNER, G. W., MONDLOCH, J. E., PETERSON, G. W., DECOSTE, J. B., HUPP, J. T. & FARHA, O. K. 2015. Effective, Facile, and Selective Hydrolysis of the Chemical Warfare Agent VX Using Zr6-Based Metal-Organic Frameworks. *Inorg Chem,* 54**,** 10829-33.
165. MOREIRA, M. A., SANTOS, J. C., FERREIRA, A. F., LOUREIRO, J. M., RAGON, F., HORCAJADA, P., SHIM, K. E., HWANG, Y. K., LEE, U. H., CHANG, J. S., SERRE, C. & RODRIGUES, A. E. 2012. Reverse shape selectivity in the liquid-phase adsorption of xylene isomers in zirconium terephthalate MOF UiO-66. *Langmuir,* 28**,** 5715-23.
166. MORENO-CASTILLA, C. 2004. Adsorption of organic molecules from aqueous solutions on carbon materials. *Carbon,* 42**,** 83-94.
167. MUELLER, U., SCHUBERT, M., TEICH, F., PUETTER, H., SCHIERLE-ARNDT, K. & PASTRÉ, J. 2006. Metal–organic frameworks—prospective industrial applications. *J. Mater. Chem.,* 16**,** 626-636.

168. NAM, S. W., CHOI, D. J., KIM, S. K., HER, N. & ZOH, K. D. 2014. Adsorption characteristics of selected hydrophilic and hydrophobic micropollutants in water using activated carbon. *J Hazard Mater,* 270**,** 144-52.
169. NI, Z. & MASEL, R. I. 2006. Rapid Production of Metal−Organic Frameworks via Microwave-Assisted Solvothermal Synthesis. *Journal of the American Chemical Society,* 128**,** 12394-12395.
170. NIELSEN, L., BIGGS, M. J., SKINNER, W. & BANDOSZ, T. J. 2014. The effects of activated carbon surface features on the reactive adsorption of carbamazepine and sulfamethoxazole. *Carbon,* 80**,** 419-432.
171. NOWOTNY, N., EPP, B., VON SONNTAG, C. & FAHLENKAMP, H. 2007. Quantification and Modeling of the Elimination Behavior of Ecologically Problematic Wastewater Micropollutants by Adsorption on Powdered and Granulated Activated Carbon. *Environmental Science & Technology,* 41**,** 2050-2055.
172. OLESZCZUK, P., PAN, B. & XING, B. 2010. Adsorption and Desorption of Oxytetracycline and Carbamazepine by Multiwalled Carbon Nanotubes. *Environmental Science & Technology,* 44**,** 4830-4830.
173. OMAR M. YAGHI, M. O. K., NATHAN W. OCKWIG, HEE K. CHAE, MOHAMED EDDAOUDI & JAHEON KIM 2003. Reticular synthesis and the design of new materials. *Nature Publishing Group,* 423**,** 705-714.
174. ORGANIZATION-WHO, W. H. 2017. *Progress on drinking water, sanitation and hygiene-Drinking Water Fact Sheet* [Online]. Available: http://www.who.int/mediacentre/factsheets/fs391/en/ [Accessed 10 March 2018 2018].
175. PARK, K. S., NI, Z., COTE, A. P., CHOI, J. Y., HUANG, R., URIBE-ROMO, F. J., CHAE, H. K., O'KEEFFE, M. & YAGHI, O. M. 2006. Exceptional chemical and thermal stability of zeolitic imidazolate frameworks. *Proc Natl Acad Sci U S A,* 103**,** 10186-91.
176. PATIL, D. V., RALLAPALLI, P. B. S., DANGI, G. P., TAYADE, R. J., SOMANI, R. S. & BAJAJ, H. C. 2011. MIL-53(Al): An Efficient Adsorbent for the Removal of Nitrobenzene from Aqueous Solutions. *Industrial & Engineering Chemistry Research,* 50**,** 10516-10524.
177. PAUL WESTERHOFF, Y. Y., SHANE SNYDER, AND ERIC WERT 2005. Fate of Endocrine-Disruptor, Pharmaceutical, and Personal Care Product Chemicals during Simulated Drinking Water Treatment Processes. *Environ. Sci. Technol.,* 39**,** 6649-6663.
178. PENG, Y., KRUNGLEVICIUTE, V., ERYAZICI, I., HUPP, J. T., FARHA, O. K. & YILDIRIM, T. 2013. Methane storage in metal-organic frameworks: current records, surprise findings, and challenges. *J Am Chem Soc,* 135**,** 11887-94.
179. PENG, Y., ZHANG, Y., HUANG, H. & ZHONG, C. 2018. Flexibility induced high-performance MOF-based adsorbent for nitroimidazole antibiotics capture. *Chemical Engineering Journal,* 333**,** 678-685.
180. PETRIE, B., BARDEN, R. & KASPRZYK-HORDERN, B. 2015. A review on emerging contaminants in wastewaters and the environment:

current knowledge, understudied areas and recommendations for future monitoring. *Water Res,* 72**,** 3-27.
181. PETROVIC´, M., GONZALEZ, S. & BARCELO´, D. 2003. Analysis and removal of emerging contaminants in wastewater and drinking water. *European Journal of Cancer,* 22**,** vii.
182. QIU, S. & ZHU, G. 2009. Molecular engineering for synthesizing novel structures of metal–organic frameworks with multifunctional properties. *Coordination Chemistry Reviews,* 253**,** 2891-2911.
183. RAHMAN, M. F., YANFUL, E. K. & JASIM, S. Y. 2009. Endocrine disrupting compounds (EDCs) and pharmaceuticals and personal care products (PPCPs) in the aquatic environment: implications for the drinking water industry and global environmental health. *J Water Health,* 7**,** 224-43.
184. REDLICH, O. & PETERSON, D. L. 1959. A Useful Adsorption Isotherm. *The Journal of Physical Chemistry,* 63**,** 1024-1024.
185. RICHARDSON, S. D. & TERNES, T. A. 2014. Water analysis: emerging contaminants and current issues. *Anal Chem,* 86**,** 2813-48.
186. RIVERA-UTRILLA, J., SANCHEZ-POLO, M., FERRO-GARCIA, M. A., PRADOS-JOYA, G. & OCAMPO-PEREZ, R. 2013. Pharmaceuticals as emerging contaminants and their removal from water. A review. *Chemosphere,* 93**,** 1268-87.
187. ROSI, N. L., ECKERT, J., EDDAOUDI, M., VODAK, D. T., KIM, J., O'KEEFFE, M. & YAGHI, O. M. 2003. Hydrogen storage in microporous metal-organic frameworks. *Science,* 300**,** 1127-9.
188. ROSSNER, A., SNYDER, S. A. & KNAPPE, D. R. 2009. Removal of emerging contaminants of concern by alternative adsorbents. *Water Res,* 43**,** 3787-96.
189. ROUQUEROL, J., ROUQUEROL, F., LLEWELLYN, P., MAURIN, G. & SING, K. S. 2013. *Adsorption by powders and porous solids: principles, methodology and applications*, Academic press.
190. RUBIO-MARTINEZ, M., AVCI-CAMUR, C., THORNTON, A. W., IMAZ, I., MASPOCH, D. & HILL, M. R. 2017. New synthetic routes towards MOF production at scale. *Chem Soc Rev,* 46**,** 3453-3480.
191. SALVESTRINI, S., SAGLIANO, P., IOVINO, P., CAPASSO, S. & COLELLA, C. 2010. Atrazine adsorption by acid-activated zeolite-rich tuffs. *Applied Clay Science,* 49**,** 330-335.
192. SANCHEZ-MARTIN, M. J., RODRIGUEZ-CRUZ, M. S., ANDRADES, M. S. & SANCHEZ-CAMAZANO, M. 2006. Efficiency of different clay minerals modified with a cationic surfactant in the adsorption of pesticides: Influence of clay type and pesticide hydrophobicity. *Applied Clay Science,* 31**,** 216-228.
193. SANDERSON, J. T., SEINEN, W., GIESY, J. P. & VAN DEN BERG, M. 2000. 2-Chloro-s-Triazine Herbicides Induce Aromatase (CYP19) Activity in H295R Human Adrenocortical Carcinoma Cells: A Novel Mechanism for Estrogenicity? *Toxicological Sciences,* 54**,** 121-127.
194. SARKER, M., AHMED, I. & JHUNG, S. H. 2017. Adsorptive removal of herbicides from water over nitrogen-doped carbon obtained from ionic liquid@ZIF-8. *Chemical Engineering Journal,* 323**,** 203-211.

195. SCHWARZENBACH, R. P., ESCHER, B. I., FENNER, K., HOFSTETTER, T. B., JOHNSON, C. A., VON GUNTEN, U. & WEHRLI, B. 2006. The Challenge of Micropollutants in Aquatic Systems. *Science,* 313**,** 1072-1077.
196. SEATON, N. A., WALTON, J. P. R. B. & QUIRKE, N. 1989. A new analysis method for the determination of the pore size distribution of porous carbons from nitrogen adsorption measurements. *Carbon,* 27**,** 853-861.
197. SEO, P. W., BHADRA, B. N., AHMED, I., KHAN, N. A. & JHUNG, S. H. 2016a. Adsorptive Removal of Pharmaceuticals and Personal Care Products from Water with Functionalized Metal-organic Frameworks: Remarkable Adsorbents with Hydrogen-bonding Abilities. *Scientific Reports,* 6**,** 34462.
198. SEO, P. W., BHADRA, B. N., AHMED, I., KHAN, N. A. & JHUNG, S. H. 2016b. Adsorptive Removal of Pharmaceuticals and Personal Care Products from Water with Functionalized Metal-organic Frameworks: Remarkable Adsorbents with Hydrogen-bonding Abilities. *Sci. Rep.***,** 34462.
199. SEO, P. W., KHAN, N. A., HASAN, Z. & JHUNG, S. H. 2016c. Adsorptive Removal of Artificial Sweeteners from Water Using Metal-Organic Frameworks Functionalized with Urea or Melamine. *ACS Appl Mater Interfaces,* 8**,** 29799-29807.
200. SEO, P. W., KHAN, N. A. & JHUNG, S. H. 2017. Removal of nitroimidazole antibiotics from water by adsorption over metal–organic frameworks modified with urea or melamine. *Chemical Engineering Journal,* 315**,** 92-100.
201. SEO, Y. S., KHAN, N. A. & JHUNG, S. H. 2015a. Adsorptive Removal of Methylchlorophenoxy-propionic Acid from Water with a Metal-organic Framework. *Chem. Eng. J.,* 270**,** 22.
202. SEO, Y. S., KHAN, N. A. & JHUNG, S. H. 2015b. Adsorptive removal of methylchlorophenoxypropionic acid from water with a metal-organic framework. *Chemical Engineering Journal,* 270**,** 22-27.
203. SHAN, D., DENG, S., ZHAO, T., WANG, B., WANG, Y., HUANG, J., YU, G., WINGLEE, J. & WIESNER, M. R. 2016. Preparation of ultrafine magnetic biochar and activated carbon for pharmaceutical adsorption and subsequent degradation by ball milling. *J Hazard Mater,* 305**,** 156-63.
204. SHANNON, M. A., BOHN, P. W., ELIMELECH, M., GEORGIADIS, J. G., MARINAS, B. J. & MAYES, A. M. 2008. Science and technology for water purification in the coming decades. *Nature,* 452**,** 301-10.
205. SHI, J., HEI, S., LIU, H., FU, Y., ZHANG, F., ZHONG, Y. & ZHU, W. 2013. Synthesis of MIL-100(Fe) at Low Temperature and Atmospheric Pressure. *Journal of Chemistry,* 2013**,** 1-4.
206. SIMAZAKI, D., FUJIWARA, J., MANABE, S., MATSUDA, M., ASAMI, M. & KUNIKANE, S. 2008. Removal of selected pharmaceuticals by chlorination, coagulation-sedimentation and powdered activated carbon treatment. *Water Sci Technol,* 58**,** 1129-35.

207. SING, K. S. 1985. Reporting physisorption data for gas/solid systems with special reference to the determination of surface area and porosity (Recommendations 1984). *Pure and applied chemistry,* 57**,** 603-619.
208. SNYDER, S. A., ADHAM, S., REDDING, A. M., CANNON, F. S., DECAROLIS, J., OPPENHEIMER, J., WERT, E. C. & YOON, Y. 2007. Role of membranes and activated carbon in the removal of endocrine disruptors and pharmaceuticals. *Desalination,* 202**,** 156-181.
209. SONG, J. Y. & JHUNG, S. H. 2017. Adsorption of pharmaceuticals and personal care products over metal-organic frameworks functionalized with hydroxyl groups: Quantitative analyses of H-bonding in adsorption. *Chemical Engineering Journal,* 322**,** 366-374.
210. SONTHEIMER, H., CRITTENDEN, J. C. & SUMMERS, R. S. 1988. *Activated carbon for water treatment*, American Water Works Association.
211. SOPHIA, A. C. & LIMA, E. C. 2018. Removal of emerging contaminants from the environment by adsorption. *Ecotoxicol Environ Saf,* 150**,** 1-17.
212. SOTELO, J. L., OVEJERO, G., RODRÍGUEZ, A., ÁLVAREZ, S., GALÁN, J. & GARCÍA, J. 2014. Competitive adsorption studies of caffeine and diclofenac aqueous solutions by activated carbon. *Chemical Engineering Journal,* 240**,** 443-453.
213. STACKELBERG, P. E., GIBS, J., FURLONG, E. T., MEYER, M. T., ZAUGG, S. D. & LIPPINCOTT, R. L. 2007. Efficiency of conventional drinking-water-treatment processes in removal of pharmaceuticals and other organic compounds. *Sci Total Environ,* 377**,** 255-72.
214. STOCK, N. & BISWAS, S. 2012. Synthesis of metal-organic frameworks (MOFs): routes to various MOF topologies, morphologies, and composites. *Chem Rev,* 112**,** 933-69.
215. STREAT, M. & HORNER, D. J. 2000. Adsorption of Highly Soluble Herbicides from Water Using Activated Carbon and Hypercrosslinked Polymers. *Process Safety and Environmental Protection,* 78**,** 363-382.
216. STREAT, M. & SWEETLAND, L. A. 1998. Removal of Pesticides from Water Using Hypercrosslinked Polymer Phases. *Process Safety and Environmental Protection,* 76**,** 127-134.
217. SUN, Y. & ZHOU, H. C. 2015. Recent progress in the synthesis of metal-organic frameworks. *Sci Technol Adv Mater,* 16**,** 054202.
218. SURIYANON, N., PUNYAPALAKUL, P. & NGAMCHARUSSRIVICHAI, C. 2013. Mechanistic study of diclofenac and carbamazepine adsorption on functionalized silica-based porous materials. *Chemical Engineering Journal,* 214**,** 208-218.
219. TAN, G., SUN, W., XU, Y., WANG, H. & XU, N. 2016. Sorption of mercury (II) and atrazine by biochar, modified biochars and biochar based activated carbon in aqueous solution. *Bioresour Technol,* 211**,** 727-35.
220. TANG, W.-W., ZENG, G.-M., GONG, J.-L., LIU, Y., WANG, X.-Y., LIU, Y.-Y., LIU, Z.-F., CHEN, L., ZHANG, X.-R. & TU, D.-Z. 2012. Simultaneous adsorption of atrazine and Cu (II) from wastewater by

magnetic multi-walled carbon nanotube. *Chemical Engineering Journal,* 211-212**,** 470-478.

221. TARAZONA, P., MARCONI, U. M. B. & EVANS, R. 1987. Phase equilibria of fluid interfaces and confined fluids. *Molecular Physics,* 60**,** 573-595.

222. TEPLENSKY, M. H., FANTHAM, M., LI, P., WANG, T. C., MEHTA, J. P., YOUNG, L. J., MOGHADAM, P. Z., HUPP, J. T., FARHA, O. K., KAMINSKI, C. F. & FAIREN-JIMENEZ, D. 2017. Temperature Treatment of Highly Porous Zirconium-Containing Metal-Organic Frameworks Extends Drug Delivery Release. *J Am Chem Soc,* 139**,** 7522-7532.

223. TERNES, T. A., MEISENHEIMER, M., MCDOWELL, D., SACHER, F., BRAUCH, H.-J., HAIST-GULDE, B., PREUSS, G., WILME, U. & ZULEI-SEIBERT, N. 2002. Removal of Pharmaceuticals during Drinking Water Treatment. *Environmental Science & Technology,* 36**,** 3855-3863.

224. THOMMES, M. 2010. Physical Adsorption Characterization of Nanoporous Materials. *Chemie Ingenieur Technik,* 82**,** 1059-1073.

225. THOMMES, M., KANEKO, K., NEIMARK, A. V., OLIVIER, J. P., RODRIGUEZ-REINOSO, F., ROUQUEROL, J. & SING, K. S. W. 2015. Physisorption of gases, with special reference to the evaluation of surface area and pore size distribution (IUPAC Technical Report). *Pure and Applied Chemistry,* 87.

226. TICHONOVAS, M., KRUGLY, E., RACYS, V., HIPPLER, R., KAUNELIENE, V., STASIULAITIENE, I. & MARTUZEVICIUS, D. 2013. Degradation of various textile dyes as wastewater pollutants under dielectric barrier discharge plasma treatment. *Chemical Engineering Journal,* 229**,** 9-19.

227. TOBISZEWSKI, M. & NAMIESNIK, J. 2012. PAH diagnostic ratios for the identification of pollution emission sources. *Environ Pollut,* 162**,** 110-9.

228. TONG, Y., MAYER, B. K. & MCNAMARA, P. J. 2016. Triclosan adsorption using wastewater biosolids-derived biochar. *Environmental Science: Water Research & Technology,* 2**,** 761-768.

229. TRICKETT, C. A., GAGNON, K. J., LEE, S., GÁNDARA, F., BÜRGI, H.-B. & YAGHI, O. M. 2015. Definitive Molecular Level Characterization of Defects in UiO-66 Crystals. *Angewandte Chemie International Edition,* 54**,** 11162-11167.

230. UNION, T. C. O. T. E. 1998. *COUNCIL DIRECTIVE 98/83/EC* [Online]. Available: http://eur-lex.europa.eu/legal-content/EN/TXT/?uri=CELEX:31998L0083 [Accessed 10 March 2018 2018].

231. V. KRUNGLEVICIUTE, K. LASK, L. HEROUX, A. D. MIGONE, J.-Y. LEE, J. LI, A. & SKOULIDAS, A. 2007. Argon Adsorption on Cu3(Benzene-1,3,5-tricarboxylate)2(H2O)3 Metal-Organic Framework. *Langmuir,* 23**,** 3106-3109.

232. VAN DE VOORDE, B., BUEKEN, B., DENAYER, J. & DE VOS, D. 2014. Adsorptive separation on metal-organic frameworks in the liquid phase. *Chem Soc Rev,* 43**,** 5766-88.

233. VIENO, N. M., HÄRKKI, H., TUHKANEN, T. & KRONBERG, L. 2007. Occurrence of Pharmaceuticals in River Water and Their Elimination in a Pilot-Scale Drinking Water Treatment Plant. *Environmental Science & Technology,* 41**,** 5077-5084.
234. VU, T. A., LE, G. H., DAO, C. D., DANG, L. Q., NGUYEN, K. T., NGUYEN, Q. K., DANG, P. T., TRAN, H. T. K., DUONG, Q. T., NGUYEN, T. V. & LEE, G. D. 2015. Arsenic removal from aqueous solutions by adsorption using novel MIL-53(Fe) as a highly efficient adsorbent. *RSC Adv.,* 5**,** 5261-5268.
235. WALTON, R. I. 2002. Subcritical solvothermal synthesis of condensed inorganic materials. *Chemical Society Reviews,* 31**,** 230-238.
236. WANG, B., LV, X. L., FENG, D., XIE, L. H., ZHANG, J., LI, M., XIE, Y., LI, J. R. & ZHOU, H. C. 2016a. Highly Stable Zr(IV)-Based Metal-Organic Frameworks for the Detection and Removal of Antibiotics and Organic Explosives in Water. *J Am Chem Soc,* 138**,** 6204-16.
237. WANG, C., LIU, X., CHEN, J. P. & LI, K. 2015. Superior removal of arsenic from water with zirconium metal-organic framework UiO-66. *Sci Rep,* 5**,** 16613.
238. WANG, C., LIU, X., KESER DEMIR, N., CHEN, J. P. & LI, K. 2016b. Applications of water stable metal-organic frameworks. *Chemical Society Reviews,* 45**,** 5107-5134.
239. WANG, J. & WANG, S. 2016. Removal of pharmaceuticals and personal care products (PPCPs) from wastewater: A review. *J Environ Manage,* 182**,** 620-640.
240. WEI, C., FENG, D. & XIA, Y. 2016. Fast adsorption and removal of 2-methyl-4-chlorophenoxy acetic acid from aqueous solution with amine functionalized zirconium metal–organic framework. *RSC Adv.,* 6**,** 96339-96346.
241. WEI, H., DENG, S., HUANG, Q., NIE, Y., WANG, B., HUANG, J. & YU, G. 2013. Regenerable granular carbon nanotubes/alumina hybrid adsorbents for diclofenac sodium and carbamazepine removal from aqueous solution. *Water Res,* 47**,** 4139-47.
242. WEI ZHOU, HUI WU, MICHAEL R. HARTMAN & YILDIRIM*, A. T. 2007. Hydrogen and Methane Adsorption in Metal-Organic Frameworks: A High-Pressure Volumetric Study. *J. Phys. Chem. C,* 111**,** 16131-16137.
243. WEITKAMP, J. 2000. Zeolites and catalysis. *Solid State Ionics,* 131**,** 175-188.
244. WORCH, E. 2012. *Adsorption technology in water treatment: fundamentals, processes, and modeling,* Walter de Gruyter.
245. XU, Y., LIU, T., ZHANG, Y., GE, F., STEEL, R. M. & SUN, L. 2017. Advances in technologies for pharmaceuticals and personal care products removal. *J. Mater. Chem. A.*
246. Y.S. HO, G. M. 1999. Pseudo-second order model for sorption processes. *Process Biochemistry,* 34**,** 451–465.
247. YAGHI, O. M., LI, G. & LI, H. 1995. Selective binding and removal of guests in a microporous metal–organic framework. *Nature,* 378**,** 703-706.

248. YAGHI, O. M. & LI, H. 1995. Hydrothermal Synthesis of a Metal-Organic Framework Containing Large Rectangular Channels. *Journal of the American Chemical Society,* 117**,** 10401-10402.
249. YAN, X. M., SHI, B. Y., LU, J. J., FENG, C. H., WANG, D. S. & TANG, H. X. 2008. Adsorption and desorption of atrazine on carbon nanotubes. *J Colloid Interface Sci,* 321**,** 30-8.
250. YANG, C. X. & YAN, X. P. 2011. Metal-organic framework MIL-101(Cr) for high-performance liquid chromatographic separation of substituted aromatics. *Anal Chem,* 83**,** 7144-50.
251. YANG, Y., OK, Y. S., KIM, K. H., KWON, E. E. & TSANG, Y. F. 2017. Occurrences and removal of pharmaceuticals and personal care products (PPCPs) in drinking water and water/sewage treatment plants: A review. *Sci Total Environ,* 596-597**,** 303-320.
252. YEE, K. K., REIMER, N., LIU, J., CHENG, S. Y., YIU, S. M., WEBER, J., STOCK, N. & XU, Z. 2013. Effective mercury sorption by thiol-laced metal-organic frameworks: in strong acid and the vapor phase. *J Am Chem Soc,* 135**,** 7795-8.
253. YILMAZ, B., TRUKHAN, N. & MÜLLER, U. 2012. Industrial Outlook on Zeolites and Metal Organic Frameworks. *Chinese Journal of Catalysis,* 33**,** 3-10.
254. YU, Z., PELDSZUS, S. & HUCK, P. M. 2008. Adsorption characteristics of selected pharmaceuticals and an endocrine disrupting compound-Naproxen, carbamazepine and nonylphenol-on activated carbon. *Water Res,* 42**,** 2873-82.
255. YU, Z., PELDSZUS, S. & HUCK, P. M. 2009. Adsorption of Selected Pharmaceuticals and an Endocrine Disrupting Compound by Granular Activated Carbon. 1. Adsorption Capacity and Kinetics. *Environmental Science & Technology,* 43**,** 1467-1473.
256. ZHANG, G., SUN, M., LIU, Y., LIU, H., QU, J. & LI, J. 2015. Ionic liquid assisted electrospun cellulose acetate fibers for aqueous removal of triclosan. *Langmuir,* 31**,** 1820-7.
257. ZHANG, W., DING, Y., BOYD, S. A., TEPPEN, B. J. & LI, H. 2010. Sorption and desorption of carbamazepine from water by smectite clays. *Chemosphere,* 81**,** 954-60.
258. ZHANG, Y., GEISSEN, S. U. & GAL, C. 2008. Carbamazepine and diclofenac: removal in wastewater treatment plants and occurrence in water bodies. *Chemosphere,* 73**,** 1151-61.
259. ZHAO, Y., SONG, Z., LI, X., SUN, Q., CHENG, N., LAWES, S. & SUN, X. 2016. Metal organic frameworks for energy storage and conversion. *Energy Storage Materials,* 2**,** 35-62.
260. ZHOU, Y., ZHANG, F., TANG, L., ZHANG, J., ZENG, G., LUO, L., LIU, Y., WANG, P., PENG, B. & LIU, X. 2017. Simultaneous removal of atrazine and copper using polyacrylic acid-functionalized magnetic ordered mesoporous carbon from water: adsorption mechanism. *Sci Rep,* 7**,** 43831.
261. ZHU, X., LI, B., YANG, J., LI, Y., ZHAO, W., SHI, J. & GU, J. 2015. Effective adsorption and enhanced removal of organophosphorus pesticides from aqueous solution by Zr-based MOFs of UiO-67. *ACS Appl Mater Interfaces,* 7**,** 223-31.

262. ZHU, X., LIU, Y., LUO, G., QIAN, F., ZHANG, S. & CHEN, J. 2014. Facile fabrication of magnetic carbon composites from hydrochar via simultaneous activation and magnetization for triclosan adsorption. *Environ Sci Technol*, 48**,** 5840-8.